Instabilities, pattern formation, localized solutions, mode-locking and stochastic effects in nonlinear optical systems and beyond

Auro Michele Perego

Doctor of Philosophy

February 7, 2018

Aston University

Instabilities, pattern formation, localized solutions, mode-locking and stochastic effects in nonlinear optical systems and beyond

Auro Michele Perego

Doctor of Philosophy

February 2018

In this thesis the results of scientific research about different nonlinear phenomena with particular emphasis to photonic systems are presented. Works about dissipation induced modulation instabilities with applications for signal amplification in nonlinear optics and mode-locking in lasers constitute the main part of the thesis. The dissipative instabilities studied are of two kinds, parametric instabilities induced by a periodic variation of spectral losses and instabilities induced by non varying but spectrally asymmetric losses. Although the main achievements are theoretical successful collaboration with experimentalists are reported too. Other results presented in this thesis concern a new fundamental theory of active mode-locking in lasers having a more general validity than Haus' one and hence useful for describing mode-locked lasers with a fast gain dynamics such as semiconductor or quantum cascade lasers; the prediction of the novel theoretical model have been successfully compared with experimental findings. Theoretical studies are also presented about collective phenomena, such as synchronization and localization, in coupled excitable lasers with saturable absorber and localized solutions on the non-vanishing background of the two-dimensional nonlinear Schrödinger equation with periodic potential: the Bogoliubov-de Gennes bullets.

Additional keywords and phrases: nonlinear optics, pulsed lasers, modulation instability, excitability.

Something to keep in mind

Le savant n'étudie pas la nature parce que cela est utile; il l'étudie parce qu'il y prend plaisir et il y prend plaisir parce qu'elle est belle. Si la nature n'était pas belle, elle ne vaudrait pas la peine d'être connue, la vie ne vaudrait pas la peine d'être vécue. Je ne parle pas ici, bien entendu, de cette beauté qui frappe les sens, de la beauté des qualités et des apparences; non que j'en fasse fi, loin de là, mais elle n'a rien à faire avec la science; je veux parler de cette beauté plus intime qui vient de l'ordre harmonieux des parties, et qu'une intelligence pure peut saisir.

H. Poincaré

Physics is like sex, sure it may give some practical results but that's not why we do it.

R. Feynman

Acknowledgements

I would like to acknowledge here many people whose constant help, encouragement and support has been decisive in obtaining the results that are presented in this thesis. From the scientific point of view I'm deeply grateful to many people I've been collaborating with during these years and that contributed substantially in achieving the results presented in this thesis: Prof. Sergei K. Turitsyn, Dr. Dimitry V. Churkin, Prof. Kestutis Staliunas, Prof. Germán de Valcárcel, Prof. Franco Prati, Prof. Stéphane Barland, Prof. Stefan Wabnitz, Dr. Sergey Sergeyev, Dr. Nikita Tarasov, Dr. Shubham Kumar, Dr. Marco Lamperti, Dr. Sergey Smirnov, Simone Gaiarin and Giuseppe Rizzelli. I hope I could have the luck and the honor to continue making science with them and sharing their friendship in the future.

I want to thank all my office colleagues at Aston for teaching me so many things when I was bothering them with questions; a special thank in this sense goes to Morteza Kamalian Kopae, Mohammad Al-Katheeb, Md. Asif Iqbal and Srikanth Sugavanam.

I particularly enjoyed hours long discussions with Nikita Tarasov on all sort of nonlinear, theoretical, experimental and numerical problems in fibre optics; I'm grateful to Morteza for stimulating conversation on inverse scattering transform, theory of integrability and solitons.

I thank my thesis Co-Supervisor Dr. Sergey Sergeyev and my Supervisor Prof. Sergei K. Turitsyn for constant support, for teaching me a lot about fundamental science, applied science and beyond science, for always being available to speak and discuss with me.

I have a special gratitude debt towards Sergei not just for teaching me a great amount

of important concepts about fibre optics and lasers and how research is linked to the society. I've received from him a constant and persistent encouragement towards being an independent researcher with my own ideas, projects and collaborations... and to fight for them!!! I'v received from him a large amount of freedom and personal trust. Those things are possibly among the most important and rare gifts a human being can receive in life. For this reason my gratitude debt will be difficult to pay back.

I want to thank Kestas for the constant help and collaboration in supervising part of the work presented in this thesis, for teaching me how to look at complicated problems in a simple way, how to go step-by-step when things are not clear or don't work, for always motivating me, engaging in passionate and creative discussions, suggesting new ideas and supporting me always, especially during the difficult start of my PhD.

A special thank goes to Franco for having introduced me to laser physics when it was still unclear that I'd have followed such research path, for his encouragement and permanent availability to discuss and think together about science.

I want to thank Germán for teaching me (beyond some important facts in laser physics, such as that "coherence matters") that when one goes to the office in the morning he should always be singing.

I want to thank all my old friends from "Il Campetto" because I'm sure I can always count on them.

I want to express a deep feeling of gratitude towards all the members of my family for having allowed me to grow up surrounded by positive and strong people.

I want to thank my parents Mauro and Tiziana and my brother Edgardo. My parents thought, and I believe still think, that education is the most important thing a person must obtain especially the early stage of the life in order to be free and autonomous in the world. I want to thank them for all the sacrifices they did in order to allow me to study in the best possible conditions always supporting, fostering and

encouraging the development of my talents. I thank them and my brother for being always supportive of my activities despite sometimes they cannot grasp why it is worth pursuing this path and why one should devote his time thinking about equations.

The constant love and the support of Matilde have been decisive in allowing my life and my research to develop in a creative and balanced way, always motivating me to do my best and bringing a ray of sun, happiness and of joy in my days.

I desire to conclude these acknowledgements with a consideration. At the end of a talk I was attending, the speaker, Prof. Sir David Payne, the inventor of the Erbium doped fibre amplifier, quoted Benjamin Disraeli saying that: *"A university should be a place of light, liberty and learning"*. I would like to correct him and say:

"A PhD must be a time of light, liberty and learning!"

I'm grateful to say that without any doubt during my PhD I experienced that sort of time. I wish the same could be true for people who will follow this path after me.

Contents

List of Figures

1 Introduction

In this thesis the results of three years of active research in nonlinear dynamics in general and in photonic systems in particular, with special interest to localized and pulsed solutions in lasers are presented. Such research activity has been carried out analytically and with help of numerical simulations; in some cases joint research works with experimentalists have been done too. The core of the thesis consists in a series of works on modulation instabilities induced by dissipative effects, the key feature of these instabilities is that, due to nontrivial nonlinear dynamics, the damped modes, counterintuitively exhibit exponential amplification. Dissipation induced modulation instabilities can occur both in presence of suitable modulation of the losses as well as in the case of stationary losses profile. Potential impact of those instabilities and of the associated pattern formation processes, both concerning signal amplification as well as mode-locking in lasers, will be discussed. To mode-locking is linked another research path I undertook concerning the derivation of a more fundamental theory for active mode-locking in lasers which accounts properly for coherent effects due to the atomic polarization and leads to a novel mathematical model more general than Haus' master equation. The predictions of the new coherent master equation have been verified experimentally and the results are summarized in a dedicated Chapter.

Pulsed solutions in lasers are not only due to mode-locking dynamics, some spontaneous Q-switching instabilities can lead to self-pulsations in lasers with saturable absorber due to the action of external perturbations. Lasers exhibiting those properties are said to be excitable in close analogy with the spiking activity of the neuronal cells. Excitable lasers are driving an emerging research direction closely linked to neuromorphic photonics. Here some preliminary results concerning collective phenomena in coupled excitable

lasers, ranging from synchronization to exponential localization of excitability due to disorder are discussed.

Finally, as the title of the thesis suggests, contributions extending "beyond" nonlinear optics are present too. In a first sense some of the works on modulation instabilities, despite I focussed on their nonlinear optics contextualization, may have applications outside of such research field due to the mathematical isomorphism that links evolution equation for dispersive and weakly nonlinear wave interaction across the most diverse areas of physics.

In a second sense some contributions presented here are about spatiotemporally localized solutions in nonlinear systems described by a two dimensional nonlinear Schrödinger equation. Such solutions can be potentially observed in Bose-Einstein condensates, however the analogue of a candidate system in photonics should still be individuated.

If we want to find a way to classify the results presented in this thesis, we can say that the topics investigated mathematically orbitate around generalised and more or less complicated forms of the nonlinear Schrödinger equation with special emphasis on instabilities, generation of pulses and localized solutions.

Since many different works and research topics are presented in this thesis, in order not to employ cumbersome notations, the meaning of the symbols used are defined consistently within each Chapter.

2 Dissipative Faraday instability in the complex Ginzburg-Landau equation

2.1 General introduction to modulation instabilities

Modulation instabilities are ubiquitous processes occurring in a great variety of natural and engineering systems. Under certain conditions homogeneous stationary states are unstable and the amplitudes of modulation modes experience exponential growth starting from noise. In this linear stage the amplitudes of the modulation modes are still much smaller than the amplitude of the homogeneous mode and the dynamics can be described by the linearized equations. When the modulation modes amplitudes become comparable in magnitude with the homogeneous mode, then the dynamics becomes nonlinear and when the growth saturates pattern formation can occur.

In the linear regime of the instabilities, is in general much easier to obtain an analytical description of the dynamics, while things become more complicated in the nonlinear stage, there numerical simulations are of great help.

It is also important to mention that, thanks to the existence of universal models that describe weakly nonlinear dynamics independently on the particular systems, results obtained in those paradigmatic models have widespread validity and impact in many physical systems. The latter fact also suggests a potential fruitful collaboration between different research areas.

It is probably very difficult to provide a rigorous mathematical classification of modulation instabilities in physics. It is however instructive to mention at least some paradigmatic instabilities that are both relevant in themselves but also are important to better emphasize and understand distinctive features of the novel modulation instabilities that are described in this thesis.

Faraday instability is probably the oldest pattern forming instability ever studied and

occurs when one parameter of a spatially extended system is periodically modulated in time. Originally it was observed in a vertically shaken mercury layer, where the excitation of surface waves was achieved as a consequence of the periodic modulation of the gravitational force [1, 2].

It has been generalised to nonlinear fibre optics where the parametric modulation is applied in space exploiting the fact that for optical fibres we have the evolution in space of a field defined in time, which is the exact opposite of what happens in spatially extended systems. Hence Faraday instabilities in optical fibres lead in general to pattern formation in time.

The Benjamin-Feir instability is probably one of the most known examples of modulation instabilities: it occurs for the homogeneous state of the nonlinear Schrödinger equation when phase matching conditions between the homogeneous mode wave and two spectral sidebands are satisfied [3, 4, 5]. Due to the universality of the nonlinear Schrödinger equation the Benjamin-Feir instability also sometimes simply called "modulation instability", has been observed in a great variety of physical systems: fluids, plasmas, Bose-Einstein condensates and nonlinear optics. In fibre optics, it occurs due to the interplay of Kerr effect and anomalous dispersion. Such instability has a particular relevance also in connection to the formation of solitons.

Another paradigmatic example that is worth mentioning is constituted by the Turing instability[6]: Alan Turing showed that such instability occurs in reaction-diffusion models for two coupled nonlinear equations describing spatially extended systems where the two key ingredients are present: local self-enhancement and lateral inhibition. Local self-enhancement is provided by a presence of nonlinearity that enhances the concentration of one the two fields in space, while the second field needs to be fast diffusing. Turing instability was particularly relevant in understanding morphogenesis process and pattern formation in biological systems. There have been attempts to generalise Turing instability to nonlinear optics. Lugiato and Lefever in the seminal paper where they presented for the first time the equation that bears their name, mentioned that the short wavelength instability (instability spectrum detached from the zero mode) exhibited by the homogenous state of such equation is the nonlinear optics analogous of the Turing instability[7]. In the Lugiato-Lefever equation diffusion is replaced by diffraction and nonlinearity is due to a self-phase modulation effect; a temporal Turing

instability has been predicted [8] and observed experimentally too [9]. Other attempts of finding analogies of the Turing instability in nonlinear optics have been performed [10], for instance considering a laser where the carrier diffusion in the gain medium plays the role of the lateral inhibiting field [11].

In nonlinear optics, modulation instabilities have attracted great interest. This interest is motivated by the following reasons: from the fundamental research point of view studying modulation instabilities is a paramount important topic because they are the key and necessary ingredients for the pattern formation and self-organization processes in nonlinear systems. Furthermore modulation instability is in general associated to soliton formation in integrable equations. From the more practical and technological point of view, instabilities are sometimes seen as detrimental effects that impair the desired operation of some optical systems, understanding their genesis and development paves the way to their suppression and control. However only a limited vision will consider instabilities as purely detrimental effects. An important research paradigm sees instabilities as important resources for solving practical problems in photonics technologies. Some reasons in this sense are the following: In the linear stage modulation instabilities are associated to exponential amplification of certain parts of the spectrum, controlling and engineering those spontaneous growth processes is of interest in the design of amplifiers of optical signals. The latter is relevant in various fields of applied optics, among others in optical communications where flexible and broadband amplification schemes are currently required. Some examples in this sense are the fibre optics parametric amplifier that exploits the Benjamin-Feir instability to amplify a broad band spectral region much larger than the one covered by the Erbium doped amplifiers currently used in optical telecommunications[12, 13]. In the nonlinear stage of modulation instabilities the formation of stable coherent structures can occur: periodic pulse trains are temporal patterns that beside the purely theoretical and scientific understanding of self-organization process are relevant for applications. In this respect modulation instabilities could be practically used as key ingredients for achieving mode-locking or generation of pulses. Among some of the fruits of this research direction is worth mentioning the "modulation instability laser" (again based on the Benjamin-Feir instability) [14, 15], and the spontaneous mode-locking induced by the Risken-Nummedal-Graham-Haken instability [16]. The Risken-Nummedal-Graham-Haken instability is due to the

coherent light-matter interaction in the laser gain medium. The coherent dynamics properly leads to the so called Rabi-splitting of the otherwise lorentzian gain curve. The generated spectral sidebands lead in this case to a spontaneous self-pulsing (harmonic mode-locking) [17]. A small remark on the notation is necessary here: across this thesis the expression "self-pulsing" will be used generically, meaning that certain pulsations arise spontaneously in a given optical system, this will not be linked to any particular case of pulsations generated precisely through Hopf bifurcations or to the phenomenon of optical bistability.

In this thesis some results will be presented about three novel kinds of modulation instabilities that are relevant both for signal amplifications as well for the generation of pulses in lasers. The *trait-d'union* of those works is the central role played by the dissipation as instability mechanism. Despite the results presented in this thesis are mainly related to the concept of Faraday instability and we will expand the discussion in this direction, we will also from time to time comment more in detail about the other instabilities we have briefly mentioned in this introduction when it will be useful for the clarification and explanation of the main results.

2.2 Classical Faraday instability: from the pendulum to spatially extended systems and optical fibres

The aim of this section is to provide the description of the dissipative Faraday (parametric) instability induced by periodic zig-zag modulation of spectral losses in the complex Ginzburg-Landau equation. It is at first however necessary to introduce the concept of parametric instability in spatially extended systems and in nonlinear fibre optics and to review the main results obtained up to now in this stimulating research field.

Parametric instabilities are a well known phenomenon that has been studied extensively for more than one century in the most diverse research areas in physics and beyond. They are instabilities developing thanks to the periodic modulation of one system's parameter. Their first study is due to Michael Faraday [1] back in 1831. As it has been briefly mentioned in the previous section, he verified experimentally that the surface of vertically shaken mercury layer exhibits the formation of waves oscillating with half the forcing frequency. In this particular case, gravity is the periodic in time modulated

parameter that destabilizes the homogeneous state of the system giving rise to the generation of the wave-pattern on top of the fluid. For this historical reason we will use interchangeably the denominations *parametric instability* and *Faraday instability* across the manuscript.

The instability generated by the external forcing is indeed related to the existence of the so-called parametric resonance. The most simple system where parametric resonance occurs is probably the pendulum. Let's consider a pendulum whose length is periodically modulated in time with angular frequency ω_p. Then it is possible to show that the pendulum will start to oscillate with a frequency equal to $\omega_p/2$. Oscillations with frequencies $n\omega_p/2$, with n integer, will also be excited but with amplitudes monotonically decreasing for increasing n. The synchronization actually occurs not for a single frequency but for a band whose width is proportional to the the strength of the forcing [18]. Faraday instabilities have been studied extensively in spatially extended systems, including fluids [1, 2], granular media [19], plasmas [20], chemical reactions [21], and Bose-Einstein Condensates [22, 23]. Those spatially extended systems can be considered in general as sets of nonlinear oscillators coupled to their neighbors through nonlocal terms which are in general differential operators (the Laplacian being probably a paradigmatic example being very generally related to diffusion processes). In spatially extended systems, the parametric resonance condition determines the frequency of the amplified modulation modes via the dispersion relation of the mode which will depend on the various parameters of the particular system considered [24].

We will now introduce the concept of parametric instabilities in fibre optics and later comment on how the parametric resonance condition can be applied to characterize the excited modes.

The propagation of light in single mode optical fibres is described by the nonlinear Schrödinger equation (NLSE) [25] (a full derivation will be given in Chapter 5):

$$\frac{\partial A}{\partial z} = -i\frac{\beta_2}{2}\frac{\partial^2 A}{\partial t^2} + i\gamma|A|^2 A \tag{2.1}$$

where A is the electric field slowly varying envelope, β_2 the group velocity dispersion coefficient, γ the nonlinearity coefficient, z is the spatial coordinate along the fibre and

t is time in a reference frame co-moving with a radiation pulse. It is evident that the mathematical structure of Eq.2.1 is identical with that of the Gross-Pitaevskii equation for a Bose-Einstein condensate in the mean-field limit [26]:

$$i\hbar\frac{\partial\psi(\mathbf{r},t)}{\partial t} = -\frac{\hbar^2}{2m}\nabla^2\psi(\mathbf{r},t) + a|\psi(\mathbf{r},t)|^2\psi(\mathbf{r},t) + V(\mathbf{r})\psi(\mathbf{r},t). \tag{2.2}$$

In Eq.2.2 ψ is the macroscopic wave function of the condensate defined in space $\mathbf{r}$ and evolving in time t, m is the mass of the atom specie the condensate is made of, a measures the atomic interaction, V is a potential and $\hbar$ is the reduced Planck's constant. Now by analogy, if the periodic in time modulation of one parameter of Eq.2.2, for instance the interaction a, could be a sinusoidal function with angular frequency ω_f and hence $a = a_0 cos(\omega_f t)$, will trigger the growth of modulation modes with wavenumber k and the corresponding pattern formation in space, then a periodic modulation of one parameter of Eq.2.1 in space with periodicity given by k_f, say for instance $\beta_2 = \beta_{av} + \beta_m cos(k_f z)$, where β_{av} and β_m are respectively the average dispersion and the dispersion modulation depth, will generate the formation of a pattern in time with angular frequency ω determined by the dispersion relation.

A first order approximation of the scaling of the Faraday instability excited frequencies for the NLSE in average normal dispersion can be obtained by applying the parametric resonance condition in the following way: the weak amplitude excitations (Bogoliubov-de Gennes modes) oscillating on top of the continuous wave (CW) solution with amplitude A_0, in the stable NLSE obey the following dispersion relation which connects their frequency ω to the wavenumber k:

$$k^2 = \frac{\beta_{2av}\omega^2}{2}\left(\frac{\beta_{2av}\omega^2}{2} + 2\gamma|A_0|^2\right) \tag{2.3}$$

being β_{2av} the average group velocity dispersion [27, 28]. Let's consider a parametric forcing that occurs with spatial period L_f and wavenumber $k_f = 2\pi/L_f$. Imposing the parametric resonance condition means assuming that modes of the electric field having $k = k_n = n\frac{k_f}{2}$, with n integer, will synchronize with the forcing and hence start to oscillate. Actually the oscillation with the strongest amplitude corresponds to $k_1 = \frac{k_f}{2}$ $(n = 1)$ and substituting this expression into Eq.2.3 gives, under the long wavelength approximation i.e. neglecting the small term $\left(\frac{\beta_{2av}\omega^2}{2}\right)^2$ the frequency of the first excited

mode:

$$\omega_1 \approx \frac{\pi}{L_f \sqrt{\beta_{2av}\gamma |A_0|^2}}. \tag{2.4}$$

Another possibility to estimate the instability frequency is to use an argument based on quasi phase-matching relations [27, 28].

The first example of Faraday instability in nonlinear fibre optics was presented by Matera and co-workers [29]. They showed that the periodic power variation experienced by the electric field propagating in a fibre transmission link in presence of attenuation and periodic lumped amplification leads to a spectral sidebands growth associated to the modulation instability. Later it was showed independently in three separate works that indeed the periodic variation of group velocity dispersion is able to excite the Faraday instability [30, 31, 32].

More recently the concept has been developed in several works and it has been proposed as a mechanism to generate pulses in an externally driven ring fibre resonator. Again both cases of modulated nonlinearity coefficient [33] and modulated group velocity dispersion [34] have been considered. The latter has been observed also experimentally thanks to the fabrication of suitable dispersion oscillating fibres, that thanks to their periodically (along the longitudinal coordinate) varying diameter exhibit and oscillating β_2 coefficient. The characteristic Faraday MI spectrum has been observed for dispersion oscillating fibres both for the simple propagation case as well as for the externally driven passive fibre resonator[34, 35]. Interestingly the competition between Faraday and temporal Turing instabilities in fibre resonators have demonstrated and characterized too [9]. Despite the considerable effort spent in this direction, the temporal Faraday pattern formation in modulated optical fibres has not been characterized yet experimentally to the best of my knowledge.

2.3 Dissipative Faraday instability

The above mentioned cases of Faraday instability in fibre optics rely on the periodic modulation of one parameter of the system which is connected to the dispersive property of the light waves (nonlinearity or dispersion). However, very recently, we have shown

that a suitable periodic modulation of spectral losses, a genuinely dissipative parameter of the system, can induce a modulation instability [36]. The scaling of such dissipative Faraday instability can be inferred from a parametric resonance condition.

This novel instability that will be discussed now is a general feature of the complex Ginzburg-Landau equation (CGLE), such equation is a universal form for nonlinear oscillations in a variety of nonlinear systems throughout the most diverse scientific disciplines [37]. We will introduce the novel dissipative Faraday instability at first in the framework of spatially extended systems and then, in the next Chapter, generalise it to fibre optics and in particular in the case of the Raman fibre laser, where its first experimental observation has been achieved.

Let's consider the following CGLE that describes the dynamics of the complex field amplitude $A(t, x)$ defined in space x and evolving in time t:

$$\frac{\partial A}{\partial t} = \mu A + (b - id)\frac{\partial^2 A}{\partial x^2} + (ic - s)|A|^2 A. \tag{2.5}$$

μ is the gain coefficient, b, d, c and s describe diffusion and diffraction, self-phase modulation and saturation respectively. Let's impose that all those coefficients are positive, in this case the homogeneous solution is Benjamin-Feir stable. Let's now consider the following modulation scheme. A spatially homogeneous field undergoes nonlinear evolution according to Eq.2.5 for a time interval of length $T_f/2$, then we damp spectral modes in the wavenumber region centered around $+k_0$ by using a lumped filter which transmits mainly in the spectral region around wavenumber $-k_0$, we let again the field evolve as described by Eq.2.5 for another time interval of length $T_f/2$ and after such evolution we damp spectral modes in the spectral region around $-k_0$ this time using a lumped filter that transmits mainly in the spectral region around wavenumber $+k_0$. If we repeat the procedure many times we have a system where spectral losses are modulated periodically in time with period T_f and in a zig-zag fashion in spectral domain. The modulation scheme is summarized in Fig. 2.1.

The periodic zig-zag modulation of spectral losses triggers an average exponential amplification of spectral modes symmetrically located with respect to the homogeneous mode ($k = 0$). The modulation has been realized by using spectral filters having the

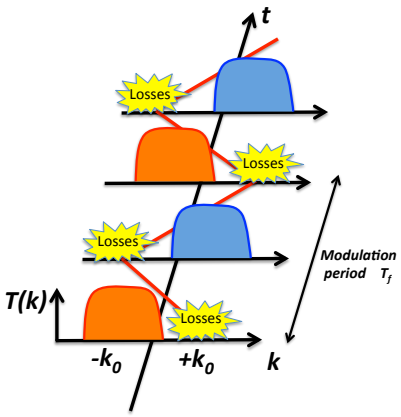

Figure 2.1: The concept of periodic, in time, and zig-zag, in frequency domain, modulation of spectral losses is illustrated here schematically: the long arrow indicates time evolution, the transmittance profile $T(k)$ of the two spectral filters used are plotted in orange and in blue respectively.

following transmission profile:

$$f_{1,2}(k) = e^{-\frac{(k\pm k_0)^8}{\sigma^8}} \tag{2.6}$$

where σ and k_0 are respectively the filters width and position in wavenumber domain. Mathematically we can express adding to Eq.2.5 the following term:

$$-\sum_{n\ even} \delta(t - nT_f/2)F_1 \star A - \sum_{n\ odd} \delta(t - nT_f/2)F_2 \star A. \tag{2.7}$$

where $F_{1,2}$ are the inverse Fourier transfoms of $f_{1,2}$ and the $\star$ denotes convolution: filters act as a multiplication operator on the field spectrum.

The growth of the modulation modes exhibits both an average amplification as well a periodic oscillation due to the lumped losses. Such oscillations occur in anti-phase for spectral modes having opposite wavenumbers $\pm k$ within the instability area. The latter anti-phase dynamics follows from the fact that when the spectral region located around wavenumber $-k_0$ suffers losses, then the spectral region around wavenumber $+k_0$ is basically unaffected (or affected only in a minor way depending on the width of the filters used).

Being the forcing considered here not described by a continuous parameter modula-

tion but by a lumped one, analytical study of the process is in principle very difficult. However some numerical tools could help to get insight on the instability and to characterize its dependence on the parameters of the system. Since we are dealing with a periodic system the stability of the homogeneous solution can be checked by simply considering the evolution of small perturbations for one single modulation period and to verify their possible growth or damping. This approach is called Floquet linear stability analysis and it is routinely applied in many studies of modulation instabilities. It consists in the following procedure: the homogeneous solution of the evolution equation of interest is computed by neglecting the parametric modulation. Then, for spectral mode with wavenumber $+k$ we add a very small real perturbation to the amplitude of one spectral mode and integrate the evolution equation in presence of the parametric modulation for a time interval corresponding to one period of the modulation. We record now the evolved amplitude of spectral mode with wavenumber $+k$ and normalize it to the modulus of the added perturbations and repeat the procedure this time adding an imaginary perturbation with wavenumber $+k$ to the homogeneous solution. We repeat this procedure by perturbing the spectral mode with wavenumber $-k$ again by adding to it first a real amplitude perturbation and then an imaginary amplitude perturbation. We can build now a stability matrix M whose entries are respectively: first and second row entries are the real and imaginary parts of the modes $+k$ and $-k$ amplitudes after the evolution of real and imaginary perturbations to mode $+k$. The third and fourth rows of M contain the real and imaginary parts of $+k$ and $-k$ mode amplitudes, respectively, after the evolution of real and imaginary perturbations of mode $-k$.

We then diagonalize the matrix M and obtain a set of eigenvalues: the Floquet multipliers. The logarithms of those eigenvalues are called the Floquet exponents. If, for a mode with wavenumber k, at least one of the Floquet exponents is greater than zero (or equivalently one of the Floquet multiplier is greater than 1) than the mode with wavenunumber $+k$ and its symmetric (-k) are unstable and their growth exponent is the Floquet exponent with largest absolute value. It is worth stressing that the 4-by-4 stability matrix gives 2 degenerate eigenvalues. In this sense most likely a simple 2-by-2 matrix could be used.

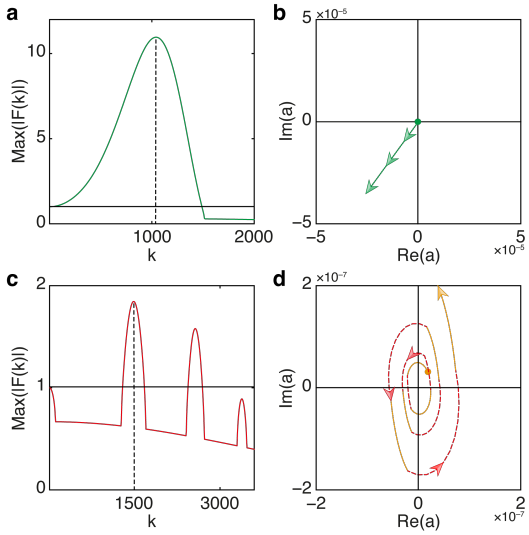

Figure 2.2: The basic features of the Benjamin-Feir and of the dispersive Faraday instability are summarized here: a) the Benjamin-Feir gain spectrum which is long-wavelength in the NLSE and in the CGLE and the monotonic growth of an unstable mode b); in c) is plotted the Faraday gain spectrum which is short-wavelength and exhibits high order harmonics, in d) the oscillatory growth dynamics of the Faraday unstable mode is depicted. The parameters used are μ=1, $s = 0.3$, $b = 0.1 \cdot 10^{-6}$, with full integration time $T = 1$. In a) and b) $c = 1$ and $d = -3 \cdot 10^{-6}$. In c) and d) $c = 4.85$, diffraction has been modulated piecewise: $d = d_1 = 5 \cdot 10^{-6}$ for $0 < t < 0.2$ orange line on d), $d = d_2 = 1 \cdot 10^{-6}$ for $0.2 < t < 0.4$ red line and so on.

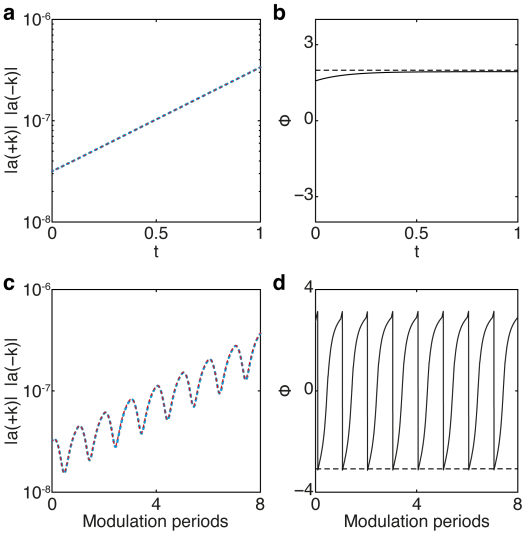

Figure 2.3: The growth of symmetric modes ($k = \pm 200\pi$) and the generalised phase is depicted for Benjamin-Feir a) and b) and dispersive Faraday instability c) and d). Blue and red dashed lines represent the modes amplitudes absolute values while the black dashed lines in b) and d) represent the values at which synchronization of the sidebands with the homogeneous mode is optimum. Parameters used are the same as in Fig.2.2.

The linear Floquet stability analysis allows to characterize the modulation instability spectrum by showing its dependence on some key parameters of the system.

In Fig.2.2 and 2.3 the features of the known Benjamin-Feir and dispersive Faraday instability are depicted, while the dynamics of the novel dissipative Faraday instability is reported in Fig.2.4. The both Faraday instabilities, besides the average growth of spectral sidebands exhibit an oscillatory dynamics induced by the periodic forcing. Oscillations are in phase for the symmetrically located spectral modes, at $\pm k$, for the dispersive Faraday instability and in anti-phase for the dissipative one. With the Benjamin-Feir instability, the dissipative Faraday instability shares the feature of being a long wavelength instability (instability spectrum attached to the $k = 0$ mode), while like the dispersive Faraday it can exhibit multiple instability tongues generated by the synchronization of the forcing with higher harmonics of the fundamentally excited mode. An analytical estimation of the dissipative Faraday instability first excited mode scaling versus other parameters of the system can be obtained. We plug the following *ansatz* into Eq.2.5

$$A(x,t) = A_0 e^{icA_0^2 t}\left[1 + a_+(t)e^{ikx} + a_-(t)e^{-ikx}\right] \tag{2.8}$$

where $A_0^2 = \mu/s$; and, linearizing with respect to the small perturbations amplitudes $a_\pm$, we obtain two coupled equations:

$$\frac{\partial a_+}{\partial t} = \mu a_+ - bk^2 a_+ + idk^2 a_+ + ic(a_+ + a_-^*)A_0^2 - s(2a_+ + a_-^*)A_0^2 \tag{2.9}$$

$$\frac{\partial a_-^*}{\partial t} = \mu a_-^* - bk^2 a_-^* - idk^2 a_-^* - ic(a_+ + a_-^*)A_0^2 - s(2a_-^* + a_+)A_0^2. \tag{2.10}$$

From these equations, by diagonalizing the coefficients matrix, it is possible to calculate the eigenvalues which are linked to the oscillation frequency and damping/amplification of the sidebands, they read:

$$\lambda_\pm = -\mu - bk^2 \pm \sqrt{-d^2k^4 - 2cdk^2\mu/s + \mu^2}. \tag{2.11}$$

For $d^2k^4 + 2cdk^2\mu/s > \mu^2$ the perturbations on top of the homogeneous state oscillate with frequency given by the imaginary part of the eigenvalues:

$$\omega_B = \sqrt{d^2k^4 + 2cdk^2\mu/s - \mu^2} \tag{2.12}$$

and their amplitude decays with rate given by the real part:

$$D = -\mu - bk^2. \tag{2.13}$$

In the long wavelength limit, $d^2k^4 << 2cdk^2\mu/s$ and assuming the parametric resonance condition, implying synchronization of the excitations with the external forcing

$$\frac{\omega_f}{2} = \omega_B, \tag{2.14}$$

since $\omega_f = \frac{2\pi}{T_f}$, where T_f is the forcing period, we have that the maximally unstable wavenumber k_{inst} (first excited mode) can be approximated as:

$$k_{inst} \approx \frac{\pi}{T_f\sqrt{2cd\mu/s}}. \tag{2.15}$$

In order to compare the analytical results with the Floquet analysis, since the detuned filters partially damp the homogeneous mode, hence making its amplitude different from the theoretical one, it is important to substitute the ratio μ/s in Eq.2.15 with the the average intensity $\langle|A_0|^2\rangle$ computed along one modulation period, otherwise an underestimation error is made. The result is quite good and it is represented in Fig.2.4 d) (dashed black line).

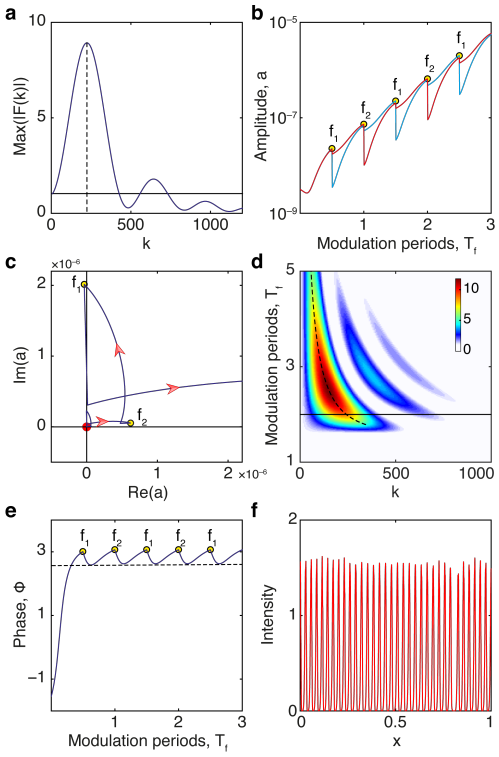

Figure 2.4: a) the dissipative Faraday instability spectrum for $T_f = 2$; b) the antiphase growth of two symmetric spectral modes amplitudes $|a_+|$ (in red) and $|a_-|$ (in blue); c) the looping in phase space of the complex amplitude. In both b) and c) the yellow dots denote respectively the action of the two filters (f_1 and f_2). In d) the instability map (Floquet multipliers with largest absolute value) is plotted in the plane "wavenumber-modulation period": colored region corresponds to instability. Beside the low frequency tongue, higher order harmonics are excited too. The horizontal black line denotes the section plotted in a). In e) the generalised phase $\Phi_0 = \phi_1 + \phi_{-1} - 2\phi_0$ is plotted where ϕ_0 is the phase of the homogeneous mode while $\phi_{\pm 1}$ those of the two sidebands. The stable spatial pattern associated to the instability for parameters corresponding to the instability spectrum shown in a) is depicted in f): the intensity pattern is taken just after the action of one spectral filter on the field. Parameters used are the following: $\mu = 1$, $s = 0.2$, $c = 3.5$, $b = 0.1 \cdot 10^{-6}$, $d = 5 \cdot 10^{-6}$, $k_0 = 1822.1$ and $\sigma = 1885$. $T_f = 2$ in all panels except for d) where T_f has been varied from 1 to 5.

In the nonlinear stage of the dissipative Faraday instability pattern formation can occur (See Fig.2.4 f)). The generated patterns, when they are stable, are oscillating periodically in time. But a stroboscopic collection of intensity distributions taken at time intervals equal to the period of the forcing can provide insight on their features and dynamics. The results are depicted in Fig.2.5.

The detuning between spectral filters is a key parameter in determining the stability of the generated patterns, if the detuning is too weak the patterns are not very stable and undergo a dynamics which sees creation and annihilation of the coherent structures. An increase in the filter's detuning allows the patterns' stabilization. In general the

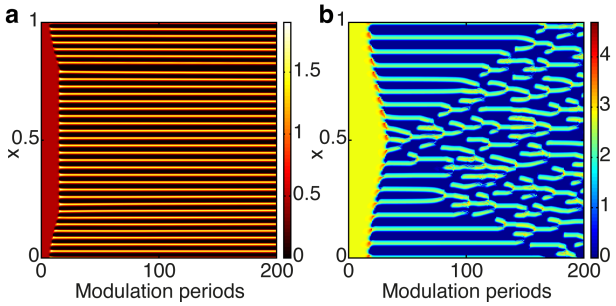

Figure 2.5: a) The slow dynamics of a stable pattern induced by the dissipative Faraday instability for the same set of parameters as Fig.2.4 f): intensity snapshots are taken every modulation period after filtering. b) reducing the filters detuning $k_0 = 1570.8$ we enter a regime where patterns are not stable anymore, but creation, destruction and merging of structures occur.

filters shape doesn't matter concerning the excitation of the instability, however it was observed that filters with steeper tails (high order supergaussian for instance) allow a more stable pattern formation.

The dissipative Faraday instability and the associated pattern formation take place in two-dimensional spatially extended systems too. Interestingly in this case more freedom is given in the choice of the filters. This allows a greater possibility concerning the choice of the patterns' features such as for instance their spatial orientation. Some examples in this respect are depicted in Figs.2.6 and 2.7. In the latter case gaussian filters with the following transmission profile have been used:

$$f_{1,2}(k_{x,y}) = e^{-\frac{(k_{x,y} \pm k_{0x,y})^2}{\sigma^2}}. \tag{2.16}$$

We remark that the patterns are stable, but they undergo a periodic dynamics in time. The individual coherent structures have a Gaussian shape after the filters, but after a temporal evolution in presence of gain and normal diffraction they develop a quasi-parabolic shape, with a dynamics resembling in this respect to that of similaritons in fibre amplifiers. Furthermore, intrapulse noise and prelude of optical wave-breaking become visible. Interestingly enough despite the fact that those waveform seem to be close to destruction, the interaction with the shifted spectral filters restores their original shape cleaning suppressing the noise. In this case we can say that the shifted spectral filters not just play the role of destabilizing the homogeneous solution leading to the pattern formation, they also play a fundamental role in keeping the patterns stable. It is worth mentioning briefly now that such a regeneration effect caused by

detuned filters is indeed known in the field of fibre optics communications and we will comment later on more in detail on this point. Results concerning the broadening of the patterns for the one- and two-dimensional case are reported in Figs.2.8 and 2.9.

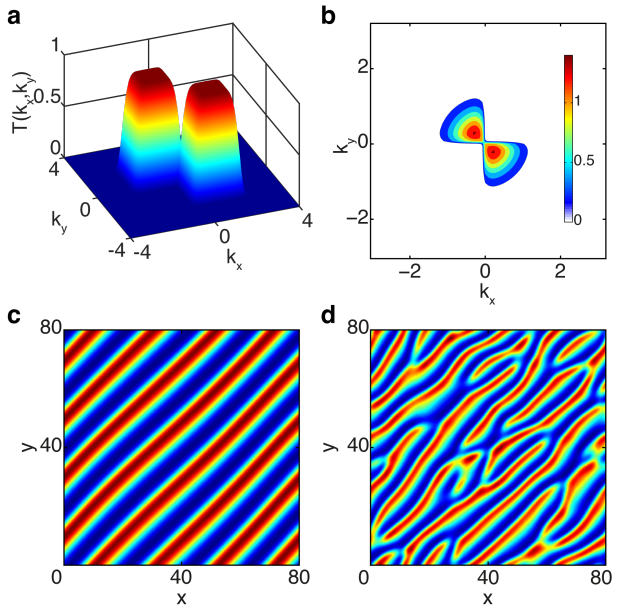

Figure 2.6: a) Filters used for exciting 2D dissipative Faraday instability, b) the unstable modes from Floquet analysis (colored area) . c) a stable intensity pattern and an unstable one d). Instability of the pattern is due to removal of diffusion (present in c) that reduces high frequency noise). Parameters used are $\mu = 1$, $d = 0.05$, $c = 0.35$, $s = 0.3$, $T_f = 5\pi$, $\sigma = 1.0905$. Filters are as in the 1D case Supergaussian and they are centered at $(k_{0x}, k_{0y}) = (-1, 1)$ and $(1, -1)$ respectively. In c) $b = 0.08$ while in d) $b = 0$.

We can expect that the two-dimensional patterns could be observed for instance in polaritonic Bose-Einstein condensates where the dynamics of the quasi-particles, coherent superpositions of excitons and photons, is described by a Ginzburg-Landau equation. Such polaritonic condensates can be realized in semiconductor microcavities where a quantum well is enclosed between two Bragg mirrors [38]. The necessary zig-zag modulation of spectral losses could be potentially implemented by a suitable engineering of the Bragg mirrors reflectivity profiles.

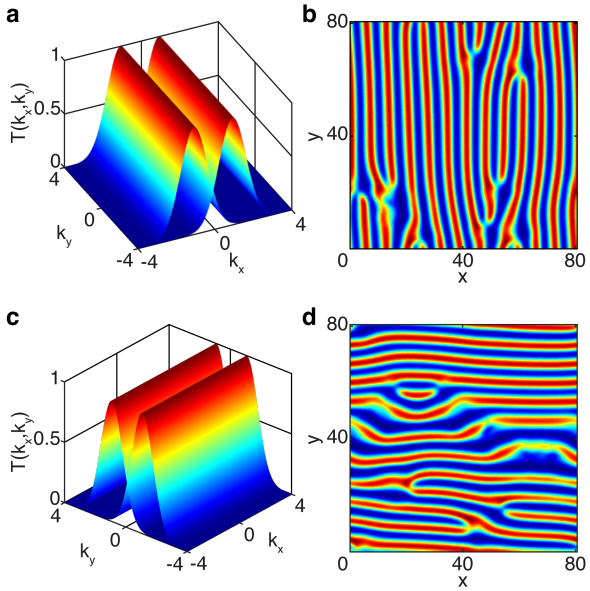

Figure 2.7: An example of 2D patterns achieved with different kind of filters compared to Fig.2.6. In a) Gaussian filters oriented parallel to the k_y axes and in b) the corresponding patterns are depicted. In c) and d) again filters and patterns are shown, but filter are rotated by $\pi/2$ in the $k_x - k_y$ plane compared to a). Parameters used are the following: $\mu = 0.2$, $d = 0.05$, $b = 0.001$, $c = 0.35$, $s = 0.3$, $T_f = 5\pi$ and $\sigma = 1$. In a)-b) filters of the form $f_{1,2} = e^{-(k_x \pm k_{x0})^2/\sigma^2}$ with $k_{0x} = 1$ are used. In c)-d) filters have the form $f_{1,2} = e^{-(k_y \pm k_{0y})^2/\sigma^2}$ with $k_{0y} = 1$.

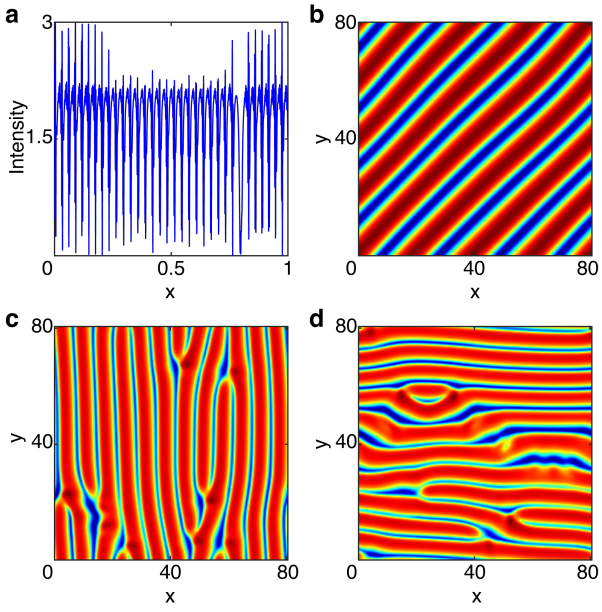

Figure 2.8: Here one- and two-dimensional patterns before the action of the filter are shown. A substantial broadening is clearly visible due to the combined action of gain, diffraction and self-phase modulation, see Figs.2.4 f), 2.6 and 2.7 for a comparison with the situation before filtering. In the 1D case a substantial amount of noise associated to optical wave breaking develops, but is later "cleaned" by the filter.

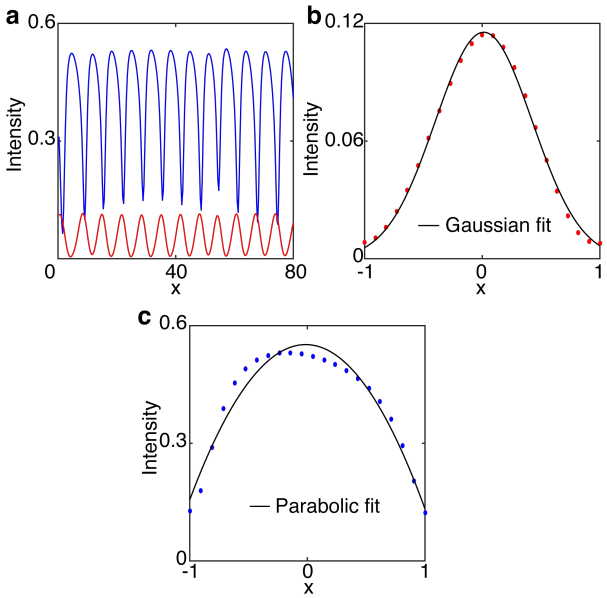

Figure 2.9: a) The comparison of 1D patterns before (blue line) and after (red line) filtering. Single structures composing the pattern are fitted by Gaussian and parabolic functions respectively after b) and before filtering c).

3 Mode-locking via Dissipative Faraday instability in a Raman laser

3.1 Experimental setup and theoretical model

Due to the mathematical isomorphism between the evolution equations describing the dynamics of spatially extended systems and fibre lasers discussed in the previous Chapter, it is natural to generalise the results obtained about the dissipative Faraday instability in the CGLE to fibre optics. In case of fibre lasers, due to the exchange of spatial and temporal coordinates in the evolution equations, the modulation of dissipation should be periodic in space and zigzagging in the temporal angular frequency ω. The associated pattern formation would then take place in time.

A very natural scheme for observing the dissipative Faraday instability in fibre optics is a linear cavity fibre laser where the cavity mirrors are fibre Bragg gratings (FBGs) with detuned reflectivity profiles in spectral domain. The photons traveling back and forth along the cavity will experience periodic lumped spectrally dependent losses for modes around ω_+ and ω_- in alternating fashion (here $\omega = 0$ is defined as the frequency of the CW solution). The modulation period of the forcing would be than equal to twice the cavity length. We have studied theoretically, numerically and experimentally (the experiment was performed by Dr. Nikita Tarasov) the dissipative Faraday instability in a linear cavity Raman laser [39]. The experimental setup, schematically depicted in Fig.3.1, consists in a 2.2 km long normal dispersion fibre. The FBGs, whose reflectivity profile in frequency domain can be controlled by Peltier elements hence achieving the necessary detuning to trigger the instability. The pump field at 1455 nm is injected in correspondence to the first cavity mirror and the first Stokes is then generated at 1550 nm along the fibre. The Bragg gratings with transmission width of 1 nm, have been detuned by about 0.75 nm. Both gratings have a chirp of -53 ps^2. Despite this fact the

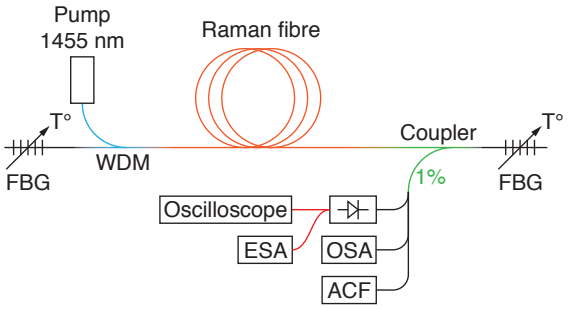

Figure 3.1: The experimental setup of the Raman laser with shifted FBG gratings.

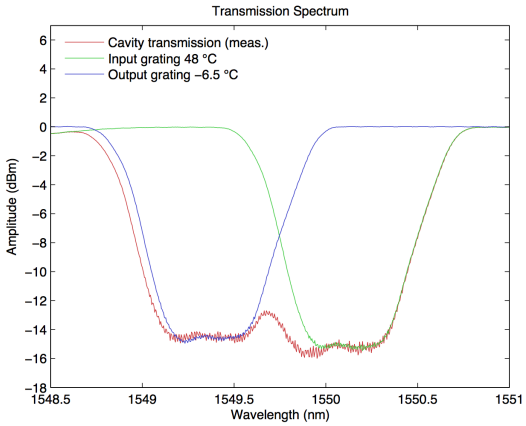

Figure 3.2: The transmission spectrum of the the gratings used experimentally is plotted in blue and green. In red is plotted instead the average transmission of the laser cavity.

net cavity dispersion remains normal due to the fact that for the Stokes wave the group velocity dispersion β_{2s}=25.49 ps^{2}km^{-1}. Once the pump field is turned on (corresponding to pump power of about 0.8 W) the laser crosses the threshold and emits a regular pulse train self-starting from noise. It has been observed that the pulse train had a repetition rate ranging from about 10 to 6 GHz depending on the pump power. The laser is described by the following coupled generalised nonlinear Schrödinger equations

$$\begin{aligned}
\pm\frac{\partial A_s^{\pm}}{\partial z} &= -i\frac{\beta_{2s}}{2}\frac{\partial^2 A_s^{\pm}}{\partial t^2} - \frac{\alpha_s}{2}A_s^{\pm} + i\gamma_s\left(|A_s^{\pm}|^2 + 2|A_p^{\pm}|^2\right)A_s^{\pm} + \frac{g_s}{2}\left(|A_p^{\pm}|^2 + |A_p^{\mp}|^2\right)A_s^{\pm} \\
\pm\frac{\partial A_p^{\pm}}{\partial z} &= -\beta_{1p}\frac{\partial A_p^{\pm}}{\partial t} - i\frac{\beta_{2p}}{2}\frac{\partial^2 A_p^{\pm}}{\partial t^2} - \frac{\alpha_p}{2}A_p^{\pm} + i\gamma_p\left(|A_p^{\pm}|^2 + 2|A_s^{\pm}|^2\right)A_p^{\pm} - \\
&- \frac{g_p}{2}\left(|A_s^{\pm}|^2 + |A_s^{\mp}|^2\right)A_p^{\pm}
\end{aligned} \tag{3.1}$$

where $A_{p,s}^{\pm}(z,t)$ are the pump and Stokes fields slowly varying envelopes defined in time t and propagating in space z, $\pm$ denotes the propagation direction of the fields in the

cavity: + from left to right and - from right to left. $\beta_{2p,s}$, $\gamma_{p,s}$, $\alpha_{p,s}$ and $g_{p,s}$ denote group velocity dispersion, Kerr nonlinearity, attenuation and Raman gain coefficient respectively, while β_{1p} accounts for the group velocity mismatch between Stokes and pump field. The suffixes, p, s indicate wether the parameter refers to pump or Stokes field respectively.

It is possible to solve numerically Eqs.3.1 in an iterative way: first the equations for the forward propagating fields are integrated with a split-step Fourier method and their intensity values along z saved, then, after computing the initial condition for the backward propagating fields after interaction of the forward propagating ones at $z = L$ with the gratings reflection functions, the equations for the backward propagating fields are integrated from $z = L$ to $z = 0$ using the previously saved values of the forward propagating fields in the cross-phase modulation terms. The values of the backward propagating fields along z are saved and used for computing the cross-phase modulation terms in the next forward propagation, that will start with initial condition given by the backward propagating fields at $z = 0$ after interaction with the grating and new injection for the pump field. Such method have been proved to be able to capture well the dynamics of Raman fibre lasers even where complex phenomena are involved[40]. For the numerical simulations and the Floquet linear stability analysis we have considered the following values of the parameters: β_{2p}=25.78 ps^{2}km^{-1}, β_{2s}=25.49 ps^{2}km^{-1}, γ_p= 8 km^{-1}W^{-1}, γ_s= 6.5 km^{-1}W^{-1}, α_p=0.6 km^{-1}, α_s= 0.6 km^{-1}, g_p=2.5 km^{-1}W^{-1}, g_s=2.32 km^{-1}W^{-1} and cavity length $L = 2.2$ km. Note that the attenuation coefficients account for both distributed and lumped losses, the latter being due to the presence of connectors. The filters have Supergaussian reflectivity profile and posses a linear chirp $\beta_{2c} = -53ps^2$; they are described by the following function acting on the Stokes field, while they are transparent for the pump:

$$f_{\pm} = Re^{-\frac{(\omega \pm \omega_{\pm})^6}{\Omega_f^6}} e^{i\beta_{2c}\omega^2}. \tag{3.2}$$

where $R = 0.98$, $\omega_{\pm} = \pm 150$ rad/ns is the detuning and Ω_f=190 rad/ns the filters' width.

Note that, as mentioned before, despite the anomalous dispersion contribution due the gratings the net cavity dispersion remains normal, hence Benjamin-Feir instability

cannot develop.

3.2 Numerical and experimental results: stability analysis and pulses

The Floquet stability analysis of Eqs.3.1 shows the dissipative Faraday instability spectrum for such laser with parameters corresponding to the experimental ones. The self-pulsing dynamics is confirmed in the case of full numerical simulations of Eqs.3.1 and the results are depicted in Fig.3.3b).

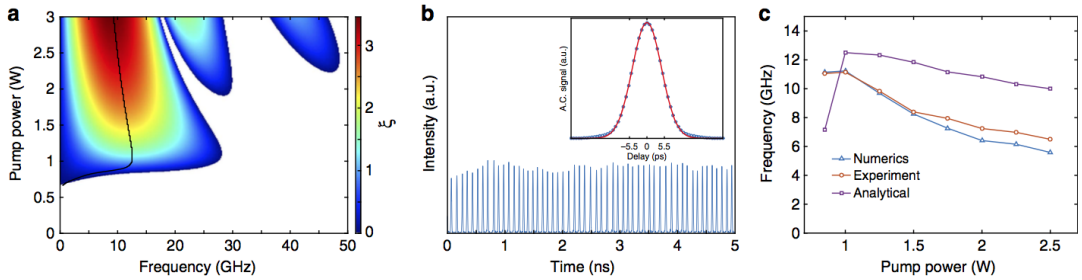

Figure 3.3: a) The instability power gain obtained from the linear Floquet stability analysis $G = 2ln(F_m)/\Lambda$ being F_m the maximum Floquet multiplier absolute value and Λ, equal twice the cavity length L, the period of dissipation modulation: colored area corresponds to unstable modes while the black line denotes the maximally unstable frequency for each value of the input pump power. b) The analogous of Fig. a) but obtained from numerical simulations. c) A comparison of the instability scaling for experimental, numerical and stability analysis predictions. Full numerical simulations agree well with the experiment while the stability analysis captures well the trend but overestimates slightly the instability frequency. The Floquet linear stability analysis for the Raman laser has been obtained following the procedure sketched in the previous chapter.

If we compare the scaling of the pulses repetition rate obtained in experiment (3.3c)), with that obtained from numerical simulations and with the prediction of the Floquet analysis, we observe that the Floquet analysis predicts an instability frequency that slightly overestimates the results from the experiment and from the numerical simulations. The discrepancy, though being a small one, is probably due to the fact that the linear stability analysis is indeed valid rigorously only in the linear regime of the instability when the spectral sidebands are still small compared to the homogeneous mode. When the modulation modes have amplitude comparable to that of the homogeneous mode than the linearized approach in general is not anymore correct and a nonlinear analysis is needed, nonlinear resonances could cause frequency shift of the

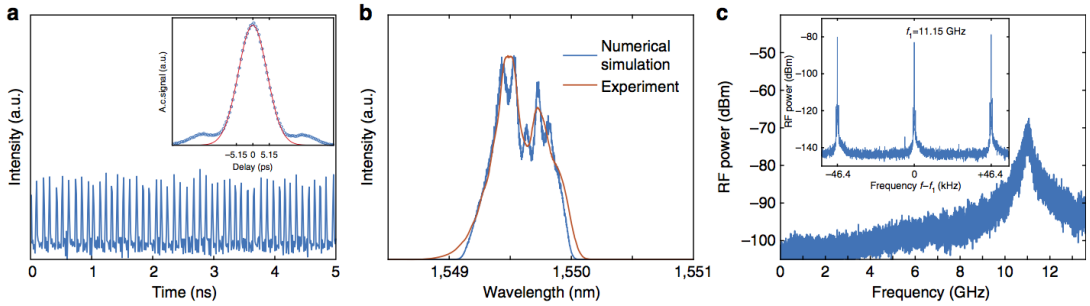

Figure 3.4: a) a pulse train recorded experimentally after the interaction with the right hand side FBG: in the inset the autocorrelation function of the single pulse shows a duration of about 9-10 ps at FWHM an it is well fitted by a Gaussian function close to the maximum. In b) the optical spectrum is depicted both for experiment and numerical simulations: there is a qualitative good agreement, despite the fact that in experiment some of the peaks observed numerically are averaged out. c) The RF spectrum shows a peak at around 11 GHz, the repetition rate of the pulses; in the inset neighbor excited cavity modes are highlighted.

modulation modes. Despite those limitations of the Floquet analysis we can still say that its predictions, despite being rigorously valid only in the linearized regime, are sufficiently accurate and informative about the behavior of the system in the nonlinear regime too. The inverse scaling of the instability frequency versus pump power is a distinctive feature of Faraday instabilities in normal dispersion regime, at least in a first approximation. Despite the fact that the Raman laser is described by complicated version of the generalised nonlinear Schrödinger equation we can still assume that the first mode excited mode by the Faraday instability obeys a scaling of the form:

$$\omega_{1Raman} \approx \frac{\pi}{L_f \sqrt{\beta_2 \gamma |A_s|^2}}. \tag{3.3}$$

where $|A_s|^2 \propto P_{in}$ being P_{in} the input pump power. We are hence justified to expect an inverse scaling of the instability frequency versus pump power.

As far as the breathing dynamics of the pulses is concerned: the pulses broaden substantially upon propagation in presence of gain, normal dispersion and nonlinear phase shift. This fact is observed with remarkably good agreement between experiment and numerical simulations (See Fig.3.5). It is also important to mention that the mode-locking regime achieved here can be most-likely described as quasi mode-locking or partial mode-locking since the cavity modes are periodically strongly damped in zig-zag fashion: the strong losses may put at risk the strict definition of cavity modes. But in any case it is also worth stressing that some form of strong phase coherence among

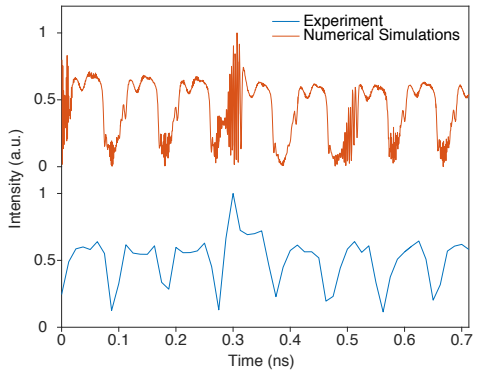

Figure 3.5: Pulses from the laser cavity just before the interaction with the gratings show the substantial broadening towards quasi-parabolic shape due to the combined effect of gain, normal dispersion and self-phase modulation. Good agreement between experimental results and numerical simulations is achieved.

the modes should exist, otherwise it would not possible to explain the regular pulse train observed.

3.3 Analysis of the coexisting instabilities

One may ask wether the phenomena observed are indeed caused by the periodic dispersion variation induced by the chirped gratings, instead of the dissipative modulation, as claimed before.

In order to understand which of the different modulations is responsible for the instability we can perform a study based on the Floquet linear stability analysis. Intuitively, since the dispersion is modulated at twice the spatial frequency of the dissipation we can expect it to excite a higher frequency instability tongue.

A first check can be done by computing the instability map, removing the chirp in the gratings (Fig.3.6 a)), in this case we don't observe any substantial difference with respect to the realistic experimental case depicted in Fig.3.3 a). As a second step we have considered non detuned chirped gratings. We can observe that the long-wavelength instability disappears and that only short wavelength (dispersive-Faraday) instability tongues survive (Fig.3.6b)). In this case the tongue due to dispersion modulation appears at around 30 GHz, close to it we see a lower frequency and weaker instability tongue. If the chirp is removed from the gratings we still see two instability tongues, one stronger at around 15 GHz the other one weaker around 30 GHz (Fig.3.6c)). Such instability is due to the periodic power variation seen by the signal and caused by the

external injection, which is taking place asymmetrically in the cavity (in correspondence to the first mirror). This last instability, is the object of a dedicated study presented in Chapter 5 and it is the equivalent for a laser of the boundary conditions induced modulation instability already studied theoretically and experimentally in externally driven passive fibre resonators [8, 41]. What happens in presence of chirped non detuned gratings (Fig.3.6b)) is that the the first excited dispersion modulation induced instability tongue overlaps with the second harmonic of the power-variation induced instability whose forcing takes place at half the frequency.

In case when dissipation only is modulated (Fig.3.6a)) a second harmonic instability tongue appears around 30 GHz. Such tongue overlaps with the first harmonic induced by dispersion modulation when both dispersion and dissipation are modulated (Fig.3.3 a)). It should also be noted that third harmonics are triggered too with both the chirped and the non chirped detuned gratings. It is important to stress that if the numerical simulations are performed with detuned unchirped gratings, pulses are observed without modifications as in the case of chirped detuned gratings; while non detuned but chirped gratings are not able to excite pulses. We can hence rule out the periodic dispersion variation as the pulse generating mechanism in the system studied here. It is left for future studies to understand if pulses from classical dispersive Faraday instability can be observed in a similar experimental configuration.

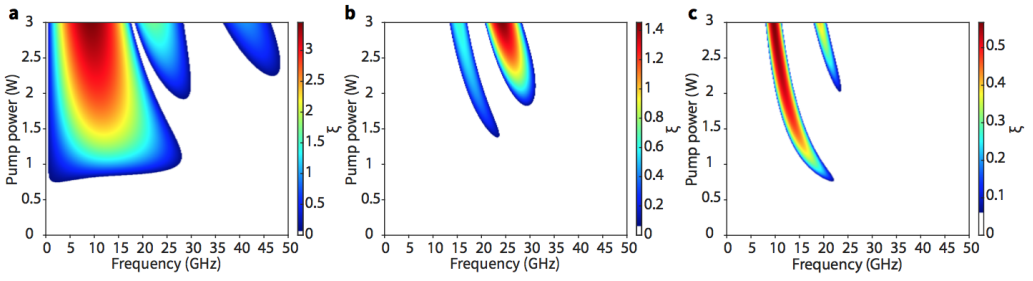

Figure 3.6: Instability spectrum dependence on pump power is plotted for different configurations: detuned and non chirped gratings a), non detuned but chirped gratings b) and nor detuned neither chirped gratings c). Apart from those variations, parameters used in the calculations are the same as those used in Fig.3.3 a).

Summarizing, the results presented in this Chapter demonstrate successfully the findings described in the previous Chapter in a realistic laser system, both theoretically and experimentally. Despite the fact that the system considered is described by a more complicated model, the dynamical equations have an underlying CGLE structure

and the laser operates in a regime where the gain, despite being not exactly uniform in space it can still be considered substantially distributed.

4 Faraday instability mode-locking with lumped amplification

4.1 Laser setup and mathematical model

In this Chapter a discussion on the flexibility and versatility of the dissipative Faraday instability induced mode-locking is presented, with particular emphasis to its implementation in fibre lasers with lumped amplification [42]. It is indeed an open scientific and engineering task understanding wether the dissipative Faraday instability could become a routinely used mode-locking technique for lasers or not. The previously discussed work on the Raman lasers constitutes a proof of principle of the concept and optimization should be performed in order to improve the quality of the mode-locking in that particular setup. It is however worth considering also different setups where such self-pulsing phenomena can be potentially achieved and practically used.

A first natural candidate setup is a fibre laser with lumped amplification, where the already existing and well developed rare-earths (Erbium and Ytterbium) amplifiers could be successfully employed.

Let us consider a ring cavity resonator where two long spans of passive normal dispersion fibres are alternated with two short active fibres which can be hence considered lumped. Before each amplifier a spectral filter is located. We consider the two spectral filters to have frequency detuned transmission profile where such detuning is needed to provide the periodic in space zig-zag in frequency modulation of spectral losses that initiates the Faraday instability. The filters have the following transmission profile:

$$f_{\pm}(\omega \pm \Delta\omega) = Te^{-\frac{(\omega \pm \Delta\omega)^4}{\sigma^4}} \tag{4.1}$$

where $\Delta\omega$ is the angular frequency detuning which is related as follows to the frequency detuning $\Delta\nu = \Delta\omega/(2\pi)$, while σ is the filter width. Note that the choice of the second order supergaussian shape is not crucial for obtaining the results, other orders could be chosen as well. The field spectrum after interacting with one of the lumped filters is given simply as a function of the input spectrum $\tilde{A}_{in}(\omega)$ and of the filter transmission function $f_{\pm}$ by $\tilde{A}_{out}(\omega) = f_{\pm}\tilde{A}_{in}(\omega)$. 4% of the power is lost from the cavity due to the presence of the output coupler.

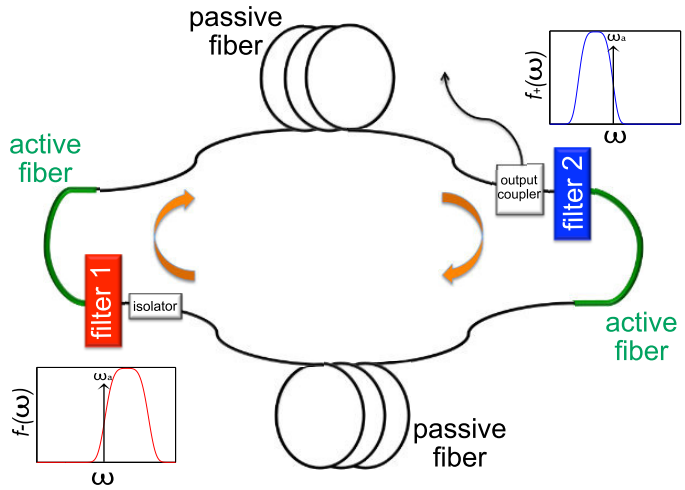

Figure 4.1: Laser setup; the unidirectional ring resonator consists of two normal dispersion passive fibres (in black) and of two active ones (in green) joined in alternate way. At the end of each passive fibre, spectral filters are located with transmissivity profile respectively positively/negatively detuned from the amplifiers frequency ω_a (indicated with black vertical arrows in the filter transmission function schematic).

A study of this setup through numerical simulations reveals indeed that self pulsing can be excited in such laser and that the generated pulse train can be stable. We have considered the following generalised NLSE to be the master model describing the dynamics of the electric field:

$$\frac{\partial A}{\partial z} = gA - \frac{\alpha}{2} + \left(\frac{1}{\Omega_g^2} - i\frac{\beta_2}{2}\right)\frac{\partial^2 A}{\partial t^2} + i\gamma|A|^2 A \tag{4.2}$$

where γ, α, β_2 denote the nonlinearity, losses and group velocity dispersion coefficients. The saturable gain reads $g = \frac{g_0}{1+\int |A|^2 dt/E_s}$, being g_0 the small signal gain and E_s the saturation energy ($g \neq 0$ only in the active fibre sections); the term proportional to Ω_g^{-2} in Eq.4.2 describes the effect of the finite gain bandwidth and is absent in the passive fibre sections.

4.2 Regular pulse train: stabilization and dispersion

The results depicted in Fig.4.2 show indeed both the stable dynamical evolution by means of spatio-temporal representation, as well as the different shape assumed by the pulses depending on the position in the cavity: before and after the filter and after the amplifier. A typical quasi-parabolic shape of the pulses after propagation in normal dispersion fibre is observed. The filters' detuning is crucial in determining

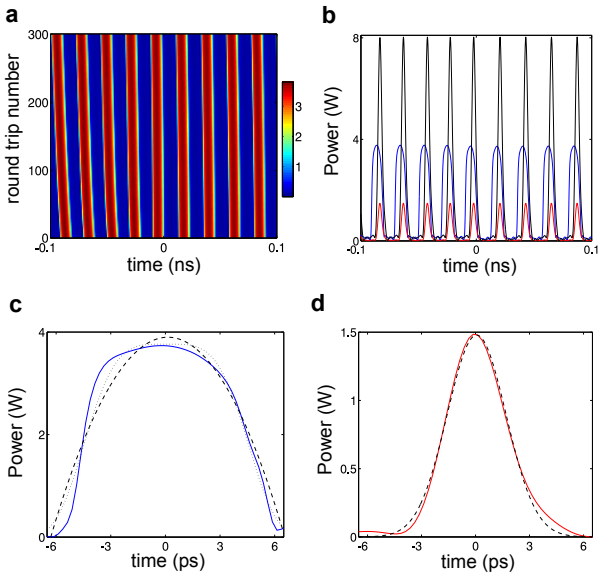

Figure 4.2: Spatio-temporal representation of a stable pulse train a): the power pictures are taken at every round trip before interaction with one of the spectral filters. In b) the pulse train is showed respectively before the interaction with the spectral filter (blue line), after the filter (red line) and after the amplifier (black line). c) A single pulse before the interaction with a spectral filter, parabolic and 2nd order Supergaussian fits are denoted with dashed and dotted lines respectively. d) A single pulse after the filter, a Gaussian fit is denoted with dashed line. Parameters used for both active and passive fibres are α =0.046 km^{-1}, while β_2=2 ps^2/km in the passive fibre and 65 ps^2/km in the amplifier and $\gamma = 1.2$ W^{-1}km^{-1} in the passive and 1 W^{-1}km^{-1} in the active fibre. Remaining parameters are $g_0 = 1011.3$ km^{-1}, $\Omega_g \approx 6$ THz, E_s=2 nJ, $\Delta\nu = 115$ GHz, $\sigma = 127.3$ GHz and $T = 1$.

the stability of the pulse train: a minimum detuning is needed in order to trigger the instability, however the resulting pulses could be unstable. Stabilization can be induced by a simple increment of the filters' detuning. The latter fact is illustrated in Fig.4.3 where a transition from a collision to a stable regime is obtained. It is important to stress that here the parabolic pulses are not wave-breaking free, since their propagation

occurs mainly in normal dispersion passive fibres where no gain is present, hence wave-breaking-free solutions are not available in such case and the pulses stability must be ensured by the filters action. Note also the fact that in Fig.4.3 a much larger value of the group velocity dispersion compared to Fig.4.2 has been used: this leads to a decreasing repetition rate according to the theory of parametric instabilities. The instability first excited mode has frequency:

$$\nu_p \propto \frac{1}{2L_f\sqrt{\beta_2\gamma\langle|A|^2\rangle}} \tag{4.3}$$

being L_f the period of the spatial forcing (total cavity length) and $\langle|A|^2\rangle$ is the power averaged along the laser cavity. Eq.4.3 is valid for a laser with distributed amplification but it results useful in estimating the dependence on the fibre parameters in the lumped case too.

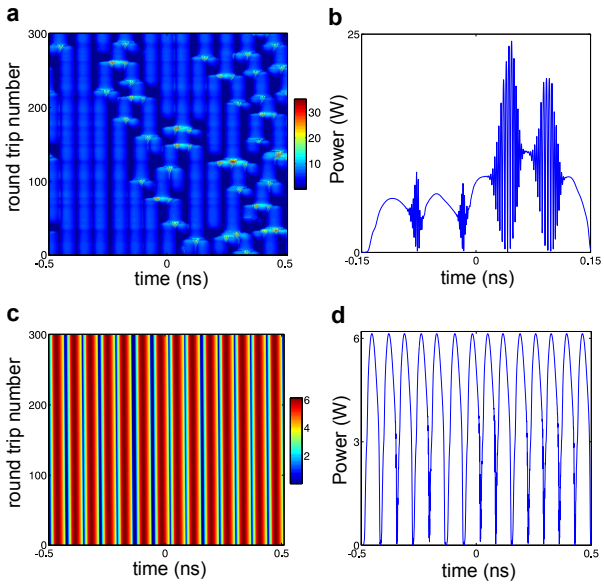

Figure 4.3: a) The spatio-temporal dynamics in the collision regime; b) collision among pulses (zoom from panel a)). c) The spatio-temporal dynamics of pulses stabilized by a detuning increment. Parameters in a) and b) are as in Fig. 4.2 except for β_2=28 ps^2/km in the passive fibre, while $\Delta\nu = 95.5$ GHz. In c) and d) parameters are identical as in a) and b), except for $\Delta\nu = 102.6$ GHz.

4.3 The transition from regular pulse train to random self-pulsing

It is important to contextualize the results discussed here and in the previous Chapter, comparing them with previous studies about lasers with detuned spectral filters. Two normal dispersion gain fibres each one followed by a spectral filter (being the two filters reflectivity profiles detuned in frequency) constitute a device called Mamyshev regenerator [43]. It has been shown by Pitois and collaborators that a series of concatenated Mamyshev regenerators can generate a train of random pulses starting from a highly incoherent light wave [44]. Later on, other authors observed experimentally the generation of random pulses in the chain of concatenated Mamyshev regenerators [45]. More recently the authors of a numerical study on a similar setup, called this laser source: *regenerative similariton laser* [46]. There seems to be a contradiction between the phenomenology described in this Chapter and the one described in [45, 46]. However the contradiction is only an apparent one. The random pulses regime bifurcates from the Faraday instability one by simply increasing the filters' detuning. The results are shown in Fig.4.4. In this sense we can ascribe the regular pulsation regime to the dissipative Faraday instability that occurs at moderate filters' detuning, while the random pulses occur in what we can call the "Mamyshev" regime corresponding to large filter detuning. In principle both regimes can be observed in the same experimental setup using the filters' detuning as control parameter. To complete the discussion it is

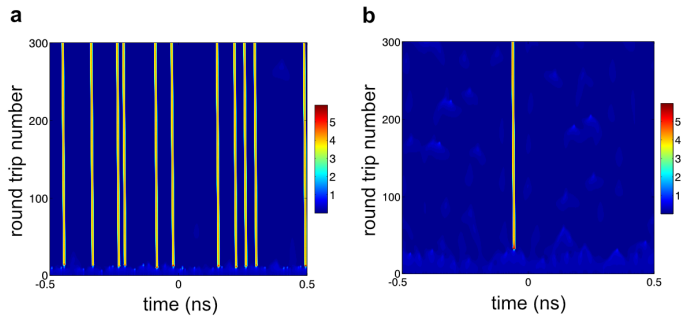

Figure 4.4: Spatio-temporal representation of the random operation regime: the intracavity power is plotted for $\Delta\nu = 124.5$ GHz in a) and $\Delta\nu = 125.4$ in GHz b) showing the random operation regime. Remaining parameters are as in Fig.4.2.

also worth remembering that a laser with detuned spectral filters can support a single stable, high peak power pulse. This behavior has been proposed in the same work by

Pitois and collaborators [44]. Two recent papers have reported on the experimental observation of such single pulse regime [47, 48]. The authors of [48] have called such laser *Mamyshev oscillator* and have demonstrated that in the stationary state the laser emits a stable pulse with peak power of the order of the Mega Watt. It is important to stress that this laser operates with a repetition rate of the order of the MHz given by the inverse of the cavity round trip time and the pulsed operational mode is not self-starting; furthermore, unlike the regime presented in this Chapter, it requires an appropriate seeding of the input field. Summarizing, the dissipative Faraday instability induced self-pulsing can be observed in all-normal dispersion fibre lasers with lumped amplification too. This fact opens potentially the way to the design of all-normal dispersion lasers, harmonically mode-locked with a repetition rate of some tens of GHz where the amplification is achieved by means of lumped gain media. This fact is a complete novelty for all-normal dispersion fibre lasers.

Another important result presented in this Chapter is the established connection between the regular and random self-pulsing regimes that can be achieved in fibre lasers with detuned filters. This fact has been shown to be due to the degree of filters' detuning, which in the extreme regime leads to the single pulse Mamyshev oscillator. A next natural step along this research line will be to experimentally study the self-pulsing dynamics excited by the dissipative Faraday instability in fibre lasers with lumped amplification in order to have more details about the practical feasibility and limitations. Furthermore it is worth stressing the practical value of the this peculiar technique for the generation of pulses: it could be particularly useful to build pulsed lasers operating at wavelengths where semiconductor based saturable absorbers are not available for instance in the mid-infrared region of the electromagnetic spectrum.

5 Gain through losses: modulation instabilities and patterns

5.1 The concept of gain through losses

There is a widespread and intuitive believe that dissipation plays a stabilizing role in dynamical systems, for instance reducing noise and hence increasing the threshold of modulation instabilities. This believe is indeed well motivated by some paradigmatic examples. Karlsson has for instance shown that the Benjamin-Feir instability gain in the nonlinear Schrödinger equation with frequency independent losses the gain is reduced for unstable modes, while the gain spectrum can slightly broaden proportionally to the amount of applied losses [49]. Another example in this direction is the study that shows how losses can suppress the onset of the coherent Risken-Nummedal-Graham-Haken instability in lasers [50].

What this Chapter wants to demonstrate is that dissipation, very counterintuitively, can destabilize homogenous solutions of nonlinear systems, provided that some specific conditions are satisfied. Here we will even simplify the action of dissipation, reducing furthermore the complexity of the (already simple) periodic zigzag modulation scheme discussed in Chapters 2, 3 and 4.

The topic we are considering here is something substantially different from what has been up to now understood about dissipation induced instabilities, both in nonlinear optics and other fields of physics.

Dissipation induced instabilities have been studied especially in classical mechanics where friction or viscosity forces cause instability of certain otherwise stationary states. An extensive review of such dissipation induced instabilities in classical mechanics has been written by Krechetnikov and Mardsen [51]. Some paradigmatic examples in this sense are the Lagrangian top that interrupts its rotation and "falls down" in presence

of friction, or a rocket that deviates from its orbit due to loss of rotational energy. In nonlinear optics one could be tempted to say that dissipation induced instabilities occur for instance by modulating the cavity losses as in case of Q-switching or active mode-locking with amplitude modulation. In this case of course the laser's off-solution and the continuous wave solution become unstable and pulses are formed in the resonator. Periodic modulation of spectral losses is also able to excite parametric instabilities and indeed some of those instabilities have been discussed in previous Chapters of this thesis.

However we are concerned, in the present Chapter, with a different concept of dissipation induced modulation instabilities, e.g. with inststabilities induced by unmodulated, unbalanced spectral losses for signal and idler waves in some nonlinear wave equations relevant to describe very popular optical systems with a wealth of applications both in fundamental and applied research. We generalise the results obtained for the first time by Tanemura and co-authors [52]. Using a 3-waves model for coupled pump, signal and idler they showed that in a normal dispersion fibre, the CW solution is unstable with respect to modulation modes if losses are applied selectively on the signal or on the idler wave. They also realized a first proof-of-principle experiment by injecting a counterpropagating probe field, shifted in frequency from the pump by an amount corresponding to the Brillouin shift ($\sim$ 9 GHz). Such probe field stimulates Brillouin scattering inducing the modulation instability of the CW solution: a signal at frequency symmetrically located with respect to the pump frequency experiences amplification.

We will show that under certain conditions, otherwise stable nonlinear optical systems could develop a modulation instability induced by spectrally unbalanced losses in a variety of nonlinear optical systems hence generalizing the original results by Tanemura and co-authors and highlighting explicitly various potential applications. The results discussed here are very general and it is most likely that similar effects could be easily predicted about (and observed in) a wealth of other nonlinear systems described by the most diverse evolution equations, even outside nonlinear optics. We define the amplification dynamics where damped mode experience amplification in virtue of the damping acting on them as *gain through losses* (GTL) process.

Conceptually we aim at considering an optical fibre with a strong frequency dependent attenuation such that given an input CW radiation field, having a quasi-monochromatic spectrum, the output will ideally result in an amplification of spectral modes where strong dissipation is present (signal) and of its symmetric ones with respect to the pump frequency (idler). The concept is summarized schematically in Fig.5.1.

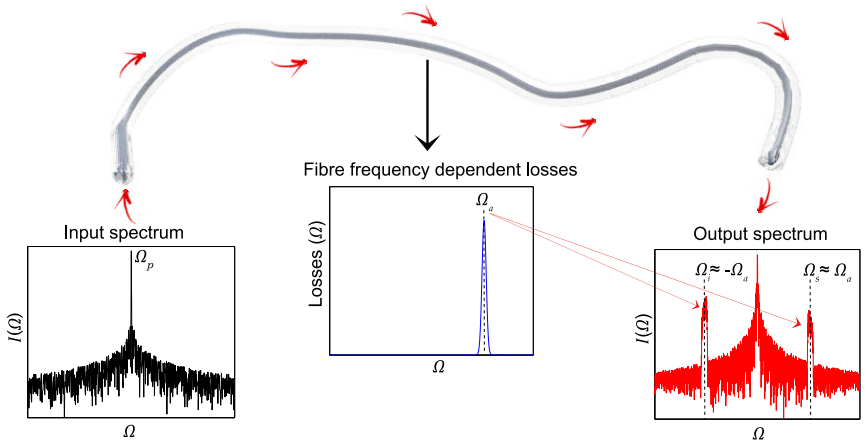

Figure 5.1: The concept of the gain through losses is summarized schematically here: a CW radiation at frequency Ω_p is injected in an optical fibre whose attenuation profile depends on the frequency and is maximum around $\Omega = \Omega_a$ in such a way that losses are not symmetric for signal and idler waves. At the fibre output the field spectrum develops two sidebands one centered at the frequency where losses are strong ($\Omega_s \approx \Omega_a$) the other one located around the symmetric mode $\Omega_i \approx -\Omega_a$ (idler).

Let's consider, without loss of generality, those filters to be complex lorentzian functions, lorentzian complex susceptibilities satisfy Kramers-Kronig relations and arise naturally as the characterizing response function of two-level atomic systems. We can indeed consider the propagation of the electric field in an optical fibre which has been doped with a set of identical homogeneously broadened two-level systems uniformly distributed along the spatial coordinate. We derive now the evolution equation for the electric field from first principles, i.e. from the Arecchi-Bonifacio (Maxwell-Bloch) equations arising from the density matrix describing the interaction of the electromagnetic field with an atomic two-level system.

5.2 The nonlinear Schrödinger equation coupled to a two-level-system

We start from the Maxwell equations in absence of free charges and current density and material magnetization, for the electric field $\vec{E}$ and the magnetic field $\vec{H} = \vec{B}/\mu_0$.

$$\nabla \times \vec{E} = -\mu_0 \frac{\partial \vec{H}}{\partial t} \tag{5.1}$$

$$\nabla \cdot \vec{H} = 0 \tag{5.2}$$

$$\nabla \cdot \vec{D} = 0 \tag{5.3}$$

$$\nabla \times \vec{H} = \frac{\partial \vec{D}}{\partial t} \tag{5.4}$$

The displacement field $\vec{D}$ and the electric field $\vec{E}$ are related by means of the constitutive relation to the medium polarization density $\vec{P}$:

$$\vec{D} = \epsilon_0 \vec{E} + \vec{P}. \tag{5.5}$$

By taking the rotor of Eq.5.1, using 5.3, 5.4 and 5.5, remembering the operator's identity $\nabla \times (\nabla \times) = \nabla(\nabla \cdot) - \nabla^2$ and the link between the vacuum permittivity ϵ_0, the vacuum permeability μ_0 and the speed of light c, $\epsilon_0 \mu_0 = 1/c^2$; we have the following wave equation:

$$\nabla^2 \vec{E} - \nabla(\nabla \cdot \vec{E}) - \frac{1}{c^2} \frac{\partial^2 \vec{E}}{\partial t^2} = \frac{1}{\epsilon_0 c^2} \frac{\partial^2 \vec{P}}{\partial t^2}. \tag{5.6}$$

It is now worth to express the three distinct contributions to the medium polarization density:

$$\vec{P} = \vec{P}_{BL} + \vec{P}_{BNL} + \vec{P}_{2LS}. \tag{5.7}$$

$\vec{P}_{BL}$ and $\vec{P}_{BNL}$ describe respectively the linear and nonlinear polarization of the fibre background material (the material of which the fibre core is made), while $\vec{P}_{2LS}$ is the contribution coming from the two-level system (2LS) coupled to the fibre. We can

assume for instance that we have doped our fibre with some atoms or ions which can be modeled as an ensemble of two level systems. The remaining contributions to the medium polarization can be expressed in term of the linear and nonlinear susceptibilities χ_L and $\chi^{(3)}$ in the following way to the temporal response function of the material R_L and R_{NL} [53] (the ˜ denotes Fourier transformed fields):

$$\vec{P}_{BL}(\vec{r},t) = \epsilon_0 \int_0^\infty dt_1 R_L(t_1)\vec{E}(\vec{r},t-t_1) \tag{5.8}$$

$$\chi_L(\omega) = \int_0^\infty dt' R_L(t_1) e^{i\omega t_1} \tag{5.9}$$

$$\begin{aligned}\vec{P}_{BNL}(\vec{r},t) &= \epsilon_0 \int_0^\infty \int_0^\infty \int_0^\infty dt_1 dt_2 dt_3 R_{NL}(t_1,t_2,t_3)\cdot \\ &\quad \vec{E}(\vec{r},t-t_1)\vec{E}(\vec{r},t-t_2)\vec{E}(\vec{r},t-t_3) \qquad (5.10)\\ \chi^{(3)}(\omega) &= \int_0^\infty dt_1 \int_0^\infty dt_2 \int_0^\infty dt_3 R_{NL}(t_1,t_2,t_3) e^{i(\omega_1 t_1+\omega_2 t_2+\omega_3 t_3)}. \qquad (5.11)\end{aligned}$$

We now consider the electric field to be a plane wave having a slowly varying (with respect to carrier frequency ω_0 in time and wavenumber k_0 in space) envelope $E_0(z,t)$, propagating along the z-coordinate (we omit the unit vector indicating the polarization direction assuming that the field is linearly polarized):

$$\vec{E}(\vec{r},t) = \frac{1}{2}\left[E_0(z,t)e^{i(k_0 z-\omega_0 t)} + c.c.\right]. \tag{5.12}$$

This assumption allows to neglect the field divergence in Eq.5.6, which by the way can be shown to be negligible in the slowly varying envelope approximation (SVEA) also if the field is not a plane wave (See [17] for more details). In the Fourier domain the field can be written as:

$$\begin{aligned}\tilde{E}(z,\omega) &= \frac{1}{2}\left[\tilde{E}_0(z,\omega-\omega_0)e^{ik_0 z} + \tilde{E}_0(z,\omega+\omega_0)e^{-ik_0 z}\right] \approx \\ &\approx \frac{1}{2}\left[\tilde{E}_0(z,\omega-\omega_0)\right]e^{ik_0 z} = \frac{1}{2}\tilde{E}_0(z,\omega-\omega_0)e^{ik_0 z} \qquad (5.13)\end{aligned}$$

where $\tilde{E}_0(z,\omega-\omega_0) = \tilde{E}_0(z,\omega)e^{-i\omega_0 t}$ and $\tilde{E}_0(z,\omega+\omega_0) = \tilde{E}_0(z,\omega)e^{+i\omega_0 t}$. Terms proportional to $\omega+\omega_0$ are rapidly oscillating and hence can be dropped [53]. Consistently with Eq.5.13 we assume that also the medium polarization obeys the SVEA and hence

reads:

$$\vec{P}(\vec{r},t) = \frac{1}{2}\left[P_0(z,t)e^{i(k_0 z-\omega_0 t)} + c.c.\right], \tag{5.14}$$

where $P_0(z,t)$ is the slowly varying envelope. In the Fourier domain:

$$\begin{aligned}\tilde{P}(z,\omega) &= \frac{1}{2}\left[\tilde{P}_0(z,\omega-\omega_0)e^{ik_0 z} + \tilde{P}_0(z,\omega+\omega_0)e^{-ik_0 z}\right] \approx \\ &\approx \frac{1}{2}\left[\tilde{P}_0(z,\omega-\omega_0)e^{ik_0 z}\right] = \frac{1}{2}\tilde{P}_0(z,\omega-\omega_0)e^{ik_0 z}.\end{aligned} \tag{5.15}$$

By assuming that the nonlinear medium response is instantaneous, then for the forward propagating electric field we have:

$$P_{0BNL} = \frac{3}{4}\chi^{(3)}|E_0|^2 E_0 \exp[i(k_0 z - \omega t)]. \tag{5.16}$$

Then we recast Eq.5.6 which we rewrite here after neglecting the divergence (as said before):

$$\nabla^2\vec{E} - \frac{1}{c^2}\frac{\partial^2\vec{E}}{\partial t^2} = \frac{1}{\epsilon_0 c^2}\frac{\partial^2\vec{P}}{\partial t^2} \tag{5.17}$$

into a form

$$\begin{aligned}\nabla^2\vec{\tilde{E}}(\vec{r},\omega) + \left(\frac{\omega^2}{c^2} + \frac{\omega^2}{c^2}\chi_B(\omega)\right)\vec{\tilde{E}}(\vec{r},\omega) &= -\frac{\omega_0^2}{\epsilon_0 c^2}\vec{\tilde{P}}_{0-2LS} \\ \nabla^2\vec{\tilde{E}}(\vec{r},\omega) + k_B(\omega)^2\vec{\tilde{E}}(\vec{r},\omega) &= -\frac{\omega_0^2}{\epsilon_0 c^2}\vec{\tilde{P}}_{0-2LS}\end{aligned} \tag{5.18}$$

where $\chi_B(\omega) = \chi_{BL}(\omega) + \chi_{BNL}(\omega)$ accounts for the material "background" response to the electric field. A "background" dielectric constant can be defined as $\epsilon_B(\omega) = 1 + \chi_B(\omega)$ similarly we can define a frequency dependent wavenumber $k_B(\omega) = \omega/c\sqrt{\epsilon_B(\omega)}$ and a frequency dependent refractive index $n_B(\omega) = \sqrt{\epsilon_B}(\omega)$.

It may look arbitrary the fact that we assume that also the nonlinear response of the material carrying contributions from $\chi_{BNL}(\omega)$ provide a response proportional to $\vec{\tilde{E}}(\omega)$. Concerning the $\chi_{BNL}(\omega)$ contribution, we know the effect in time domain (see Eq. 5.16) hence in frequency domain we can express $\chi_{BNL}(\omega)$ as a convolution operator acting

on $\vec{\tilde{E}}(\omega)$. We will keep such an implicit definition since then Eq.5.18 will be rewritten in the time domain. To be specific we can determine k_{BNL} in the following way taking into account the intensity dependent refractive index. The propagation constant reads $\omega n_B(\omega)/c = \omega\sqrt{\epsilon_B}(\omega)/c$. We have that, considering the $\chi^{(3)}$ effects perturbatively with respect to the background linear dispersive effects:

$$\begin{aligned}
&\sqrt{\epsilon_B} = \sqrt{1+\chi_{BL}+\frac{3}{4}\chi^{(3)}|E_0|^2} = \sqrt{1+\chi_{BL}}\sqrt{1+\frac{3\chi^{(3)}|E_0|^2}{4(1+\chi_{BL})}} \approx \\
&\approx \sqrt{1+\chi_{BL}}\left(1+\frac{3\chi^{(3)}|E_0|^2}{8(1+\chi_{BL})}\right) = \\
&= n_{BL}+\frac{3\chi^{(3)}|E_0|^2}{8n_{BL}(\omega)}
\end{aligned} \tag{5.19}$$

hence the propagation constant reads:

$$\begin{aligned}
&k_B = k_{BL}+k_{BNL} = \frac{\omega n_{BL}(\omega)}{c}+\frac{\omega}{c}\frac{3\chi^{(3)}|E_0|^2}{8} \approx \\
&\approx \frac{\omega n_{BL}(\omega)}{c}+\frac{\omega_0}{c}\frac{3\chi^{(3)}|E_0|^2}{8}+i\frac{\alpha}{2}
\end{aligned} \tag{5.20}$$

where we have assumed, consistently with the perturbative approach, that the nonlinear contribution to the propagation constant can be considered constant, and depending only on the carrier frequency ω_0. We have also added phenomenologically the frequency independent damping damping α. Furthermore we recall that whenever the expression k_{BNL} appears multiplied, in the frequency domain, by the field Fourier transform one should consider such product as a convolution of both terms in frequency, however we leave it tacitly assumed, in order to have a more compact notation. At the end of the derivation, the evolution equation will be expressed in time domain and in this case we will have a simple product between the field and k_{BNL} defined as a function of time.

We see that the SVEA and plane wave approximation allow to simplify the evolution equation for the electric field (Eq.5.18). While $\nabla_\perp^2 = \partial_x^2+\partial_y^2$ acting on the field gives "zero" due to plane wave approximation, the SVEA allows to approximate

$$\frac{\partial^2 E_0(z,t)e^{i(k_0 z-\omega_0 t)}}{\partial z^2} \approx \left[2ik_0\frac{\partial E_0(z,t)}{\partial z}-k_0^2 E_0(z,t)\right]e^{i(k_0 z-\omega_0 t)} \tag{5.21}$$

or analogously in frequency domain:

$$\frac{\partial^2 \tilde{E}_0(z,\omega-\omega_0)}{\partial z^2} \approx \left[2ik_0 \frac{\partial \tilde{E}_0(z,\omega-\omega_0)}{\partial z} - k_0^2 \tilde{E}_0(z,\omega-\omega_0)\right] e^{ik_0 z}; \tag{5.22}$$

and the "nonlinear" Helmholtz equation (Eq.5.18) after dividing left hand side and right hand side by $e^{i(k_0 z-\omega_0 t)}$ reads:

$$\begin{aligned} &2ik_0 \frac{\partial \tilde{E}_0(z,\omega-\omega_0)}{\partial z} - k_0^2 \tilde{E}_0(z,\omega-\omega_0) + k_B(\omega)^2 \tilde{E}_0(z,\omega-\omega_0) = \\ &= -\frac{\omega_0^2}{\epsilon_0 c^2} \tilde{P}_{0-2LS}(z,\omega-\omega_0). \end{aligned} \tag{5.23}$$

Assuming that in a perturbative approximation the actual wavenumber $k(\omega)$ differs only slightly from the carrier wavenumber k_0, we can write $k_B(\omega)^2 - k_0^2 \approx 2k_0(k_B(\omega) - k_0)$ and hence we arrive at:

$$i\frac{\partial \tilde{E}_0(z,\omega-\omega_0)}{\partial z} + (k_B(\omega)-k_0)\tilde{E}_0(z,\omega-\omega_0) = -\frac{\omega_0^2}{2k_0\epsilon_0 c^2}\tilde{P}_{0-2LS}(z,\omega-\omega_0). \tag{5.24}$$

Indeed, mathematically, the SVEA means assuming that for a given field A $(|\partial_t A|) << \omega|A|$ and $(|\partial_x A|) << k|A|$. Before determining explicitly the wavenumber $k_B(\omega)$ we calculate now $\tilde{P}_{2LS}(\omega-\omega_0)$.

The propagation equation for the electric field is coupled via $\vec{P}_{2LS}$ to the equations, which describe respectively the population inversion and the polarization of the two-level system. Let's define the transition frequency of the two-level system

$$\omega_a = \frac{E_1 - E_2}{\hbar} \tag{5.25}$$

where E_1 and E_2 are respectively the energies of the upper and lower state and $\hbar$ is the Planck's constant divided by 2π. Starting from the interaction hamiltonian in the dipole approximation it is possible to write down the Liouville-Von Neumann equation for the density operator ρ describing the temporal evolution of the two-level system interacting with an external electric field, a two-by-two matrix whose diagonal elements describe respectively the population of the upper and lower state while the off-diagonal ones describe the coherence, i.e. the average polarization of the atomic population which oscillates coherently with the electric field. It is assumed that the atomic dipoles get the

spatial dependence of the electric field interacting with them and oscillate at the same frequency. Consistently with the derivation of the NLSE the electric field is assumed to be a quasi monochromatic plane wave having an envelope which varies in time and space much more slowly than its carrier wave. Under the plane wave approximation, the slowly varying envelope approximation and the rotating-wave approximation which consists in neglect rapidly varying material terms that oscillate much faster then the carrier frequency of the electric field slowly varying envelope, the equations governing the matter dynamical evolution read (see Appendix for more details):

$$\frac{\partial r}{\partial t} = -i\delta r - \frac{i}{2}\Omega r_3 - \gamma_\perp r \tag{5.26}$$

$$\frac{\partial r_3}{\partial t} = i(\Omega r^* - \Omega^* r) - \gamma_{||}(r_3 - \sigma). \tag{5.27}$$

The actual atomic polarization describing the density of dipoles oscillating in phase with the field reads in reality $P_{2LS} = 2Ndr(z,t)$ where N is the number of atoms per unit volume. Similarly $r_3 N$ has the meaning of population inversion per unit volume and $\delta = \omega_a - \omega_0$ is a detuning between the atomic and the electric field frequency ω_0. $\Omega = dE_0(z,t)/\hbar$ is the so called Rabi frequency which is indeed proportional to the electric field slowly varying envelope $E_0(z,t)$ times the dipole moment of the atomic transition d and divided by $\hbar$. $\gamma_{||}$ is the population inversion decay rate, $\gamma_\perp$ is the dipoles dephasing rate, which determines the HWHM of the atomic transition line. The non dimensional parameter σ, can assume values between 1 and -1. In case of the two level medium acting as *absorber* (which will be the case we are interested in) $\sigma \approx -1$, while if the two-level medium acts as an *amplifier* σ assumes values between 0 and 1.

We leave for the moment the equations for the matter fields expressed in such a compact form, but later on in the derivation we will make the notation coherent to the classic NLSE one. It is important to stress that Eq.5.26 and Eq.5.27 are obtained within approximations (the SVEA, the rotating wave approximation and the plane wave approximation) which are fully consistent with the assumptions which are made to derive the NLSE. The exact details of their derivation from the Liouville-Von Neumann equation can be found in [16, 53] or in other classical textbooks or, as mentioned before, in the Appendix.

We proceed now to obtain $\chi_{2LS}(\omega)$. Apart for very short transient dynamics where coherent exchange of energy between the field and the two-level atoms, atomic polarization and inversion relax to an equilibrium value [16, 54]. We study this equilibrium state by setting $\partial_t r = \partial_t r_3 = 0$. From Eqs.5.26 and 5.27 we obtain the stationary solution:

$$r_{3s} = \frac{\sigma(1+\Delta^2)}{1+\Delta^2+|F|^2} \approx \sigma = -1 \tag{5.28}$$

where $F = \Omega/\sqrt{\gamma_{||}\gamma_{\perp}}$, $\Delta = \delta/\gamma_{\perp} = (\omega_a - \omega_0)/\gamma_{\perp}$ is the normalized detuning and the limit $1 + \Delta^2 << |F|^2$ has been taken. Note that within this approximation we neglect saturation of the two-level system, however since we aim to describe the effect of the losses on weak sidebands and not on the strong pump field, the approximation is well justified and allows considerable simplifications in the stability analysis.
From Eq.**??** and recalling the relation $2Ndr = P_{0-2LS}$ we obtain multiplying left and right by $2Nd$:

$$\frac{\partial P_{0-2LS}}{\partial t} = -i\delta P_{0-2LS} - iNd\Omega\sigma - \gamma_{\perp} P_{0-2LS} \tag{5.29}$$

I recall now that according to the SVEA we have the following Fourier transform relation:

$$P_{0-2LS}(z,t) = \frac{1}{2\pi}\int_{-\infty}^{+\infty} d(\omega-\omega_0) e^{-i(\omega-\omega_0)t} \tilde{P}_{0-2LS}(z, \omega-\omega_0). \tag{5.30}$$

In the Fourier domain and dividing left and right by $\gamma_{\perp}$ Eq.5.30 reads:

$$-\frac{i\,(\omega-\omega_0)}{\gamma_{\perp}}\tilde{P}_{0-2LS} = -i\Delta\tilde{P}_{0-2LS} - i\frac{Nd\sigma}{\gamma_{\perp}}\tilde{\Omega} - \tilde{P}_{0-2LS}. \tag{5.31}$$

Solving Eq.5.31 with respect to $\tilde{P}_{0-2LS}$ and recalling the definition of $\Omega(z,t)$ in terms of $E_0(z,t)$ yields:

$$\tilde{P}_{0-2LS}(\omega-\omega_0) = -i\frac{Nd^2\sigma}{\hbar\gamma_{\perp}}\frac{\gamma_{\perp}}{\gamma_{\perp}+i(\omega_a-\omega)}\tilde{E}_0(\omega-\omega_0). \tag{5.32}$$

Eq.5.32 can be rewritten more conveniently as a function of the two "frequency shifts":

$$\Omega = (\omega - \omega_0) \tag{5.33}$$

$$\Omega_a = (\omega_a - \omega_0) \tag{5.34}$$

as:

$$\tilde{P}_{0-2LS}(\Omega) = -i\frac{Nd^2\sigma}{\hbar\gamma_\perp}\frac{\gamma_\perp}{\gamma_\perp + i(\Omega_a - \Omega)}\tilde{E}_0(\Omega). \tag{5.35}$$

We substitute now Eq.5.32 into Eq.5.24 which becomes now

$$\frac{\partial\tilde{E}_0(z,\Omega)}{\partial z} = i(k_{BL}(\omega) + k_{BNL} - k_0)\tilde{E}_0(z,\Omega) - \frac{\omega_0^2 Nd^2}{2k_0\epsilon_0 c^2\hbar\gamma_\perp}\chi_{2LS}(\Omega)\tilde{E}_0(z,\Omega) \tag{5.36}$$

where we have recalled that $\sigma \approx -1$ and split $k_B(\omega)$ into its linear frequency dependent part $k(\omega)_{BL}$ and the Kerr contribution k_{BNL}which we assume realistically to be independent on frequency over the field spectrum considered. We also define a coupling parameter between the electric field and the two-level system

$$g = \frac{\omega_0^2 Nd^2}{2k_0\epsilon_0 c^2\hbar\gamma_\perp} \tag{5.37}$$

and a susceptibility for the two-level system:

$$\begin{aligned}\chi_{2LS}(\Omega) &= \frac{\gamma_\perp}{\gamma_\perp + i(\Omega_a - \Omega)} = Re(\chi_{2LS}(\Omega)) + iIm(\chi_{2LS}(\Omega)) = \\ &= \frac{\gamma_\perp^2}{\gamma_\perp^2 + (\Omega_a - \Omega)^2} - i\frac{(\Omega_a - \Omega)\gamma_\perp^2}{\gamma_\perp^2 + (\Omega_a - \Omega)^2}.\end{aligned} \tag{5.38}$$

We observe that the two level system gives both a dispersive and a dissipative contribution to the field. Absorption takes place in a frequencies range of FWHM given by $2\gamma_\perp$ in the vicinity of Ω_a (ω_a in terms of absolute frequency) with a strength g. Dispersion and group velocity of the wave packet are also affected and are described by the imaginary part of the susceptibility.

We now expand $k_{BL}(\omega)$ in Taylor series around the carrier frequency ω_0:

$$k_{BL}(\omega) \approx k_0 + (\omega - \omega_0)\left(\frac{\partial k_{BL}(\omega)}{\partial \omega}\right)_{\omega=\omega_0} + (\omega - \omega_0)^2 \frac{1}{2}\left(\frac{\partial^2 k_{BL}(\omega)}{\partial \omega^2}\right)_{\omega=\omega_0}. \quad (5.39)$$

The coefficient at the first order of the expansion is the inverse of the group velocity (v_g) of the wavepacket

$$\beta_1 = \left(\frac{\partial k_{BL}(\omega)}{\partial \omega}\right)_{\omega=\omega_0} = \frac{1}{v_g} \quad (5.40)$$

while the coefficient at the second order of the expansion is the group velocity dispersion

$$\beta_2 = \left(\frac{\partial^2 k_{BL}(\omega)}{\partial \omega^2}\right)_{\omega=\omega_0}. \quad (5.41)$$

Taking the inverse Fourier transform of Eq.5.36 and taking into account Eqs.5.20,5.38 and 5.39 we obtain the evolution equation:

$$\begin{aligned} &\frac{\partial E_0(z,t)}{\partial z} + \frac{1}{v_g}\frac{\partial E_0(z,t)}{\partial t} = \quad (5.42)\\ &= -i\frac{\beta_2}{2}\frac{\partial^2 E_0(z,t)}{\partial t^2} + i\gamma|E_0(z,t)|^2 E_0(z,t) - g\mathcal{F}^{-1}\left\{E_0(z,\Omega)\chi_{2LS}(\Omega)\right\} - \frac{\alpha}{2}E_0(z,t) \end{aligned}$$

where we leave the term responsible for the coupling with the two-level system written implicitly as a function of the inverse Fourier transform operator $\mathcal{F}^{-1} = (2\pi)^{-1}\int_{-\infty}^{+\infty} d\Omega e^{-i\Omega\tau}$ and the coefficient $\gamma = \frac{\omega_0}{c}\frac{3\chi^{(3)}}{8n_{BL}(\omega_0)}$ describes the Kerr nonlinearity.

By performing a change of variable we can consider the evolution of the electric field in a reference frame co-moving with the field itself and traveling at velocity v_g. We introduce the retarded time

$$\tau = t - \frac{z}{v_g} \quad (5.43)$$

a new spatial variable $z' = z$ and a new field $A(z', \tau)$ which depends on the new

variables. According to the chain rule we have that:

$$\frac{\partial E_0(z,t)}{\partial z} = \frac{\partial A(z',\tau)}{\partial z'}\frac{\partial z'}{\partial z} + \frac{\partial A(z',\tau)}{\partial \tau}\frac{\partial \tau}{\partial z} = \frac{\partial A(z',\tau)}{\partial z'} - \frac{1}{v_g}\frac{\partial A(z',\tau)}{\partial \tau}$$
$$\frac{\partial E_0(z,t)}{\partial t} = \frac{\partial A(z',\tau)}{\partial z'}\frac{\partial z'}{\partial t} + \frac{\partial A(z',\tau)}{\partial \tau}\frac{\partial \tau}{\partial t} = \frac{\partial A(z',\tau)}{\partial \tau} = \frac{\partial A(z',\tau)}{\partial \tau}. \quad (5.44)$$

In this way, removing the primes on the spatial variable in order not to overburden the notation, the evolution equation finally reads:

$$\frac{\partial A}{\partial z} = -i\frac{\beta_2}{2}\frac{\partial^2 A}{\partial \tau^2} + i\gamma|A|^2 A - g\mathcal{F}^{-1}\left\{A(\Omega)\chi_{2LS}(\Omega)\right\} - \frac{\alpha}{2}A. \quad (5.45)$$

5.3 Gain through losses in a passive fibre: the amplifier

Let's consider the evolution equation

$$\frac{\partial A}{\partial z} = -i\frac{\beta_2}{2}\frac{\partial^2 A}{\partial \tau^2} + i\gamma|A|^2 A - \theta \star A \quad (5.46)$$

where $\theta = \mathcal{F}^{-1}\left\{\chi_{2LS}(\Omega)\right\}$ and frequency independent losses have been neglected for simplicity. A linear stability analysis of the nonlinear Schrödinger equation with filter can be performed by inserting the following *ansatz*:

$$A(z,\tau) = A_s\left[1 + a_+(z)e^{-i\Omega t} + a_-(z)e^{i\Omega t}\right] \quad (5.47)$$

into Eq.5.46. $A_s = \sqrt{P}e^{i\gamma P z}$ where P is the power of the homogeneous solution. Linearizing with respect to the perturbation amplitudes $a_\pm$ we obtain the evolution equations for the sidebands:

$$\frac{\partial a_\pm}{\partial z} = i\Omega^2\frac{\beta_2}{2}a_\pm + i\gamma P\left(a_\pm + a_\mp^*\right) - g\frac{\gamma_\perp}{\gamma_\perp + i\left(\Omega_a \mp \Omega\right)}a_\pm. \quad (5.48)$$

From Eqs. 5.48 it is possible to build a stability matrix whose rows entries are the coefficients which multiply the amplitudes a_+ and a_-^* in the equation for a_+ and the coefficients multiplying the amplitudes a_+ and a_-^* in the equation for a_-^* (obtained from conjugation of the a_- one). The largest real part of the stability matrix' eigenvalues is the so called instability increment λ_m. The spectral modes whose stability increment is larger than zero experience exponential amplification with a rate given by the instability

increment. Indeed, by plotting λ_m we can verify that the damped frequencies and the corresponding symmetric idler waves experience exponential growth. The process is more efficient for modes close to the pump frequency; however, gain can take place for a large frequency interval. Theoretical results are confirmed by the full numerical simulations of Eq.5.46 and are depicted in Fig. 5.2.

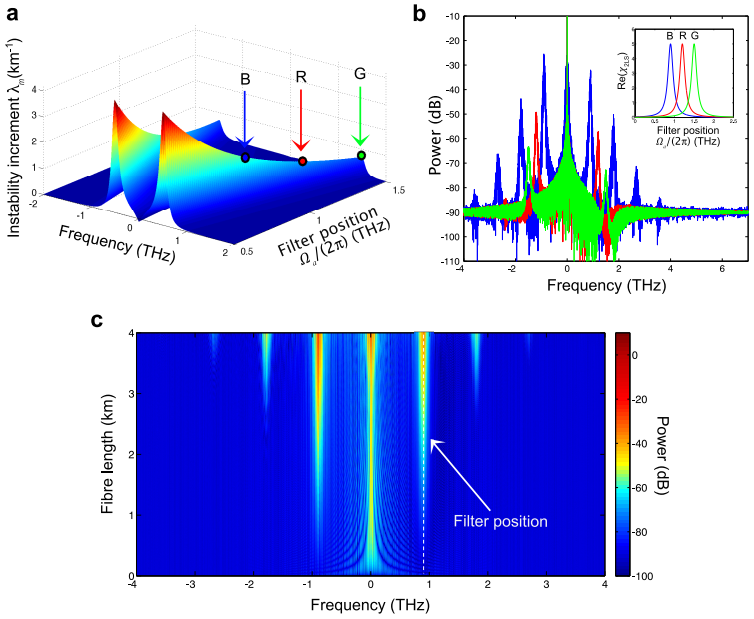

Figure 5.2: The instability increment λ_m is plotted in a) and shows that spectral modes damped by the distributed frequency dependent losses centered at frequency $\Omega_a/(2\pi)$ experience exponential gain, the process is more efficient if losses are applied close to the pump frequency Ω=0. In b) three spectra obtained from numerical simulations of Eq.5.46 for filters having respectively Ω_a=2π 0.9 (B), 2π 1.2 (R) and 2π 1.5 rad/ps (G) are depicted. In the inset of b) the real part of the 2LS-filter susceptibility is depicted with colours corresponding to the associated spectrum. Parameters common to all the simulations are: P = 5W, fibre length L=4 km, γ=15 (W km)$^{-1}$, β_2=1 ps^{2}km^{-1}, $g = 5km^{-1}$ and $\gamma_\perp$= 0.5 ps^{-1}. In c) the spectral evolution along the fibre shows that the gain is obtained for the spectral region where losses are applied (dashed white line) and for the symmetrically located idler wave; higher harmonics appear when signal's and idler's amplitudes have grown substantially. In c) parameters used are the same as for the blue spectrum in b).

From the results of numerical simulations we can observe the amplification of higher harmonics of the damped frequencies too. As far as the technical aspect of numerical simulations is concerned, the convolution appearing in time in domain in Eq.5.46 can be easily computed in the Fourier domain as a simple multiplication using the standard split-step integration method. It is important to stress that in case where the filters are applied symmetrically to both signal and idler waves simultaneously, then the well known stabilizing effect of dissipation is observed as expected. The results of both

theory and numerical simulations for symmetric losses are depicted in Fig.5.3

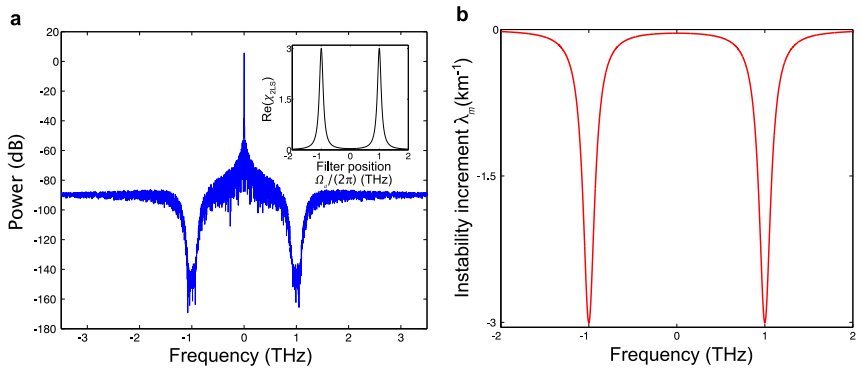

Figure 5.3: If losses are applied symmetrically to both signal and idler waves the well known stabilization takes place. In a) the results of numerical simulations are shown: the spectrum $|A(\Omega/(2\pi))^2|$ exhibits two "holes" in correspondence to the losses maxima (losses profiles corresponding to 2 symmetrically located 2LSs is shown in the inset). In b) the prediction of the stability analysis is shown. Parameters used are $L = 4$ km, P= 5 W, γ=15 (km W)$^{-1}$ and β_2=1 ps^{2}km^{-1}. The losses are described by 2 2LSs each one having g=3 km^{-1}, $\gamma_\perp$=0.5 ps^{-1} and $\Omega_a = \pm 2\pi$ rad/ps.

The dependence of the instability gain on other fibre parameters has been investigated and some results are depicted in Fig.5.4. We can observe that the GTL process is enhanced by increasing the input pump power or increasing the losses strength. We also mention the fact that lower dispersion favors the process too. Note that frequency independent losses can also be included in Eq.5.46 if it is needed for accurate modeling of some real world system. However the results will not be qualitatively affected, frequency independent losses would just reduce the instability gain as one could naturally expect. It is important to stress that the process is of purely dissipative origin. If the dispersive part of the 2LS susceptibility is neglected, than the results are not affected. A fundamental understanding of the ultimate cause of such fascinating phenomenon is still missing, possibly an analysis at the quantum level could be of help in this sense.

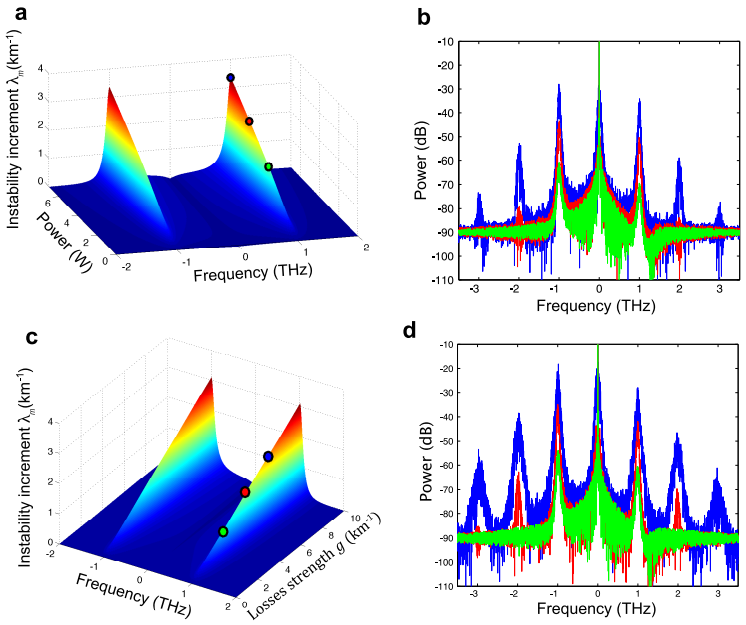

Figure 5.4: The instability increment is plotted versus pump power a): the GTL process is more efficient in the higher the pump power, this fact is confirmed by full numerical simulations; b): the three different plots of the spectrum $|A(\Omega/(2\pi))^2|$ have been obtained for the values of P indicated with the corresponding colored dots on a). The same dynamics can be observed by increasing the losses strength g: c)-d). Parameters used in a) and b) are: fibre length L=4 km, γ=15 (km W)$^{-1}$, β_2=1 ps^{2}km^{-1}, g = 8 km^{-1}, Ω_a=2π rad/ps and $\gamma_\perp$ = 0.5 ps^{-1}. Parameters used in c) and d) are: fibre length L=8 km, γ=15 (km W)$^{-1}$, β_2=1 ps^{2}km^{-1}, P = 5 W, Ω_a=2π rad/ps and $\gamma_\perp$ = 0.5 ps^{-1}.

5.4 Imaging of losses into gain

The GTL process is naturally linked to another interesting phenomenon: the imaging of the spectral losses profile into the modulation instability gain spectrum. Indeed through numerical simulations we can observe that it is indeed possible to achieve a mapping between the shape of the filter used and the resulting shape of the spectral sidebands. In order to perform this observation we consider the case where we have a set of identical normal dispersion fibre spans; at the end of each span we put a filter, being the filters identical at the end of each span. Now we can join such fibre spans with filters to form a long chain. We inject a CW pump field at the beginning of the chain ad record the spectrum at the output. We can see that by varying the shape and frequency position of the filter we get a a mapping of the filter profile into the modulation instability gain curve. We have verified the imaging of losses into gain for three different filters' shapes: Gaussian, Supergaussian and triangular (See Fig.5.5).

It is important to stress that in order to guarantee physical validity to our results the

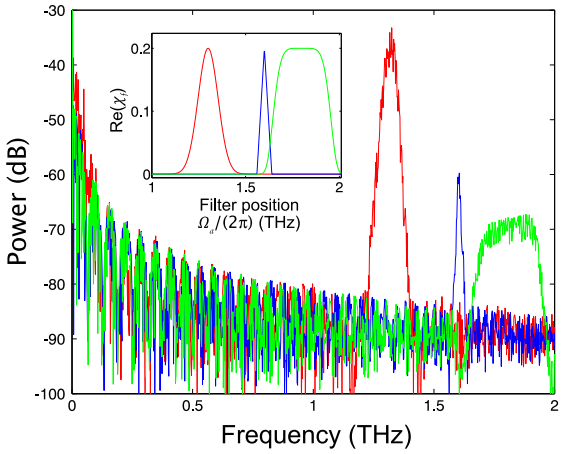

Figure 5.5: The imaging of losses into gain: the recorded spectra after the evolution of an input CW radiation propagating through a chain of identical fibre spans each one followed by a filter. Three kind of filters, differing in shape and spectral position have been considered and their reflectivity profiles are shown in the inset. Spectra are related to the corresponding filter by the same color convention. The shape of the filter is mapped into a gain profile. Parameters used are the following: for the Gaussian filter ω_f=2$\pi\cdot$ 1.3 rad/ps, σ_f=2$\pi\cdot$0.075 rad/ps; for the triangular filter ω_f=2$\pi\cdot$ 1.3 rad/ps, σ_f=2$\pi\cdot$0.075 rad/ps; while for the Supergaussian one ω_f=2$\pi\cdot$ 1.3 rad/ps, σ_f=2$\pi\cdot$0.075 rad/ps. Parameters common to all three simulations are filter strength g_f=0.2, P= 5 W, γ=15 (km W)$^{-1}$ and β_2=1 ps^{2}km^{-1}; the fibre span length between consecutive filters has been chosen to be equal to 5 m and a propagation of 180 spans have been simulated.

filters' transmission functions includes together with the dissipative part a dispersive contribution calculated using the Kramers-Kronig relations [55]. After each fibre span, the field amplitude Fourier transform is multiplied by the complex filter susceptibility $\chi_f\cdot$

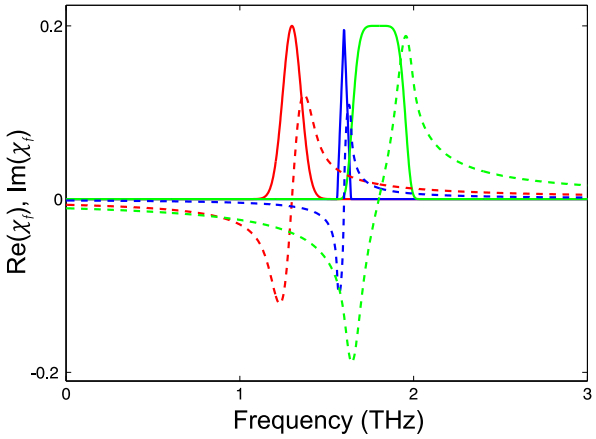

Figure 5.6: Real and imaginary parts of the filters susceptibilities corresponding to the filters used in Fig.5.5 are shown with continuous and dashed lines respectively.

5.5 Gain through losses in a ring fibre resonator: temporal patterns and frequency combs

Up to now we have focussed on linear stage of the dissipation induced modulation instability that results in the amplification of the damped spectral modes. It is also interesting and instructive to study the associated pattern formation. We perform this investigation in a different physical setup which is more suitable for the observation of stable patterns. Stable patterns are not possible in the NLSE coupled to a 2LS due to the fact that energy is gradually depleted from the field due to the presence of losses and the absence of any source or gain term.

We now study the GTL process in an externally driven passive fibre ring cavity resonator. It is well known that the temporal Lugiato-Lefever equation is the mean-field description of such kind of resonator. It is worth mentioning that the Lugiato-Lefever equation has been originally derived for a passive Kerr medium located in a cavity with external monochromatic driving in the context of spatial pattern formation [7, 56]. Later on Haelterman, Trillo and Wabnitz derived the temporal version of the Lugiato-Lefever equation for fibre resonators [8]. Despite its simplicity it captures a wealth of nonlinear phenomena both concerning spatial and temporal phenomena, among them cavity solitons and frequency combs play surely the lion' share [56]. The mean field approximation assumes that changes suffered by the electric field per cavity roundtrip

due to various physical effects and intracavity elements are small.

Since we want to study the impact of spectrally dependent losses in such system, we should derive a generalised Lugiato-Lefever equation that also includes the effect of the spectral filter. Let's consider an unidirectional ring fibre resonator of length L with the electric field envelope $E(z,t)$ defined in space z and time t whose propagation along the fibre is described by a nonlinear Schrödinger equation with group velocity dispersion β_2 and Kerr nonlinearity coefficient γ:

$$\frac{\partial E}{\partial z} = -i\frac{\beta_2}{2}\frac{\partial^2 E}{\partial t^2} + i\gamma|E|^2 E. \tag{5.49}$$

We also assume that the injection takes place very close in space to the position where the spectral filter is located, then the Fourier transform of the field $\tilde{E}(z,\omega)$ obeys the following boundary conditions:

$$\tilde{E}^{(n+1)}(0,\omega) = \sqrt{1-\alpha L}\sqrt{1-\theta}\sqrt{1-\tilde{F}(\omega)}\tilde{E}^{(n)}(L,\omega-\delta_0) + \sqrt{\theta P_{in}}\delta(\omega) \tag{5.50}$$

where θ describes the resonator output coupler defining the fraction of power that leaves the cavity at each round trip, α accounts for the remaining cavity losses, P_{in} is the power of the monochromatic external injection while $\tilde{F}(\omega) = f_0 e^{-(\omega-\omega_f)^2/\sigma_f^2}$ describes the spectral dependent reflectivity profile of a lumped filter ideally located close to the coupler where the injection takes place and having width σ_f and strength f_0 (a real number between 0 and 1) that is maximum around the frequency ω_f (from previous considerations about the dissipative origin of the gain through losses process we exclude here for simplicity the dispersive contribution of the filter). δ_0 describes the detuning between the monochromatic injection frequency and the closest cavity resonance and n is an integer valued index that stands for the cavity round trip number. We assume now a first order approximation such that the boundary conditions become:

$$\tilde{E}^{(n+1)}(0,\omega) = \left[1-\alpha_0-\frac{1}{2}\tilde{F}(\omega)\right]\tilde{E}^{(n)}(L,\omega-\delta_0) + \sqrt{\theta P_{in}}\delta(\omega) \tag{5.51}$$

where $\alpha_0 = (\alpha_L + \theta)/2$. Now we can express the field envelope at the end of each cavity round trip as follows:

$$E^{(n)}(L,t) = E^{(n)}(0,t) + L\frac{dE}{dz}|_{z=0} = \\ = E^{(n)}(0,t) + \left[-iL\frac{\beta_2}{2}\frac{\partial^2}{\partial t^2} + iL\gamma|E^{(n)}|^2\right]E^{(n)}(0,t) + \sqrt{\theta P_{in}} \quad (5.52)$$

By using Eq.5.52 into the inverse Fourier transform of Eq.5.51, discarding high order terms and approximating the term $e^{-i\delta_0} \approx 1 - i\delta_0$, we end up with the following difference equation:

$$E^{(n)}(L,t) - E^{(n)}(0,t) = \\ = \left[\alpha_0 - i\delta_0 - \frac{1}{2}F(t) \star -iL\frac{\beta_2}{2}\frac{\partial^2}{\partial t^2} + iL\gamma|E^{(n)}|^2\right]E^{(n)}(0,t) + \sqrt{\theta P_{in}} \quad (5.53)$$

where $\star$ denotes convolution and $F(t)$ is the inverse Fourier transform of $\tilde{F}(\omega)$. Now we replace the discrete map index n with a continuous slow time T' in this way we can define a new mean field $E(nt_R, t) = E^{(n)}(0,t)$ such that:

$$E^{(n)}(L,t) - E^{(n)}(0,t) = t_R\frac{\partial E}{\partial T'} \quad (5.54)$$

where t_R is the round trip time. In this way we end up with the generalised Lugiato-Lefever mean-field equation:

$$t_R\frac{\partial E}{\partial T'} = \left[\alpha_0 - i\delta_0 - \frac{1}{2}F(t) \star -iL\frac{\beta_2}{2}\frac{\partial^2}{\partial t^2} + iL\gamma|E|^2\right]E + \sqrt{\theta P_{in}}. \quad (5.55)$$

It is possible to express Eq.5.55 in a normalized form:

$$\frac{\partial \Psi}{\partial T} = -\Psi - i\Delta\Psi - i\frac{\partial^2\Psi}{\partial\tau^2} + i|\Psi|^2\Psi + f \star \Psi + S \quad (5.56)$$

where we have defined the slow time $T = \alpha_0 T'/t_R$, the fast time $\tau = t\sqrt{(2\alpha_0)/(|\beta_2|L)}$, the normalized field envelope $\Psi = E\sqrt{(\gamma L/\alpha_0)}$, the normalized detuning $\Delta = \delta_0/\alpha_0$ and the injection $S = \sqrt{(\gamma\theta P_{in}L)/(\alpha_0^3)}$. We have furthermore considered that the fibre has normal dispersion. The spectral filter is described now by the Fourier transform of $f(t)$ which reads $\tilde{f}(\omega) = \mu e^{-(\omega-\omega_f)^2/\sigma_f^2}$ where the term $\mu = f_0/(2\alpha_0)$ measures the filter's strength. We will consider here only the normal dispersion case; the anomalous

dispersion fibre can be described by changing to plus the minus sign in front of the second derivative with respect to τ.

A numerical simulation of Eq.5.56 leads to the observation that indeed the GTL process can potentially take place in externally driven passive fibre resonators too. The results are summarized in Fig.5.7, where spectrum (Fig.5.7a)), an intensity trace (Fig.5.7b)) and the slow evolution of the patterns along the coordinate T (Fig.5.7c)) have been plotted once the field has reached a stable stationary state. The resulting

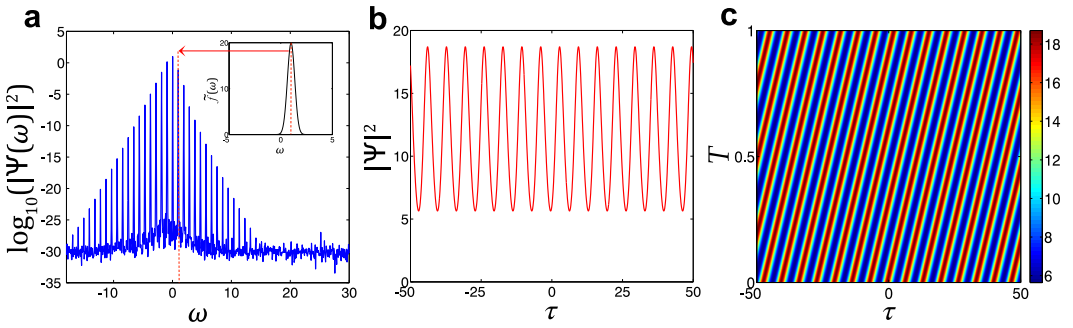

Figure 5.7: Pattern formation in the generalised Lugiato-Lefever equation: a) The spectrum $|\Psi(\omega)|^2$ in log scale in the stationary state: peaks are separated by $\Delta\omega = 1$ equal to the filter frequency shift from the pump. The first excited mode is highlighted with a red dashed line, while the filter's profile is shown in the inset. b) the stable temporal pattern: a train of pulses on the finite field background with a repetition rate given by the frequency position of the filter $\omega_f/(2\pi)$. In c) the stability of the temporal pattern is shown: only a drift is present but the structures are robust over the slow-time evolution. Parameters used are $\mu = 20$, S=40, Δ=0, ω_f=1 and σ_f=0.5.

spectrum (Fig.5.7a)), in semilogarithmic scale, exhibits the characteristic triangular shape typical frequency combs associated to periodic multisolitonic temporal dynamics [57]. The frequency separation between nearest neighbors spectral modes is given by the frequency shift of the filter's position from the pump field and the field configuration in the time domain consists of a stable train of pulses on the finite background. Those results stress the potentiality of the GTL process both for frequency comb generation as well as mechanism for the production of high repetition rate pulse trains. The dynamics of the Lugiato-Lefever equation is known to be very rich in terms of multistability, pattern formation and dynamical instabilities [56], the investigation of the coexistence of those phenomena with the GTL process appears to be an interesting research direction for future studies.

Some of the possible issues that need to be addressed in the first place are the following: estimation of the differences in predictions between the mean field model derived here

and the Ikeda map approach for the resonator modelling; experimental study of the phenomena discussed here in ring fibre resonators and consideration of the feasibility of observing some analogous dynamics in the spatial Lugiato-Lefever equation.

5.6 Gain through losses in an optical parametric oscillator

The GTL principle may have potentially relevant impact in a wealth on systems where nonlinear wave dynamics is involved. As a simple example of its far reaching consequences I illustrate here the simple case of an optical parametric oscillator (OPO) for a χ_2 medium. Such a device can be described by the coupled evolution equations for signal A_s and conjugate idler wave A_i^* conjugate, in the regime of strong and undepleted pump [53]:

$$\frac{\partial A_s}{\partial z} = -\alpha_s A_s - i\Delta k_s A_s + M_s A_i^* \tag{5.57}$$

$$\frac{\partial A_i^*}{\partial z} = -\alpha_i A_i^* + i\Delta k_i A_i^* + M_i A_s. \tag{5.58}$$

Where $\alpha_{s,i}$ are the signal and idler losses respectively and $\Delta k_{s,i}$ represent here the detunings that for simplicity we consider satisfying $\Delta k_s = \Delta k_i = \Delta_k/2$, being $\Delta_k = k_p - k_s - k_i$ a mismatch parameter ($k_{p,s,i}$ are the pump, signal and idler wavenumbers respectively). The coupling constants $M_{s,i}$ depend on the pump intensity $|A_p|^2$ through the following relation $M_s M_i = \rho|A_p|^2$ being ρ a proportionality factor. If one performs the linear stability analysis of Eqs.5.57 and 5.58 obtains the following eigenvalues:

$$\lambda_\pm = \frac{1}{2}\left[-(\alpha_s + \alpha_i) \pm \sqrt{(\alpha_s - \alpha_i - i\Delta k)^2 + 4\rho|A_p|^2}\right]. \tag{5.59}$$

If losses are neglected then gain occurs for modes satisfying the standard phase-matching conditions $\Delta k^2 = 4\rho|A_p|^2$. If losses are symmetric ($\alpha_s = \alpha_i$) then the OPO gain is simply reduced. It is however not trivial what happens if losses are different for signal and idler waves ($\alpha_s \neq \alpha_i$). For simplicity we will focus from now on, on the case where $\alpha_i = 0$ and $\alpha_s \neq 0$. We also define the growth exponent which quantifies the amount of gain $\lambda = max\,[Re(\lambda_\pm)]$. We observe that unbalanced losses lead to amplification of

waves outside the phase-matched area. In Fig.5.8, the results are presented. The facts

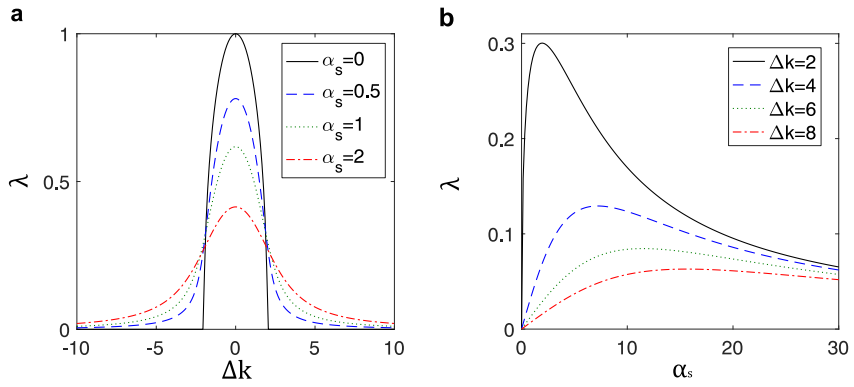

Figure 5.8: a) The growth exponent λ is plotted versus mismatch parameter Δk for different values of the losses α_s. By increasing losses strength we see that gain decreases in the phase matched region but becomes possible and increases outside the phase-matched area. In b) it is shown how the amount of losses that maximizes the out of phase-matching gain depends on the wavenumber.

presented here have the goal to illustrate the essence of a new physical phenomenon and to motivate a further and more detailed investigation of the GTL principle in OPOs, which of course should be undertaken taking carefully into account the experimental constraints and conditions. It remains however clear that the GTL principle could potentially be used to achieve gain in OPOs in the case when obtaining phase matching is difficult, or to enhance the gain bandwidth of phase matched OPOs.

6 Self-induced Faraday instability in lasers

6.1 Self-induced Faraday instability in the complex Ginzburg-Landau equation

We discuss in this Chapter another kind of dissipative Faraday instability that could be engineered to achieve generation of pulses in lasers. As we have already mentioned in Chapter 2, the first example of Faraday instability in nonlinear fibre optics was discussed by Matera and co-authors [29], in the case where periodic amplification along an optical fibre communication link due to the periodically induced variation of the effective nonlinearity.

Let's consider now the case of a linear laser cavity where the gain, for some reasons, exhibits a non homogeneous profile along the propagation direction of the light in the resonator. Such inhomogeneity could arise due to the attenuation of the pump field or due to its partial depletion during the process of stimulated emission. It is evident in this case that the laser field traveling back and forth in the cavity experiences a periodic gain profile. Such periodic gain profile corresponds to a periodic nonlinearity landscape seen by the propagating electric field as it is schematically illustrated in Fig.6.1. In the first place we study this dynamics with a simplified but paradigmatic model: the CGLE with a periodically varying gain coefficient; which mimics the periodic gain variation that may spontaneously arise due to the internal dynamics of the laser. It is important to stress that we choose such simplified model with periodically varying gain in order to obtain an insight into the problem, I'll later comment on a system where such periodic gain variation arises spontaneously due to the intrinsic dynamics of the laser solutions. The CGLE for a fibre laser, describing the evolution along the space coordinate z of

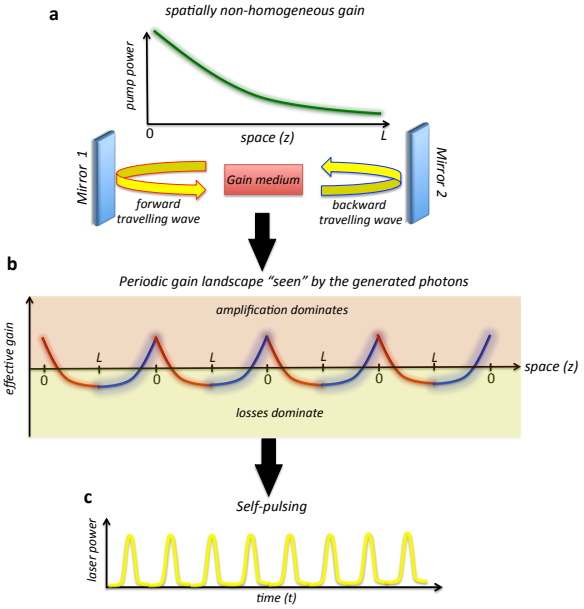

Figure 6.1: The concept of self-induced Faraday instability laser is illustrated schematically: The spatially inhomogeneous gain profile arises naturally from the solutions of the nonlinear laser equations a gives rise to an effective periodic gain (and consequently nonlinearity) landscape profile b) seen by the generated photons that travel back and forth in the linear cavity. The periodic gain and nonlinearity variations results in a parametric forcing leading to self-pulsing with high repetition rate c).

the electric field envelope A defined in time t reads:

$$\frac{\partial A}{\partial z} = \mu(z)A + (b - id)\frac{\partial^2 A}{\partial t^2} + (ic - s)\left|A\right|^2 A \tag{6.1}$$

where d and b account respectively for dispersion and diffusion (finite gain bandwidth), c describes self-phase modulation and s the gain saturation. $\mu = \mu_{av} + \delta_\mu cos(k_m z)$ is the gain coefficient that is constituted by an average part μ_{av} and an oscillating one with modulation depth $\delta\mu$ and modulation wavenumber $k_m = 2\pi/L_m$ being L_m the spatial modulation period. A Floquet stability analysis of the continuous wave solution helps us in understanding that indeed a Faraday-like instability is taking place in the system; in particular if δ_μ exceeds μ_{av} (i.e. there are spatial regions along the cavity where gain dominates and other where losses dominate) certain spectral modes experience exponential growth ($\mathcal{G} > 0$). The power gain coefficient is defined as $\mathcal{G} = 2ln(|\lambda_m|)/L_m$ where λ_m is the Floquet multiplier with the largest absolute value while the procedure for the Floquet analysis has been described already in Chapter 2. Two typical features of Faraday instability are observed: the synchronization area increases with increasing modulation depth (Fig.6.2a); furthermore there is an inverse scaling of the frequency of

unstable modes versus the modulation period L_m and versus the nonlinearity coefficient c. The instability leads to a pattern formation: stable patterns are generated. They are periodic with a period double to the forcing one as in the Faraday instability induced by dispersion modulation [34]. The results are summarized in Fig. 6.2.

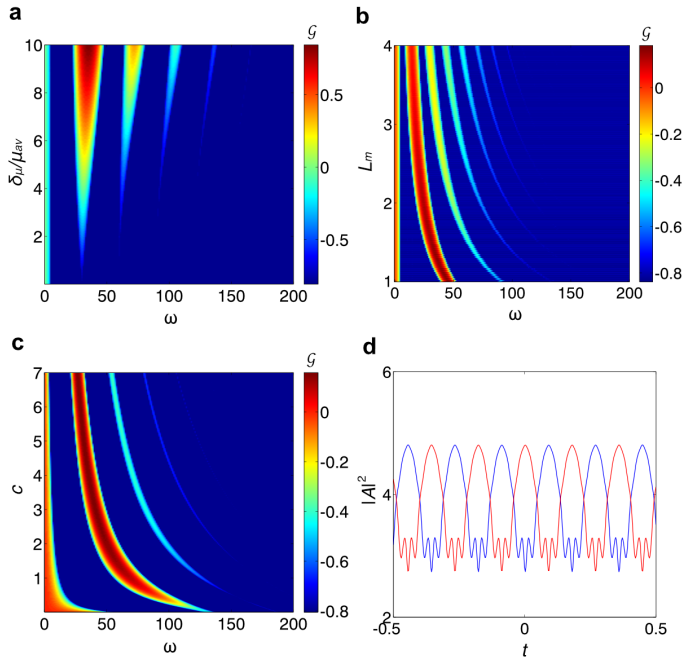

Figure 6.2: a) the instability $\mathcal{G}$ is plotted in the $\omega - \delta_m$ plane instability takes place for $\mathcal{G} > 0$. In b) and c) $\mathcal{G}$ is plotted in the $\omega - L_m$ and in the $\omega - c$ plane respectively. In d) an example of a stable pattern -pulse train- is shown: blue and red lines correspond to the field modulus squared plotted at even (blue) an odd (red) modulation periods respectively (this is similar to what observed in longitudinally modulated ring resonators). Common parameters used in all subplots are $c = 5$, $s = 0.1$, $d = 1.18 \cdot 10^{-4}$, $\mu_{av} = 0.4$, $\delta_\mu = 5\mu_{av}$, $L_m = 1.5$ and $b = 0$. In a) δ_μ has been varied from 0 to $10\mu_{av}$, in b) L_m has been varied from 1 to 4 and in c) c has been varied from 0 to 7.

Interestingly we can observe that under certain conditions the Faraday patterns can coexist with spatiotemporal chaos. If the gain bandwidth b is different from zero, from an initially Faraday patterns dominated regime spatiotemporal chaos develops: islands of Faraday patterns appear and disappear along the slow dynamics of the system (see Fig. 6.3a)). Very counterintuitively, the patterns are stabilized by reducing the value of b (see Fig. 6.3c)). If diffusion is reduced to below $b = 10^{-6}$ (for the set of parameters chosen Fig.6.3), the dynamics is dominated by stable Faraday patterns without any signature of turbulence. The latter fact is quite unexpected since in general diffusion helps the stabilization in pattern formation processes, by suppressing high frequency noise and has to be considered in case of real world laser design operating in self-pulsing

regime caused by the self-induced Faraday instability.

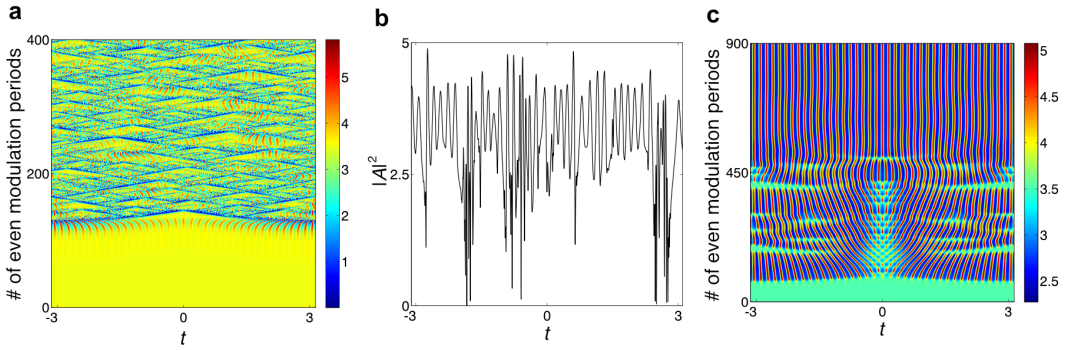

Figure 6.3: a) The coexistence of Faraday patterns with spatiotemporal chaos; b) a section of a); parameters used are: c=5, $s = 0.2$, $d = 1.18 \cdot 10^{-4}$, $\mu_{av} = 0.8$, $\delta_\mu = 5\mu_{av}$, $L_m = 1.5$, $b = 1.97 \cdot 10^{-5}$. In c) we can appreciate the stabilization of the patterns by setting $b = 0$.

6.2 Self-induced Faraday instability in a Raman fibre laser

We have verified indeed that periodic gain variation can lead to a Faraday instability in the CGLE, let's now enter in more details about a possible candidate for the experimental realization of the Faraday instability laser. Let's consider a linear cavity Raman fibre laser such as the one described in Chapter 2 but this time without detuning in frequency the cavity mirrors (See Fig.6.4a). The cavity is pumped in correspondence of the first mirror at 1455 nm and lasing occurs at 1555 nm. The dynamics of the laser is described by the following coupled generalised nonlinear Schrödinger equations for the Stokes A_s and pump A_p slowly varying envelopes:

$$\begin{aligned} \pm\frac{\partial A_s^{\pm}}{\partial z} &= -i\frac{\beta_{2s}}{2}\frac{\partial^2 A_s^{\pm}}{\partial t^2} - \frac{\alpha_s}{2}A_s^{\pm} + i\gamma_s|A_s^{\pm}|^2 A_s^{\pm} + \frac{g_s}{2}\left(|A_p^{\pm}|^2 + |A_p^{\mp}|^2\right)A_s^{\pm} \\ \pm\frac{\partial A_p^{\pm}}{\partial z} &= -\beta_{1p}\frac{\partial A_p^{\pm}}{\partial t} - i\frac{\beta_{2p}}{2}\frac{\partial^2 A_p^{\pm}}{\partial t^2} - \frac{\alpha_p}{2}A_p^{\pm} + i\gamma_p|A_p^{\pm}|^2 A_p^{\pm} - \frac{g_p}{2}\left(|A_s^{\pm}|^2 + |A_s^{\mp}|^2\right)A_p^{\pm} \end{aligned} \tag{6.2}$$

where $\beta_{2p,s}$, $\gamma_{p,s}$, $\alpha_{p,s}$ and $g_{p,s}$ denote group velocity dispersion, Kerr nonlinearity, attenuation and Raman gain coefficient respectively. $\pm$ denotes the propagation direction in the cavity: + from left to right and - from right to left, while β_{1p} accounts for the group velocity mismatch between Stokes and pump field.

Due to the combined action of pump depletion and attenuation the pump field exhibits a non homogeneous distribution along the spatial coordinate z. Such inhomogeneity increases proportionally to the pump input power as it is shown in Fig.6.4a), where the gain profile experienced by the laser field upon a four cavity round trip propagation is depicted. A Floquet stability analysis of the Raman lasers CW solution shows that for a pump power exceeding a certain threshold a Faraday instability appears (Fig.6.4b). We observe that such instability triggers the generation of a pulse train (Fig.6.4d) and e)). Note that at variance with results reported in Chapter 3 the repetition rate of the pulses is almost 10 times higher since the cavity length is about 10 times shorter.

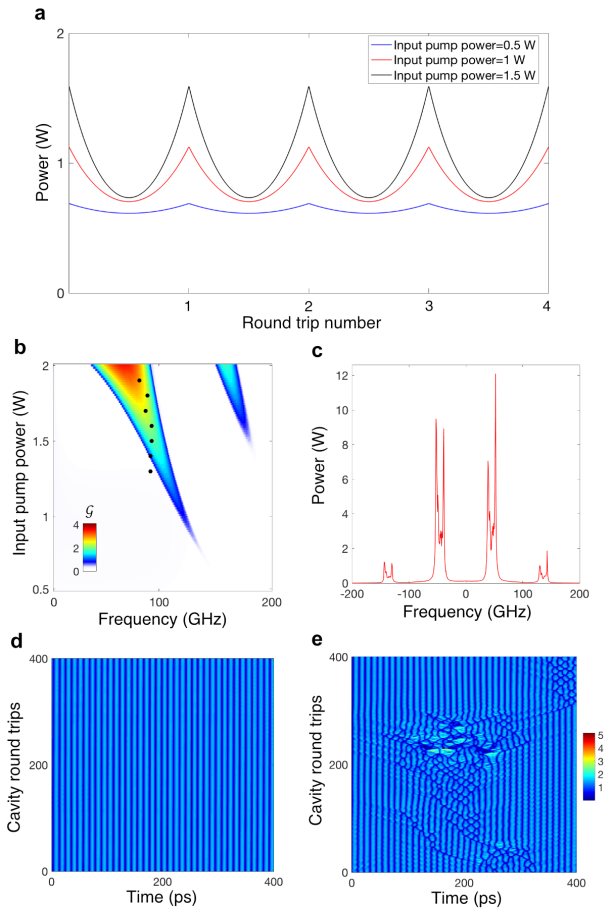

Figure 6.4: a) The spatial inhomogeneity in the pump field increases by incrementing the input pump power P_{in}. b) The Faraday instability gain: instability corresponds to the colored area. Black dots denote the peak position of the power spectrum in the stationary state obtained in numerical simulations. c) The field spectrum modulus squared. Faraday instability induced self-pulsing obtained from numerical simulations of Eqs.6.2: stable d) and collision dynamics e). Parameters used are γ_p=3 (W km)$^{-1}$, γ_s=2.57 (W km)$^{-1}$, g_p=1.51 (W km)$^{-1}$, g_s=1.3 (W km)$^{-1}$, α_s=0.8 km^{-1}, α_p=0.5 km^{-1}, fibre length L = 0.37 km. The cavity mirrors are modeled as having Supergaussian profile of order 3 (without chirp) reflecting at the Stokes wavelength, with a width of about 1nm. For subplots c), d) and e) the pump power used is P_{in}=1.5 W.

The self-induced Faraday instability has been discussed in its basic features and some preliminary steps towards its potential observation in real-world systems have been presented too. Of course future studies, specially experimental ones, will help clarifying wether it could result in a technologically relevant tool for achieving mode-locking with high repetition rates in lasers. Further effort is needed also for establishing a mathematically rigorous theory of such modulation instability.

7 A new master equation for active mode-locking in lasers

7.1 Haus theory for active mode-locking: is it the end of the story?

An example of mode-locking was discussed before, concerning the dissipative Faraday instability in a Raman fibre laser. In this Chapter some more fundamental results about the theory of mode-locking in lasers will be presented. It is a well known fact that the paradigmatic mathematical model which describes the dynamics of mode-locked lasers is the so-called Haus master equation (HME), a milestone in laser physics. Derived in 1975 by Hermann Haus for active mode-locking induced by modulation of losses with a period equal to the cavity roundtrip time [58], HME can be generalised to a variety of mode-locking techniques: active mode-locking by phase modulation, passive mode-locking with a saturable absorber, Kerr-lens mode-locking, soliton-mode-locking, additive pulse mode-locking etc [59]. We distinguish between active and passive mode-locking techniques for the following reason, the first ones do require the presence of a device, in general an electro-optic or an acusto-optic modulator, that is driven by an external source of energy (different from the laser medium itself) while the latter don't. Since we will focus in this Chapter on active mode-locking by amplitude modulation it is worth remembering that it is based on the periodic modulation of the cavity losses. Such modulation is preformed either using an electro-optic or an acusto-optic modulator that periodically reflect light out of the cavity. If the period of losses modulation corresponds to about the cavity round trip time we have the so-called fundamental mode-locking and only one pulse is circulating in the cavity, if instead the modulator is driven with the frequency which is an integer multiple of the cavity free-spectral range, than we

have harmonic mode-locking and many pulses are present in the cavity. Before Haus' work there have been attempts to estimate features of pulses in active mode-locking, for instance, Siegman and Kuizenga [60, 61] developed a self-consistent approach that allows to calculate the stationary state pulse features such as duration, spectral width and chirp as a function of the modulator's and active medium parameters. However such an approach is not very useful when the dynamics of pulses is of interest, for instance when the modulator frequency is detuned with respect to the cavity free spectral range, or when other physical effects are involved.

HME is derived under the hypothesis that the electric field envelope inside the cavity suffers only from a smooth variation at each interaction with the optical elements present in the cavity and that its net change per roundtrip is small. The dynamical equation for the field is coupled with an equation describing the gain dynamics. Before entering into details about our new model it is worth reporting a brief and phenomenological derivation of HME.

The most general solution for the electric field in a laser cavity is a sum over all the longitudinal cavity modes:

$$E(z,t') = \sum_{n=0}^{n=\infty} E_n \exp i(\Omega_n t' - K_n z). \tag{7.1}$$

We consider modes propagating only in one direction and with a small frequency spacing so that we can pass to the continuum and replace the sum with an integral:

$$E(z,t') = \int_0^{+\infty} E(K) \exp i(\Omega(K)t' - Kz)dK \tag{7.2}$$

Since we are interested in pulsed solutions we introduce a slowly varying envelope. In order to do this we define a central frequency ω_0, a central wave number k_0 and we make the following changes of variable:

$$k = K - k_0, \tag{7.3}$$

$$\omega(k) = \Omega(K - k_0) - \omega_0 \tag{7.4}$$

$$E(k) = E(K - k_0). \tag{7.5}$$

The electric field can then be written as

$$E(z,t') = \left(\int_{-\infty}^{+\infty} E(k)\exp i(\omega(k)t' - kz)dk\right) e^{i(\omega_0 t' - k_0 z)}, \tag{7.6}$$

and the slowly varying envelope takes the form:

$$A(z,t') = \int_{-\infty}^{+\infty} E(k)\exp i(\omega(k)t' - kz)dk. \tag{7.7}$$

By defining two temporal variables: $T = t'$ and $t = t' - z/v_g$, with v_g group velocity of the envelope, we have the final expression for the envelope

$$A(T,t) = \int_{-\infty}^{+\infty} E(k)\exp\{i\left[(\omega(k) - v_g k)T + k v_g t\right]\}dk. \tag{7.8}$$

T is a slow temporal variable introduced to describe the pulse change on the cavity roundtrip time scale, while t describes fast variations which occur on time scales of the order of a typical pulse duration.

The key hypothesis of smooth change per cavity roundtrip allows to write the amplitude variation at each roundtrip as a derivative with respect to the slow time scale T:

$$\frac{\partial A(T,t)}{\partial T} = \frac{\sum_i \Delta A_i}{T_R} \tag{7.9}$$

where T_R is the cavity round trip time and ΔA_i the amplitude variation due to the i-th cavity element. We analyze now how each element affects the electric field slowly varying envelope.

The gain medium action can be described naturally in the frequency domain by the following transmission function $\exp\left[\overline{G}(\omega)\right]$ acting on the Fourier transformed amplitude $\tilde{A}(\omega)$. $\exp\left[\overline{G}(\omega)\right]$ is related to the gain medium susceptibility and has the following form:

$$\exp\left[\overline{G}(\omega)\right] = \exp\left[\frac{\overline{G}}{1+\left[\frac{2(\omega-\omega_0)}{\Delta\omega_G}\right]^2}\right] = \exp\left[\frac{\overline{G}}{1+\left[\frac{(\omega-\omega_0)}{\Omega_G}\right]^2}\right] \approx \exp\left[\overline{G}\cdot\left[1-\frac{(\omega-\omega_0)^2}{\Omega_G^2}\right]\right]. \tag{7.10}$$

where ω_0 is the laser central frequency, $\Delta\omega = \omega - \omega_0$, $\Omega_G = \Delta\omega_G/2$ the gain medium bandwidth, and $\overline{G}$ the single-pass gain. The Taylor approximation can be done by

assuming that the electric field spectrum is smaller than the amplifying bandwidth. Hence, since the effect of the gain should be small, the exponential can be approximated to the first order:

$$\exp\left[\overline{G}(\omega)\right]\tilde{A}(\omega) \approx \left[1+\overline{G}\left(1-\frac{\Delta\omega^2}{\Omega_G^2}\right)\right]\tilde{A}(\omega) = \left[1+\overline{G}-\overline{G}\frac{\Delta\omega^2}{\Omega_G^2}\right]\tilde{A}(\omega), \tag{7.11}$$

so

$$\Delta\tilde{A_G}(\omega) = \overline{G}\left[1-\frac{\Delta\omega^2}{\Omega_G^2}\right]\tilde{A}(\omega). \tag{7.12}$$

Taking the inverse Fourier transform on both sides of Eq. (7.12) we have

$$\Delta A_G(T,t) = \overline{G}\left[1-\frac{1}{\Omega_G^2}\frac{\partial^2}{\partial t^2}\right]A(T,t). \tag{7.13}$$

Cavity losses are described in the following way: the amplitude at the roundtrip $n+1$ is the amplitude at the roundtrip n attenuated by an exponential factor $\exp(-l)$. Since the amplitude suffers just a small attenuation per roundtrip:

$$A_{n+1}(T,t) = e^{-l}A_n(T,t) \approx (1-l)A_n(T,t) \tag{7.14}$$

and

$$\Delta A_l(T,t) = -lA(T,t). \tag{7.15}$$

The modulator is assumed to induce a cosinusoidal amplitude modulation, with period much larger than a typical pulse width, which is a very realistic case; its effect is described through a suitable transmission function so that:

$$A_{n+1}(T,t) = \exp\left(-M\left[1-\cos(\omega_M t)\right]\right)A_n(T,t) \tag{7.16}$$

where M is the modulation depth, and ω_M the modulation frequency. Approximating the exponential at the first order we obtain

$$\Delta A_M(T,t) = -M\left[1-\cos(\omega_M t)\right]A(T,t). \tag{7.17}$$

The previously commented assumption that the modulation period is much larger than a typical pulse width, allows to consider that the pulse, which passes through the

modulator around the point of minimum losses, "sees " the modulator just around this point. If the time origin is assumed to be coincident with the pulse transit we can use the parabolic approximation and write

$$\Delta A_M(T,t) = -\frac{M\omega_M^2 t^2}{2} A(T,t). \tag{7.18}$$

We are now able to write the HME for active mode-locking:

$$T_R \frac{\partial A(T,t)}{\partial T} = \left[\bar{G}\left(1 + \frac{1}{\Omega_g^2}\frac{\partial^2}{\partial t^2}\right) - l - \frac{Mt^2\omega_M^2}{2} \right] A(T,t). \tag{7.19}$$

Eq.7.19 is in general coupled to a gain equation (see e.g. [62])

$$\frac{\partial \overline{G}(T)}{\partial T} = -\frac{\overline{G}(T) - g_0}{\tau_L} - \overline{G}\frac{W(T)}{P_L} \tag{7.20}$$

where g_0 is the small signal gain, τ_L the gain medium relaxation time, P_L the saturation power of the gain and $W = \int |A(T,t)|^2 dt$ is the total energy stored in the cavity at the instant of time T.

It is worth mentioning that the basic assumptions underlying its derivation are: (i) the gain recovery time is much slower than the cavity roundtrip time, hence the pulses sees only an average gain and (ii) all the physical effects induce small changes in the electric field from roundtrip to roundtrip. Recent studies have evidenced the limits of HME in describing accurately features of the pulses in lasers with a fast gain recovery time, such as semiconductor lasers. In this cases the gain can change substantially on a time scale comparable with the cavity round trip time hence violating the assumptions of HME validity. Asymmetric pulses significantly deviating from the predicted Gaussian shape have been observed too. Such substantial discrepancies between HME predictions and experimental results, has motivated some attempts to develop new theoretical models for the description of mode-locking in lasers. A good example is the delay-differential equation model developed by Vladimirov and Turaev [63] which describes passive mode-locking in a semiconductor laser with saturable absorber, reproducing some of the features of the experimentally observed pulses such as for instance their asymmetric tails [64]. The results presented in this Chapter describe a new complete theory for active mode-locking in lasers: a new master equation is de-

rived from first principles, i.e. from the Arecchi Bonifacio (AB) equations describing, from the fundamental point of view the coherent light-matter interaction in the gain medium[65, 17]. In the literature those equations are generally referred to as Maxwell-Bloch equations. Some reasons to pay credit to the original discover of those equations, Tito Arecchi and Rodolfo Bonifacio, are given for example in a recent editorial [66]. The new master equation, a partial differential equation coupled to a gain equation, describes active mode-locking in lasers and has an extended range of validity compared to HME. In the limit where the gain recovery time is much longer than the cavity round trip time, as for instance in solid state lasers, then the well-known predictions by Haus are recovered, but our model is valid also in the opposite limit, e.g. when the gain recovery time is comparable or smaller than the cavity round trip time. In the latter case our model predicts substantial discrepancies from HME solutions, showing that stable pulses are no longer symmetric, they could exhibit skew-*sech* shape or even a pronounced "bump". Such novel predictions are validated by a comparison with experimental results obtained with an actively mode-locked semiconductor laser.

7.2 The derivation of the coherent master equation

We start our derivation from the AB equations. How the AB equations can be obtained starting from the density matrix formalism describing a two-level system coupled to the electromagnetic field, whose dynamics obeys the Maxwell equations, has been reported in Appendix; here we simply rewrite them (with a simple change in notation that will be useful during the exposition) as the starting point of our work:

$$\frac{1}{v_0}\frac{\partial f}{\partial t} + \frac{\partial f}{\partial z} = \frac{a}{2}p \tag{7.21}$$

$$\frac{\partial p}{\partial t} = \Omega_G(Df - p) \tag{7.22}$$

$$T_G\frac{\partial D}{\partial t} = 1 - D - Re(p^* f) \tag{7.23}$$

where f is the electric field slowly varying envelope, p the atomic polarization, D is the population inversion, v_0 is the cold cavity group velocity, a the unsaturated gain and $T_G = \gamma_{||}^{-1}$ the inverse of the population inversion decay rate, Ω_G is the half-width at half-maximum of the gain curve, also usually denoted with the symbol $\gamma_\perp$ in laser physics. We consider the case where no detuning between the laser frequency and the atomic resonance is present.

We consider a unidirectional ring cavity resonator. The presence of the modulator in the cavity imposes the following boundary conditions for the electric field:

$$f(0,t) = (1-l)e^{-m(t-t_m)} f(w, t-t_e) \tag{7.24}$$

where we have assumed that the entrance and exit plane of the gain medium are located at coordinates $z = 0$ and $z = w$, l are the cavity losses in absence of the modulator, t_m is the light time of flight from the modulator to the gain medium entrance face, while t_e is the light time of flight from the medium exit face to the medium entrance face. We chose m to be the following function of t: $m(t) = M\left[1 - cos(\Omega_M t)\right]$ where M is a modulation depth while $\Omega_M = 2\pi/T_M$ being T_M the period of the modulator.

As an intermediate step towards obtaining the master equation we start with transforming the field equation (Eq.7.21) into a map relating $f(0,t)$ to $f(0, t-T_R)$, e.g. to its value at the previous cavity round trip. Due to the fact that the "hot" cavity group velocity v is unknown and differs from the "cold" cavity one, the effective cavity roundtrip time $T_R = t_e + w/v$ is unknown too, we introduce the roundtrip time difference $\delta T_R = w\left(\frac{1}{v} - \frac{1}{v_0}\right)$ and write $\left(v^{-1}\partial_t + \partial_z\right) f = s$ being $s = \frac{ap}{2} + \frac{\delta T_R}{w}\partial_t f$. The equation for f can be solved formally and the solution reads $f(w,t) = f(0, t - w/v) + \int_0^w s(z, t - w/v + z/v)dz$. If s is a wave-packet propagating at speed v we have $f(w,t) = f(0, t-w/v) + ws(0, t-w/v)$. From the fact that $w/v = T_R - t_e$ we have $f(w, t - t_e + T_R) = f(0,t) + ws(0,t)$. Defining $\mathcal{F}(t) = f(0,t)$ and $\mathcal{P}(t) = f(0,t)$ we can obtain the map:

$$\Delta_R \mathcal{F} = -[l + m(t)]\mathcal{F}(t) + \frac{aw}{2}\mathcal{P}(t) + \delta T_R \partial_t \mathcal{F}(t). \tag{7.25}$$

The following definition has been used $\Delta_R \mathcal{F} = \mathcal{F}(t + T_R) - \mathcal{F}(t)$. Furthermore, by shifting the origin of time, we have written $m(t)$ instead of $m(t + T_R - t_m)$, assuming m and $l << 1$, approximated $e^{-m(t)} \approx 1 - m(t)$ and discarded higher order terms.

The atomic polarization captures indeed the coherence in the light-matter interaction, but if we want to get to a simple equation for the field coupled to a gain equation, like in HME, which simplifies significantly the problem, the equation for p should be adiabatically eliminated. This way of proceeding is justified by the fact that p evolves on a much faster time scale compared to f and D. However such adiabatic elimination must be performed in a careful way. In general people simply set $\dot{p} = 0$ and obtain two closed equations for f and D. However this cannot be done in our case since the information on the finite gain bandwidth would be lost and we will have a gain medium that amplifies all the spectral modes of the electric field having hence an instantaneous response. A proper way of performing the adiabatic elimination in an advanced way [67, 68], based on the expansion of differential operators, allows to formally write

$$p = (1 + \Omega_G^{-1}\partial_t)^{-1}(Df) \tag{7.26}$$

and then Taylor expand the differential operator in virtue of the smallness of the parameter Ω_G^{-1} up to the second order, hence obtaining the following expression for p:

$$p = (1 + \Omega_G^{-1}\partial_t)^{-1}(Df) \approx \left[1 - \Omega_G^{-1}\partial_t + \Omega_G^{-2}\partial_t^2\right](Df). \tag{7.27}$$

In this way we see that a second order derivative in time appears which describes the finite gain bandwidth, the first order term is a drift while the zero order term is just the result one would obtain by performing the standard adiabatic elimination technique. The map (Eq.7.25) becomes hence

$$\Delta_R \mathcal{F} = (l\mathcal{G} - l - m)\mathcal{F} + \delta T_R \partial_t \mathcal{F} + l\hat{L}(\mathcal{G}\mathcal{F}) \tag{7.28}$$

with $\mathcal{G}(t) = rD(0,t)$ being $r = \frac{aw}{2l}$ the dimensionless pump parameter (equal to 1 at the laser threshold). The information about the coherence is contained in the differential operator $\hat{L} = -\Omega_G^{-1}\partial_t + \Omega_G^{-2}\partial_t^2$, while from Eq.7.23 it is easy to derive an equation for

$\mathcal{G}$:

$$T_G d_t \mathcal{G} = r - \mathcal{G}\left(1 + |\mathcal{F}|^2\right) - Re\left[\mathcal{F}^* \hat{L}(\mathcal{G}\mathcal{F})\right] \tag{7.29}$$

and the laser is now described by two equations only.

We now separate the time variable in a fast and a slow scale. Let's define $\chi(t = nT_R + t')$ being $\chi = \mathcal{F}, \mathcal{G}, m$. Hence we have that $\chi_n(t' + T_R) = \chi_{n+1}(t')$. By limiting $t' \in [0, T_R]$ we have that n counts the number of cavity roundtrips while t' the roundtrips fractions. With such notation Eq.7.28 reads the same but with $\chi(t) \to \chi_n(t')$, $\chi(t+T_R) \to \chi_{n+1}(t')$ and $m(t) \to m_n(t') = M\left\{1 - \cos\left[\Omega_M(t' - \theta n T_R)\right]\right\}$, being $\theta = (T_M - T_R)/T_R$. All the temporal derivatives are redefined as $\partial_t \to \partial_{t'}$.

Now we want to pass from the discrete to the continuum limit transforming the map into a differential equation. For this purpose we define the continuous slow time variable T' and the continuous fields $X(T', t')$ such that $X'(T' = nT_R, t') = \chi_n(t')$; we also impose the asynchronous boundary conditions $X'(T', t' + T_R) = X'(T', t')$ which follows from $\chi_n(t' + T_R) = \chi_{n+1}(t')$. The right hand side of Eq.7.28 can be hence written as $F'(T' + T_R, t') - F(T', t')$, that in the limit of sufficiently small $\Delta_R \mathcal{F}$ can be approximated as $T_R \partial_{T'} F'(T', t')$. In this way we obtain the coupled differential equations:

$$T_R \partial_{T'} F' = (lG' - l - m')F' + \delta T_R \partial_{t'} F' + l\hat{L}' G' F' \tag{7.30}$$

$$T_G \partial_{t'} G' = r - G'\left(1 + |F'|^2\right) - Re\left[F'^* \hat{L}'(G'F')\right] \tag{7.31}$$

where $m'(T', t') = M\left\{1 - \cos\left[\Omega_M(t' - \theta T')\right]\right\}$ and $\hat{L}' = -\Omega_G^{-1}\partial_{t'} + \Omega_G^{-2}\partial_{t'}^2$.

Eq.7.30 and Eq.7.31 exhibit two inconvenient features, (i) the fields satisfy non synchronous boundary conditions $X'(T', t' + T_R) = X'(T' + T_R, t')$ and (ii) the modulation function m' moves with speed θ. Both undesired features can be eliminated by introducing the new time variables $T = T' + t'$ and $\tau = t' - \theta T'$ and the new fields $X(T, \tau) = X(T', t')$. In this fashion the fields obey the periodic boundary conditions $X(T, \tau) = X(T, \tau + T_M)$ which confine the problem in the interval $\tau \in (-T_M/2, +T_M/2)$.

Following the chain rule for differentiation we have

$$\partial_{T'} \rightarrow \partial_T - \theta\partial_\tau,\ \partial_{t'} \rightarrow \partial_T + \partial_\tau \tag{7.32}$$

and using the fact that $\theta = l\tau_d/T_R$, after defining $\tau_d = (T_M - T_R)/l$ and $\mu = M/(2l) =$ the equations for the field and the gain read:

$$l^{-1}T_R\partial_T F = (G - 1 - \mu^2\Omega_M^2\tau^2)F + (\tau_d + l^{-1}\delta T_R)\partial_\tau F + \hat{L}_\tau(GF) \tag{7.33}$$

$$T_G(\partial_T + \partial_\tau)G = r - G\left(1 + |F|^2\right) - Re\left[F^*\hat{L}_\tau(GF)\right] \tag{7.34}$$

with $\hat{L}_\tau = -\Omega_G^{-1}\partial_\tau + \Omega_G^{-2}\partial_\tau^2$. In the right hand side of both equations we have approximated $[\partial_T + \partial_\tau](GF) \approx \partial_\tau(GF)$ because the electric field changes only slowly from round trip to round trip but can vary substantially in the same roundtrip (typically it will be very small far away from the modulator minimum losses point, it will grow substantially in the vicinity of such point before decaying in a similarly fast fashion). In order to gain a physical insight into the equations we split the gain variable in a fast and slow part $G(T,\tau) = \overline{G}(T) + g(T,\tau)$ where $\bar{G}$ is the average gain over one modulation period. Note that such average gain as well as other average quantities $\overline{X}$ appearing in the next equations are computed as follows: $\overline{X}(T) = \frac{1}{T_M}\int_{-T_M/2}^{T_M/2} X(T,\tau)d\tau$. Coming back to our gain-splitting procedure, $g(T,\tau)$ has zero average but can potentially vary significantly in one modulation period. In the left hand side of the equation for g the term $\partial_T g$ can be neglected because it is much smaller than $\partial_\tau g$; indeed as mentioned above the changes of the fields from round trip to round trip are considered small while variations of the pulse intensity in the vicinity of the modulator minimum losses point and consequently of the gain close to the pulse peak are substantial. Hence we have

$$l^{-1}T_R\partial_T F = (\overline{G} - 1 - \mu^2\Omega_M^2\tau^2 + \tau_d\partial_\tau + \overline{G}\Omega_G^{-2}\partial_\tau^2)F + gF + \hat{L}_\tau(gF) \tag{7.35}$$

$$T_G d_T\overline{G} = r - \bar{G}\left(1 + \overline{|F|^2}\right) - \overline{g|F|^2} - \overline{G}Re\left[\overline{F^*\hat{L}_\tau F}\right] - Re\left[\overline{F^*\hat{L}_\tau(gF)}\right] \tag{7.36}$$

$$T_G\partial_\tau g = \overline{G}\left(\overline{|F|^2} - |F|^2\right) + \overline{g|F|^2} - g|F|^2 - g - \overline{G}Re\left[F^*\hat{L}_\tau F\right] +$$

$$+ \overline{G}Re\left[\overline{F^*\hat{L}_\tau F}\right] - Re\left[F^*\hat{L}_\tau(gF)\right] + Re\left[\overline{F^*\hat{L}_\tau(gF)}\right]. \tag{7.37}$$

Note that we have approximated also $\delta T_R \approx \frac{aw}{2\Omega_G}\bar{D}$. We motivate here the reason. $\delta T_R = w(v^{-1} - v_0^{-1})$ can be computed from the dispersion relation of the medium. If we have a monochromatic wave $f(z,t) = f_0(z)e^{-i\omega t}$ propagating through the amplifying medium, then the resulting polarization will have the form $p(z,t) = p_0(z)e^{-i\omega t}$ let's consider D for the moment as a free variable. Plugging those definitions into the AB equations gives that $f(z)$ should be of the form $f(z) = f(0)e^{ik(\omega)z}$ with

$$k(\omega) = \left(\frac{\omega}{v_0} + \frac{aD}{2}\frac{\Omega_G\omega}{\Omega_G^2 + \omega^2}\right) - i\frac{aD}{2}\frac{\Omega_G^2}{\Omega_G^2 + \omega^2}. \tag{7.38}$$

The group velocity $v = (dk/d\omega)^{-1}_{\omega=0}$ is determined by the real part of $k(\omega)$ while the absorption/amplification by the imaginary one; note that $\omega = 0$ is the resonance frequency. It is easy to see that hence $\delta T_R = \frac{aw}{2\Omega_G}D$. When mode-locking is considered, f is a superposition of monochromatic waves and hence D is not constant any more. D can be split into its average value over a modulation period, $\overline{D}$, and a remainder. Such remainder can be considered small and has null average (by definition); its effect on the pulse velocity should be much less than that of $\overline{D}$ and affect mainly its shape; hence we can write for the multimode operation $\delta T_R \approx \frac{aw}{2\Omega_G}\overline{D}$. Even if $\overline{D}$ still depends on time, this dependence is very slow (null in the steady state). In the transient regime (or in cases of pulse instability) $\overline{D}$ has some inter-roundtrip variation, but not intra-roundtrip, hence $\overline{D}$ is a constant during the time taken by the pulse to cross the medium and the formal solution of Eq.7.21 is valid.

By checking that approximating $\hat{L}_\tau \approx -\partial\tau(gF)$ and neglecting the term $\hat{L}_\tau(gF)$ still preserves the key coherent feature such as the Risken-Nummedal-Graham-Haken instability (RNGHI), we can neglect higher order terms in the equations for $\overline{G}$ and g. Within this approximation $\overline{F}^*\hat{L}_\tau F = -(\Omega_G^{-1}/2)\overline{\partial_\tau|F|^2} = 0$ thanks to the periodic boundary conditions. In this way we arrive at the final master equation for active mode-locking in lasers:

$$l^{-1}T_R\partial_T F = (\overline{G} - 1 - \mu^2\Omega_M^2\tau^2 + \tau_d\partial_\tau + \overline{G}\Omega_G^{-2}\partial_\tau^2)F + gF + \hat{L}_\tau(gF) \tag{7.39}$$

$$T_G d_T\overline{G} = r - \overline{G}\left(1 + \overline{|F|^2}\right) - \overline{g|F|^2} \tag{7.40}$$

$$T_G\partial_\tau g = \overline{G}\left(\overline{|F|^2} - |F|^2\right) + \overline{g|F|^2} - g|F|^2 - g + \overline{G}\Omega_G^{-1}Re\left[F^*\partial_\tau F\right]. \tag{7.41}$$

If we neglect the terms involving the fast gain g, then HME is recovered:

$$l^{-1}T_R\partial_T F = (\overline{G} - 1 - \mu^2\Omega_M^2\tau^2 + \tau_d\partial_\tau + \overline{G}\Omega_G^{-2}\partial_\tau^2)F \quad (7.42)$$

$$T_G d_T\overline{G} = r - \overline{G}\left(1 + \overline{|F|^2}\right). \quad (7.43)$$

It is worth recalling that HME admits the following Gaussian pulse solution:

$$F(\tau) = \sqrt{I_p}e^{i\phi}e^{-\frac{1}{2}\left(\frac{\tau-\tau_0}{\tau_p}\right)^2} \quad (7.44)$$

where the peak intensity is given by $I_p \approx \sqrt{2\mu\Omega_G T_R}(r/r_{th} - 1)$, the width $\tau_p = (\mu\Omega_G\Omega_R)^{-1/2}$ and the position of the pulse by $\tau_0 = -(\tau_d\Omega_G)/(2\mu\Omega_R)$; ϕ is an arbitrary phase. The threshold r_{th} is equal to 1.

Before proceeding to a detailed investigation of mode-locking dynamics, it is worth mentioning that is possible to show that a linear stability analysis of the set of Eqs.7.39, 7.40 and 7.41 (without the modulator terms) predicts instability of the homogeneous solution $F_s = \sqrt{r-1}$, $\overline{G}_s = 1$, $g_s = 0$ with respect to the following modulation modes $\delta F = \delta F_0 e^{\lambda lT/T_R + iq\tau}$ and $\delta g = \delta g_0 e^{iq\tau}$, being $q = \alpha\gamma\Omega_G$ and $\gamma = (T_G\Omega_G)^{-1/2} << 1$. The normalized eigenvalue λ, at the second order expansion in the parameter γ reads

$$\lambda = 2i(r-1)\alpha/\gamma - \left[\alpha^4 - 3(r-1)\alpha^2 + 2r(r-1)\right]\alpha^2\gamma^2. \quad (7.45)$$

Its real part is positive for wavevectors α satisfying $\alpha_- < \alpha < \alpha_+$ with

$$2\alpha_\pm^2 = 3(r-1) \pm \sqrt{(r-1)(r-9)} \quad (7.46)$$

which is the condition for the RNGHI in class-B lasers [69].

7.3 The fast gain and the differences with Haus

As a first result we can observe that the new master equation reproduces the HME results in the limit $T_G >> T_R$ which is typical for instance of solid state or gas lasers. However if $T_G \approx T_R$ or $T_G < T_R$ than our model predicts a very different solution. It is important to stress that in the limit $T_G >> T_R$, $g(\tau)$ is very small, while for $T_G \approx T_R$ or $T_G < T_R$, $g(\tau)$ acquires a more significant magnitude. We can hence ascribe to

the fast gain component arising from the coherent light matter interaction, neglected in the original approach by Haus, the qualitative change in the pulse shape when the condition $T_G >> T_R$ doesn't hold any more (See Fig. 7.1).

It is important to stress that in HME if no detuning is applied then the pulse will always be located at the minimum losses point of the modulator. We see that when T_G approaches T_R this is not anymore true, the fast gain medium exerts a force on the pulse shifting it towards negative temporal coordinates, this means that the maximum of the pulse is located before the minimum losses point of the modulator. The pulse stationary position is determined by the balance between the modulator and the gain "forces".

By applying a certain amount of detuning $\Delta = T_M^{-1} - T_R^{-1}$ we can maximize the pulse intensity and indeed we see that this occurs when the amount of applied detuning is large enough to bring the pulse at the $\tau = 0$ coordinate. However we observe that the pulse in this case still preserves a slight asymmetry in its tails hence deviating from the Gaussian shape predicted by Haus theory. Note that despite a detuning τ_d is already present in the equations we have defined the new one Δ in order to ease the comparison with experimental results.

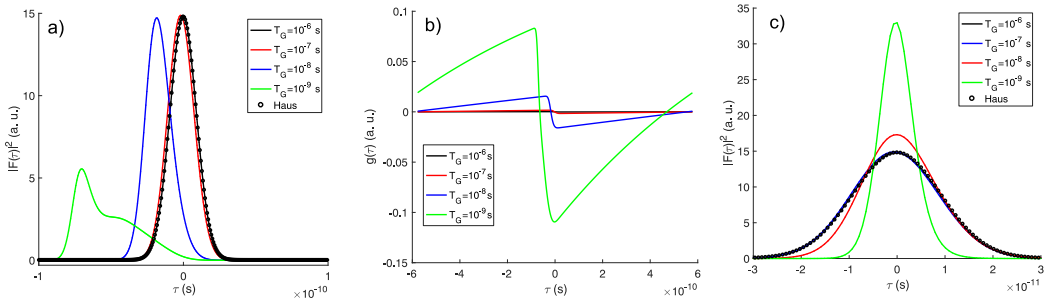

Figure 7.1: In a) the pulses obtain from the coherent master equation are compared with HME for different values of T_G showing an asymmetry arising for small T_G. In b) the corresponding value of the fast gain is shown: $g(\tau)$ increases in magnitude for fast gain media, e.g. by decreasing T_G. In c) applying a detuning we can optimize the pulse intensity counteracting the gain medium force that pushes the pulse away from the modulator minimum losses position; a very slight asymmetry in the pulses still persists. Parameters used are $\Omega_G = 1.1 \cdot 10^{12}$ s^{-1}, $t_R = 1.155 \cdot 10^{-9}$s, $l = 0.6$, $M = 1.2$, $r = 1.3$. The detuning Δ applied in c) to center the pulses is respectively 283.32 kHz for $T_G = 10^{-9}$ s, 69.5 kHz for $T_G = 10^{-8}$ s, 5.75 kHz for $T_G = 10^{-7}$s and 0 for $T_G = 10^{-6}$s.

7.4 The experimental validation of the coherent master equation predictions

The predictions of the new master equation have been compared with experimental results obtained in a ring cavity semiconductor laser, mode locked through amplitude modulation. The experimental setup is depicted in Fig.7.2. It consists in a semiconductor optical amplifier emitting at 970 nm, having carrier lifetime estimated in the order of 10 ns, with an extended cavity constituted by an optical fibre. The total cavity length is about 9 m. The unidirectionality of the propagation is guaranteed by the presence of an optical isolator, the mode-locker is an active electro optical modulator driven at a frequency of around 866 MHz, corresponding to the 25-th harmonic of the cavity free spectral range. This leads to the generation of 25 pulses in the cavity. The choice of such an extremely long cavity was motivated by the will of exploring more extreme scenarios that could emphasize the limitations of Haus theory and the potentialities of the coherent master equation. In order to justify the application of

Figure 7.2: The experimental setup: a semiconductor gain medium (OA) is used as gain medium and the extended cavity is provided by an optical fibre for a total cavity length of 9 m, the modulator is denoted by the acronym (MZM). An isolator guarantees the unidirectionality of the ring cavity.

our model, derived for fundamental mode-locking, to the analysis of these experimental results where harmonic mode-locking is achieved; we can consider the fact that the various pulses coexisting in the cavity do not interact at all, due to the strong modulation of losses and hence regard them as virtually belonging to different independent lasers [70]. We can hence just consider in the simulations of Eqs.7.39, 7.40 and 7.41 that $T_R = T_{Rexp}/25$ where T_{Rexp} is the true experimental cold cavity round trip time: $T_{Rexp} = 9\text{m}/c$. The other parameters we have chosen reflect the remaining features of

the experimental setup.

The stationary state pulsed solutions have been plotted versus the amount of modulator detuning for both the experimental case and the numerical simulations, showing a good agreement. We have also compared the tails of the high intensity pulses in both cases showing that they deviate significantly from the Gaussian shape. Finally we observe that the detuning interval over which stable pulses can be found is very similar in simulations and in the experiment. It is important to tell that in experiment it is not known which pulse corresponds to the zero detuning case. Hence the zero of the detuning Δ in experiment (Fig.7.3) is arbitrary. An important fact predicted by our model is that the action of detuning is not a symmetric one. In the HME indeed applying a certain amount of positive detuning or the same amount of negative detuning will have no effect on the pulse shape and simply shifts is position by a quantity proportional to the magnitude of the detuning itself; detuned pulse solutions are simply shifted Gaussians [62]. In our model things are different because the sign of the detuning matters substantially: the pulse shape is dramatically different depending on which sign of the detuning is chosen. This fact is due to the asymmetry introduced by the fast gain action. Mathematucally this fact is described by the first derivative of gF in Eq. 7.39.

The results depicted in Fig.7.3 show a quantitative agreement between theory and experiments concerning the detuning interval over which pulses are stable in simulations. The theory captures qualitatively all the relevant features observed in experiment: asymmetry of the detuning action, asymmetric pulses, and pulses with bump (See also Fig.7.4).

We can notice that the pulse duration is typically much shorter in experiment than in theory. While the theory reproduces perfectly the pulses shapes in various mode-locking regimes, as shown in Fig.7.4, the quantitative agreement concerning the pulse duration is present only for the optimized *sech*-like pulse (Fig.7.4 c) and d)). When the pulse deviates significantly from *sech* shape the duration predicted by the theory is much longer than in experiment (still being the predicted duration of the same order of magnitude). The broadening in experiment is limited by some effect which is not accounted properly in the theory. Furthermore the pulse with the clear bump observed has the highest intensity among the three in experiment but not in the theory. The

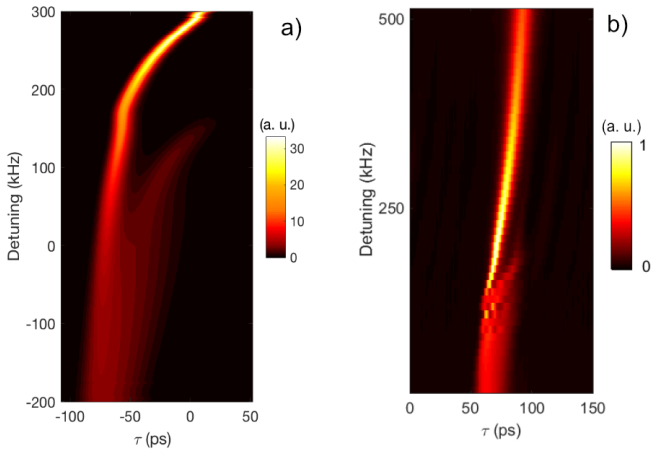

Figure 7.3: The intensity of the stable pulse in the stationary state obtained numerically a) is depicted for different values of the modulators detuning Δ and is compared with experimental results b). In both cases only the detuning range where stable pulses exist has been plotted showing a good agreement between theory and experiment. The theory captures the essential features of mode-locking observed in experiment: asymmetric effect of the detuning, pulse with the bump, typical pulse duration and range of detuning where pulses are stable. Parameters used in the simulations are $\Omega_G = 1.1 \cdot 10^{12}$ s^{-1}, $t_R = 1.155 \cdot 10^{-9}$s, $l = 0.6$, $M = 1.2$, $r = 1.3$ and $T_G = 10^{-9}$ s.

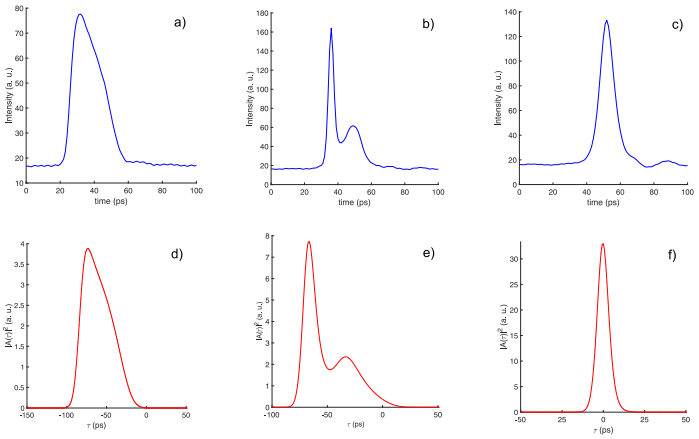

Figure 7.4: Three paradigmatic pulse shapes observed experimentally a), b) and c) are compared with their theoretically predicted counterparts: d), e) and f). A good agreement is present concerning the shape of the pulses, while the duration is overestimated in theory in d) and e). The ordinate axes in experimental data refer to the photocurrent measured by the detector and the deep after the right pulse tail in c) is an effect due to the detector. Parameters used in the simulations are $\Omega_G = 1.1 \cdot 10^{12}$ s^{-1}, $t_R = 1.155 \cdot 10^{-9}$s, $l = 0.6$, $M = 1.2$, $r = 1.3$ and $T_G = 10^{-9}$ s; Δ has been taken equal to -115.03, 57.512 and 283.32 kHz in d), e) and f) respectively.

above mentioned discrepancies can be potentially attributed to many physical effects that are not described in our model: the fibre group velocity dispersion and Kerr nonlinearity or the linewidth enhancement factor (alpha-factor) of the semiconductor

laser gain medium. Furthermore it may be that the parabolic approximation of the modulator transmission function is accurate only in the vicinity of the minimum losses point, if in experiment the losses increase with a faster law than a parabolic one, then such fact could explain the longer pulse duration observed in the theory for those pulses which are not close to the modulator minimum losses point.

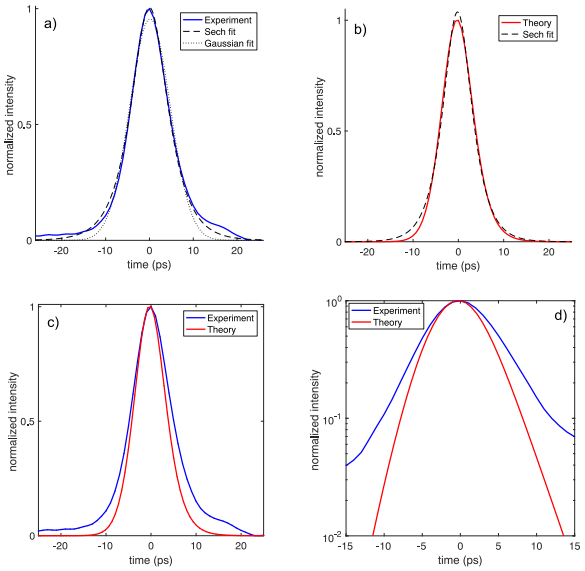

Figure 7.5: The normalized intensity of the most symmetric experimental pulse with Gaussian and hyperbolic secant fit is depicted in a): the hyperbolic secant fits better the experimental results, but cannot account for the skewness. In b) the normalized intensity calculated theoretically is fitted by an hyperbolic secant function. In c) the normalized intensities obtained in experiment and in the theory are compared (plot in linear scale). In d) the same quantities plotted in c) are represented in logarithmic scale to emphasize the skewness. The data used correspond to Fig.7.4 c) and f).

Another important feature of the pulses generated through active mode-locking outside the Haus limit is their skewness which persists even when the pulses are the closest possible to a symmetric shape. The skewness is predicted by the theory and observed experimentally (See Fig.7.5). The hyperbolic secant is the function that better describes the data, anyway being symmetric doesn't account for the skewness. It is in the end relevant to recall the fact that we are are applying a theory valid for fundamental mode-locking to describe harmonic mode-locking. An accurate modeling aiming at the exact reproduction of the experimental results should most likely include the physical effects mentioned above. Anyway, at the moment we can notice that the our model captures remarkably well qualitatively and in various circumstances even quantitatively the essential physics of laser mode-locking outside of the Haus limit.

The above presented results show that coherence in light-matter interaction, an often neglected feature in applied laser physics, can play significant roles in mode-locking by affecting in a crucial way the shape and the dynamics of pulses. This is due to the fact that coherence entails the presence of a fast gain component that varies on a typical pulse duration time scale and becomes physically relevant when the inversion life time is comparable or even shorter than the cavity round trip time. With the derivation of the new master equation a substantial innovation in the theory of mode-locking in lasers has been provided. Our coherent master equation, whose predictions have been confirmed experimentally, can be potentially generalised to a variety of mode-locking mechanisms and can include various physical effects such as Kerr nonlinearity, group velocity dispersion, linewidth-enhancement factor for semiconductor lasers gain media or even the presence of an intracavity saturable absorber. Our model could be particularly promising in describing mode-locking in semiconductor lasers but also in actively mode-locked quantum cascade lasers with external cavity, which are good candidates for the generation of frequency combs in the mid-infrared frequency range[71, 72]. Quantum cascade lasers have a gain lifetime of the order of the tens of ps, hence they can significantly violate HME validity assumptions; up to now they have been modeled by the heavy formalism of the full AB equations which is highly unpractical and not amenable to a straightforward analytical treatment [73, 74]. Furthermore in such lasers active mode-locking is preferred compared to passive one due to the very fast gain dynamics that prevents obtaining stable pulses with saturable absorbers; the coherent master equation can be potentially generalised to describe such systems even when the pump current, and not the losses, is modulated.

8 Synchronization and disorder-induced localization in coupled excitable lasers

8.1 Excitability in semiconductor lasers with a saturable absorber

Excitability is an interesting phenomenon common to various dynamical systems but most known in biology and especially associated to the spiking activity of the neuronal cells[75, 76]. Excitability takes place when a system originally at a stationary state exhibits an all-or-nothing response to a strong enough perturbation, undergoing a large excursion in phase space and generating a spike-like signal. After the generation of the spike the system relaxes back to the stationary state and, after a so called refractory time, is hence ready to be excited again. Excitability is an emerging research paradigm in nonlinear optics too. Probably the first theoretical prediction of excitability in lasers dates back to when Dubbeldam, Krausskopf and Lenstra showed analytically and with help of numerical simulations that a semiconductor lasers with an intracavity saturable absorber can exhibit excitability in a parameter range realistically accessible for experimental observation[77]. The excitable behavior is due to the fact that the laser off-solution is an attractor close to a saddle-point: a strong enough perturbation can hence bring the system across the saddle point and subsequently back to the off-solution attractor through a limit cycle. Such prediction has been later verified experimentally by Barbay and co-authors [78]. A variety of studies on excitability in lasers and amplifiers has been undertaken. It is particularly worth mentioning that semiconductor lasers with saturable absorber support the existence of temporally excitable spatially localized cavity solitons [79]; also they allow the generation of pulsating excitable solitons, and exhibit the intriguing potentiality for pulse reshaping, due to the fact that the

output pulses features are independent of the intensity and duration of the triggering perturbations [80]. Furthermore it has been demonstrated that semiconductor lasers with saturable absorber can be used in order to exploit excitability for coincidence detection and for creating optical switches but also to achieve spatiotemporal pattern recognition [81, 82, 83].

The first studies of collective dynamics in a population of coupled excitable semiconductor lasers with saturable absorber, including both the synchronization properties and the localization of excitability in presence of disorder in the coupling strengths have been presented in two recent publications [84, 85] whose most relevant points will be summarized in this Chapter.

Let's first recall, by help of numerical simulations, how the single semiconductor laser with saturable absorber exhibits excitability following the original work by Dubbeldam and co-authors[77]. They considered the rate equation model for the normalized field intensity I, gain G and absorption Q:

$$\begin{aligned} \dot{I} &= (G - Q - 1)I + \sigma, \\ \dot{G} &= \gamma(A - G - IG), \\ \dot{Q} &= \gamma(B - Q - aQI). \end{aligned} \tag{8.1}$$

A describes the bias current of the gain, B the absorption, and a is the differential absorption relative to the differential gain. γ is the relaxation rate of the gain which is assumed to be equal to the one of the absorber and is in general much smaller than unity. σ is a small additive delta correlated ($\langle\sigma(t_1)\sigma(t_2)\rangle = \sqrt{2D}\delta(t_1 - t_2)$) noise term with amplitude D that is the key element in triggering excitability.

If the laser is kept in the off-solution below threshold but very close to it, then additive noisy perturbations may trigger the stimulated emission process which will rapidly deplete the gain with consequent emission of a giant light pulse. In this way the gain medium is depleted and a refractory time is necessary to restore the population inversion. During the refractory time pulses cannot be emitted. Once the inversion has been restored thanks to the pumping mechanism the laser is ready to be excited again.

The excitable behavior can be appreciated from a phase space plot in the $(G - I)$ plane too (See Fig.8.2). Another relevant feature of the excitable laser is the presence

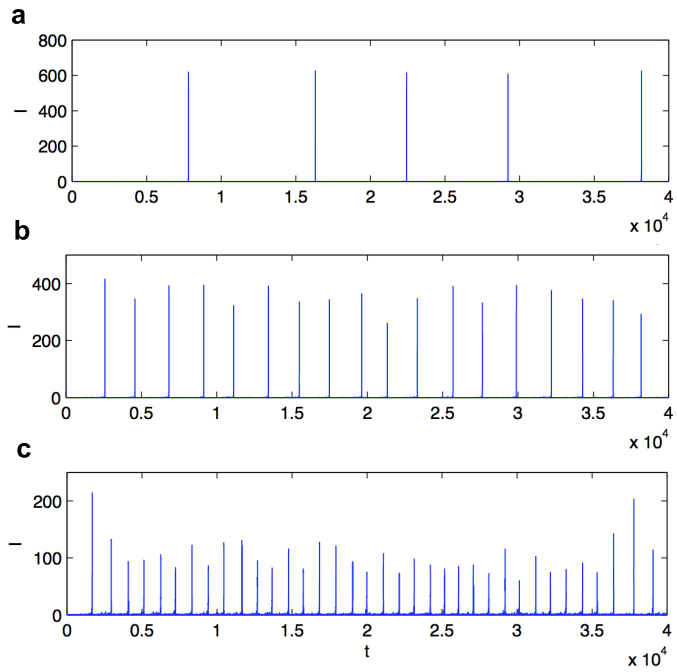

Figure 8.1: Excitability in semiconductor laser with saturable absorber: a quasi-periodic spiking activity is observed. Increasing the noise strength the repetition rate is enhanced and the intensity of the pulses is reduced. Parameters used are A=6.5, B=5.8, a=1.8, $\gamma = 10^{-3}$ while D=0.004, 0.015 e 0.04 in a), b) and c) respectively.

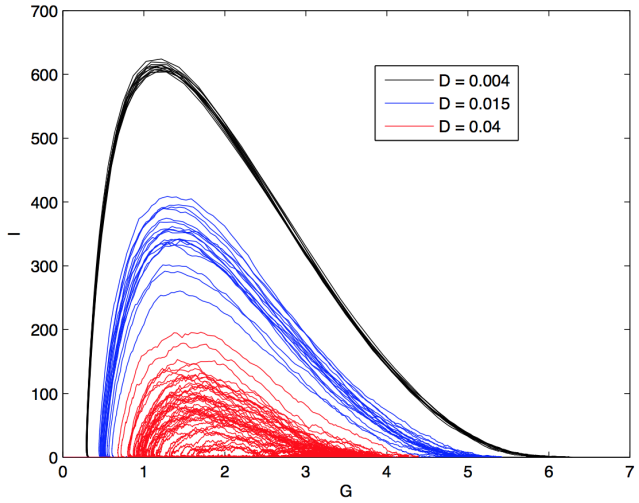

Figure 8.2: The intensity I is plotted versus gain G for many firing events: after firing (large value of I) the refractory time is determined by the recovery time of the gain. For stronger noise intensity D (values shown in the inset), the refractory time is reduced and the pulses peak intensity exhibit larger fluctuations. Parameters used are A=6.5, B=5.8, a=1.8 and $\gamma = 10^{-3}$.

of the coherence resonance phenomenon. Coherence resonance means actually that it exists an optimum value of the noise strength that maximizes the coherence of the system: for lower or larger values a worse coherence is observed. Coherence resonance

can be measured by plotting the normalized jitter R of the pulse train versus noise strength D. The normalized jitter is defined as $R = \sigma_T/\langle T\rangle$ where σ_T is the standard deviation and $\langle T\rangle$ the average temporal interval between consecutive pulses. Numerical simulations that reproduce the results of the coherence resonance obtained for the first time in [77] are depicted in Fig. 8.3. Another important feature of the excitable

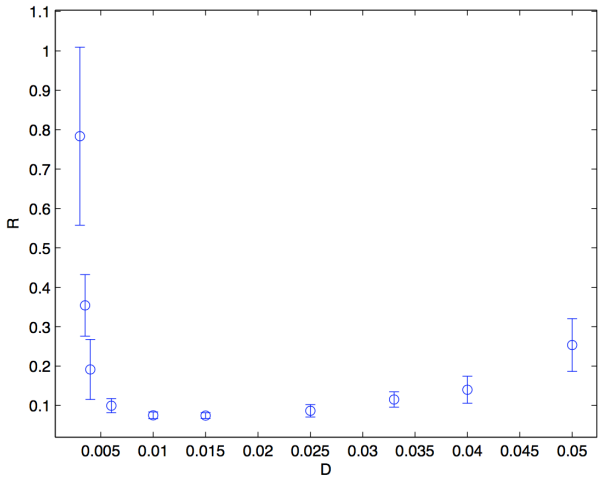

Figure 8.3: The normalized jitter R exhibits a minimum when plotted versus noise strength D. Parameters used are A=6.5, B=5.8, a=1.8 and $\gamma = 10^{-3}$

semiconductor laser with saturable absorber, which is worth mentioning but that will not be discussed here in detail, is its ability to perform pulse reshaping, e.g. to give the same pulse output independently on the temporal shape of the input perturbation [77, 80].

8.2 Synchronization and array-enhanced coherence resonance

I present now some recent results about the collective dynamics of coupled excitable lasers.

Initially we have considered a one-dimensional array of n coupled identical semiconductor lasers with saturable absorber. The i-th laser's normalized dynamical variables, complex electric field amplitude F_i, inversion G_i, and absorption Q_i obey the following set of coupled nonlinear equations (the dot denotes temporal derivative):

$$
\begin{aligned}
\dot{F}_i &= \frac{1}{2}(G_i - Q_i - 1)F_i + \sigma_i + \frac{K}{2}\left[F_{i+1} + F_{i-1} - 2F_i\right], \\
\dot{G}_i &= \gamma_i(A_i - G_i - I_i G_i), \\
\dot{Q}_i &= \gamma_i(B_i - Q_i - a_i Q_i I_i).
\end{aligned} \tag{8.2}
$$

The subscript i denotes the laser number, while $I_i = |F_i|^2$ is the field intensity, A_i the bias current of the gain, a_i the differential absorption relative to the differential gain, B_i the background absorption. γ_i is the absorber and gain decay rate that is considered to be smaller than unit. This fact gives to the field amplitudes F_i the role of the slow variables of the system. The normalization is the one given in [86]. σ_i is a delta correlated Gaussian noise term with $\langle \sigma_i(t_1)\sigma_j(t_2)\rangle = \sqrt{2D}\delta(t_1 - t_2)\delta_{ij}$: as it has been mentioned before, such noise term provides the necessary perturbations to the close to threshold off-solution in order to induce the excitable behavior.

Concerning the coupling term K, lossy coupling has been considered, describing a non-delayed mutual and reciprocal injection between closest neighbor lasers. The phenomenological coupling term K describes the exchange of radiation between first neighbor lasers scaled to the intensity damping rate of the single laser and in this section we have considered the couplings identical for all lasers. The interaction can be physically implemented using semitransparent mirrors with the desired transmittance, which couple light from one laser cavity to the adjacent ones. Periodic conditions at the array boundaries have been assumed. During all the study the value of K has been chosen to be constant along the whole array. The presence of the coupling induces the appearence of a discrete one dimensional Laplace operator that acting as an effective diffusion spreads the local electric field intensity gradients which form in the laser array induced by the stochastic fluctuations caused by the random noise. In order to study the synchronization properties of the array we have first considered various numbers of coupled identical lasers described by the following set of parameters which hold for all the results reported in this section: $A_i = 6.5$, $B_i = 5.8$, $a_i = 1.8$ and $\gamma_i = 10^{-3}$ $\forall i$. With K=0 the single laser exhibits excitability for $A_i \in [6.06, 6.8]$[77]. If we numerically simulate the dynamics of a certain number of coupled lasers and compare the emitted intensity traces with the uncoupled situation we can immediately observe some signif-

icant qualitative differences: When the lasers are coupled they emit pulses in a highly synchronized fashion (Fig. 8.4). This fact motivates the need of a more quantitative

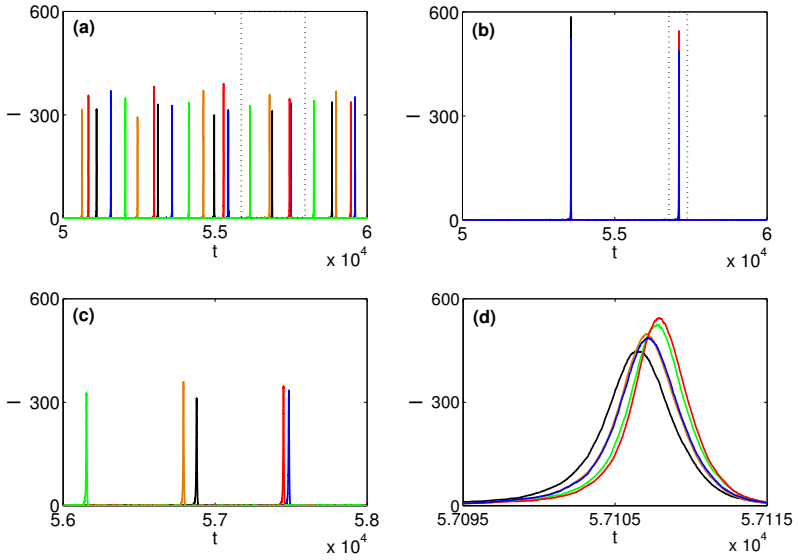

Figure 8.4: a): an example of intensity evolution for 5 uncoupled lasers, different colors correspond to different lasers, obtained for $D = 0.015$ and $K = 0$. In b) the simulation results obtained with the same parameters as in a) but with $K = 0.2$ shows a clear example of temporal synchronization. c) and d): zooms of the regions indicated by a dashed-line box for the uncoupled a) and coupled b) configuration respectively.

study of the synchronization There are many way of quantifying synchronization, as far as the temporal synchronization is concerned, we have followed here the one used in a similar study of coupled FitzHugh-Nagumo oscillators [87] and proposed originally in [88]. To each oscillator a phase can attributed:

$$\phi_i(t) = \frac{t - \tau_k}{\tau_{k+1} - \tau_k} + 2k\pi \tag{8.3}$$

where τ_k is the time of the k-th firing event, i.e. the position in time of the k-th pulse. In order to describe the degree of synchronization the following quantity has been considered:

$$s_i = \sin\left(\frac{\phi_i - \phi_{i+1}}{2}\right)^2 \tag{8.4}$$

which after performing a spatiotemporal average gives the S indicator that provides a measure of the synchronization degree

$$S = \lim_{T\to\infty} \frac{1}{T} \int_0^T \quad \frac{1}{n} \sum_{i=1}^{n} s_i \Bigg) \, dt. \tag{8.5}$$

The maximum synchronization occurs when $S = 0$ while in complete absence of synchronization $S = 0.5$. In Fig. 8.5a)-d) we have depicted $\log_{10}(S)$ as a function of coupling strength and noise amplitude for different values of n. As far as intensity synchronization is concerned the linear correlation coefficient ρ for the intensity pulse peak of closest in time pulses of consecutive lasers in the chain has been computed. The results are depicted in Fig. 8.5e)-h). In order to take into account the stochasticity of the system, for each quantity of interest a map obtained from an average of 10 independent realizations has been plotted. Each realization consists of a simulation performed for a temporal interval of length T=100000. The white areas in the plots correspond to situations where less than ten pulses were observed. Such procedure and conditions apply to Figs. 8.6 and 8.7 too.

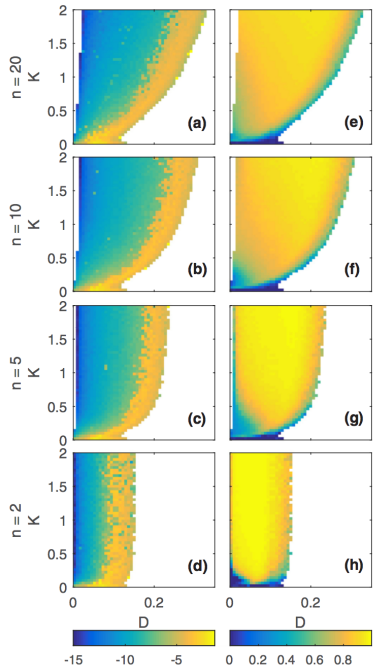

Figure 8.5: $\log_{10}(S)$ is plotted in the (K-D) plane for various values of n, panels a)-d). The minimum synchronization theoretically achievable corresponds to $\log_{10}(S) \approx -0.69$. The intensity linear correlation coefficient ρ_I is depicted, panels in panels e)-h).

Results similar to those illustrated in Fig. 8.5 can be obtained by considering a

population of lasers each one having a different value of pump parameter A_i that has been chosen as uniformly distributed random number in the interval $[6.3, 6.7]$. This choice basically guarantees that all the lasers are in the excitability regime, but each one of them would fire with a different frequency (repetition rate of the pulse train) if considered separated from the others. What indeed occurs is that synchronization is robust also for different coupled lasers with a small reduction of the synchronization area (See Fig.8.6). This fact is relevant towards the experimental observation of the phenomena considered here, since in the real world imperfections are present and differences in the pump parameters of the lasers are unavoidable.

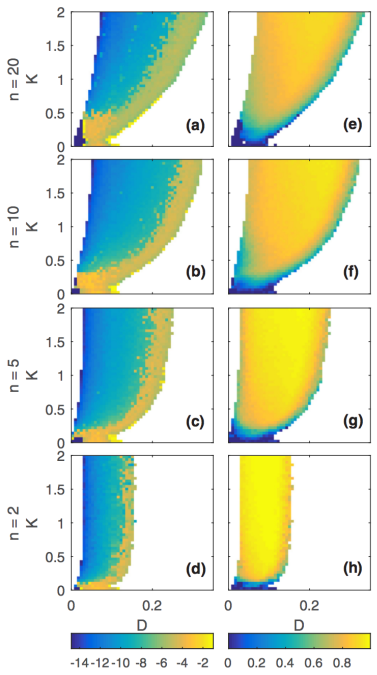

Figure 8.6: The analogous of Fig.8.5 but for a population of nonidentical lasers. The large inhomogeneity among different lasers implies, as intuitively expected, the necessity of a stronger coupling in order to achieve the same degree of synchronization compared to the case of identical lasers.

Another important aspect that is worth mentioning is how the collective behavior influences the single laser performance. We can indeed notice improved performances of the single laser coherence in terms of reduced jitter in its generated pulse train and reduced variance in the pulse peaks heights (see Fig.8.7). Concerning the single laser jitter an *array-enhanced coherence resonance* [87, 89] can be observed: the interval of noise strength that excites a low jitter pulse train becomes larger by increasing the number of coupled lasers.

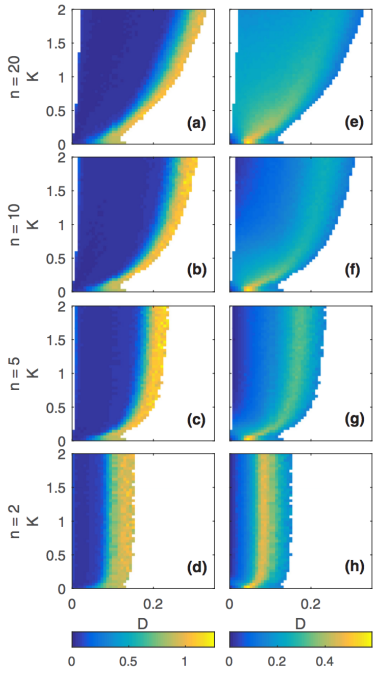

Figure 8.7: The normalized jitter R, panels a)-d), and intensity peak standard deviation σ_I, panels e)-h), are plotted as function of coupling strength K and noise intensity D in left and right column respectively for values of n indicated on the figures. Array-enhanced coherence resonance is observed.

8.3 Disorder-induced localization of excitability

The second phenomenon that is presented in this Chapter is the localization of excitability in an array of coupled lasers with saturable absorber, induced by the presence of disorder in the coupling strengths of the array [85]. Exponential localization of the electronic wave function in an atomic lattice, caused by disorder has been predicted by Anderson in a seminal paper published in 1958 [90]. Such localization of the electronic wave function being associated with the wave phenomenon of quantum interference. Anderson's paper has initiated an entire research field and what has been called *Anderson localization* is now an active research area which encompasses a variety of physical systems ranging from solid state physics [91], its original starting point, to acoustics [92], microwaves [93], Bose-Einstein condensates [94] and optics. In optics, phenomena connected with localization induced by disorder has been extensively studied for instance in [95] and [96], where light localization propagating in semiconductor powders takes place. Other examples include the inhibition of light diffraction and consequent localization in disordered photonics crystals [97, 98] and in waveguide arrays [99, 100].

The disorder causing localization can be diagonal, as in the case of the original work by Anderson, if the energy of the individual lattice sites is randomized; or out-of-diagonal, in case where the randomness appears in the coupling strength between neighbor lattice sites[101]. The latter is the case studied in [99, 100]. As I have already mentioned before, excitability in optics is a research topic that is acquiring substantial momentum due to the possible applications in computational tasks, detection and simulation of neural networks dynamics. It is hence quite natural to investigate wether the excitable waves generated in arrays of coupled lasers are subject or not to localization in presence of disorder.

Let's look hence at the impact of disorder on the propagation of excitable waves in an array of coupled lasers with saturable absorber where randomness in the coupling strengths is present. We consider again a 1D chain of lasers with local nearest neighbor couplings and periodic boundary conditions described by the model:

$$\begin{aligned}
\dot{F}_i &= \frac{1}{2}(G_i - Q_i - 1)F_i + \sigma_i + \frac{K_{i,i+1}}{2}F_{i+1} + \frac{K_{i,i-1}}{2}F_{i-1} - \left(\frac{K_{i,i-1}}{2} + \frac{K_{i,i+1}}{2}\right)F_i \\
\dot{G}_i &= \gamma_i(A_i - G_i - I_i G_i) \\
\dot{Q}_i &= \gamma_i(B_i - Q_i - a_i Q_i I_i)
\end{aligned} \tag{8.6}$$

which are basically Eqs.8.2 with a more accurate specification of the couplings allowing for a clear discussion of the randomness. $K_{i,i\pm1}$ describes local coupling between first neighbor lasers scaled to the intensity damping rate of the single uncoupled laser. Note that across all the studies only the case of reciprocal couplings $K_{i,i+1} = K_{i+1,i}\forall i$, is considered. Throughout all the study on the localization of the excitability the following set of parameters values has been chosen: $A_i = 6.5$, $B_i = 5.8$, $a_i = 1.8$ and $\gamma_i = 10^{-3}$, $\forall i$; the noise strength D has been kept constant across all the array and periodic boundary conditions have been assumed.

The disorder has been implemented by making $K_{i,i\pm1}$ vary randomly from laser to laser following a uniform distribution. In particular, $K_{i,i\pm1} = K_0 + \rho_{i,i\pm1}$, where K_0 is an average coupling and $\rho_{i,i\pm1}$ a random number constant in time drawn from a uniform distribution in the interval $[-r, +r]$ with $\rho_{i,i+1} \neq \rho_{i,i-1}$ in general. In the solid state physics analogy this choice would correspond to a randomization of the hopping probability between neighbor sites of the atomic lattice (out-of-diagonal disorder). We

consider, without loss of generality, that the additive noise is present only in one laser of the array, the central one and keep all the other lasers in the off-solution but very close to threshold in order to study the conditions under which excitability waves propagate through the lasers chain. If no randomness is present and the couplings are all equal, each laser has in its field amplitude equation a discrete laplacian operator of the form $K_0\left(F_{i+1}+F_{i-1}-2F_i\right)$ then, once the central lasers fires an excitability wave propagates through the chain both left and right with respect to the central laser. Roughly speaking we can say that the lasers are synchronized: they all fire in a temporal interval much shorter than the central laser refractory time. Furthermore the laser phases are locked in correspondence to the firing events as it is shown in Fig. 8.8 b). Such free propagation dynamics is what we can define as the ballistic or diffusive

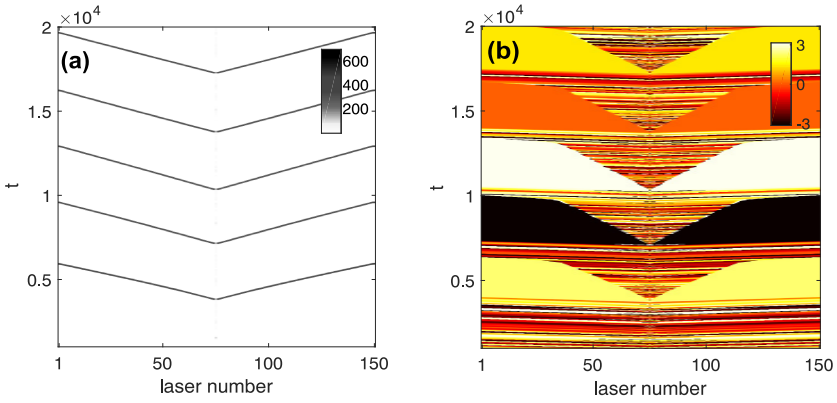

Figure 8.8: The spatiotemporal dynamics corresponding to the diffusive regime: the excitability wave emanates from the center of the array where the noise is added. Field intensity is plotted versus laser (x-axis) and time (y-axis) in (a). In (b) the corresponding phase evolution is shown: a strong phase locking occurs in correspondence to every firing event. Parameters used are $D=0.1$ and $K_{i,i\pm1}=K_0=0.1\ \forall i$.

regime.

If the randomness is introduced in the coupling strengths a very different dynamics takes place: the excitable behavior of the laser array remains spatially localized to a small set of lasers located in the vicinity of the central one (See Fig.8.9a)).

In order to characterize quantitatively the localization we have defined a "firing-event" as the small temporal window located around the interval of time, the coupled lasers generate an excitable wave. Within the "firing-event" temporal window we have recorded the maximum intensity emitted by each laser and averaged it over all the "firing-events" occurring during one simulation. After averaging the intensity distribution over many different realization of the disorder in the system (i.e. different draws of

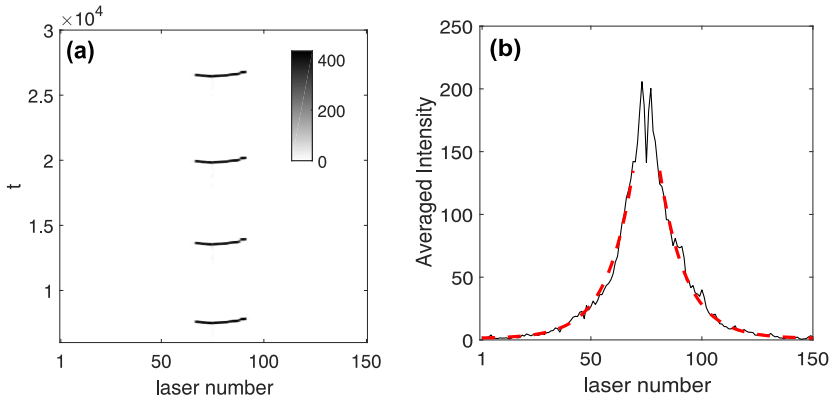

Figure 8.9: When the disorder is turned on with a sufficient strength in the laser array, excitability becomes localized as the spatio-temporal dynamics depicted in (a) shows. The average intensity across the array averaged over the "firing-events" of 150 multiple realizations of the disorder in the coupled lasers' system, is fitted by an exponential function (Eq.8.7), dashed red line in (b). Parameters used are $r = 0.4$, $D = 0.1$ and $K_0 = 0.5$.

the $K_{i,i\pm1}$'s for fixed r) we have then fitted the tails of such resulting averaged intensity distribution with an exponential function (see Fig.8.9b))

$$f = b + e^{-\alpha|i-i_0|} \tag{8.7}$$

being i_0 the position of the central laser. Repeating the above mentioned procedure for five times allows to obtain the average localization exponent $\langle\alpha\rangle$ and the relative standard deviation. The localization length can be hence defined as the inverse of $\langle\alpha\rangle$. Note that the method used is reliable and takes into account the fluctuations in the height of the different spikes emitted. Indeed although in a single "firing-event" some lasers may emit higher spikes than others, lasers that emit the most intense pulses change randomly (within the localization length) in successive "firing-events" and in different realizations of the disorder, so that the average is justified.

A critical amount of disorder must be present in the system in order to observe exponential localization of excitability, by repeating the simulations for arrays having different number of lasers, a decreasing trend of the critical point r_c at which excitability becomes localized versus the number of lasers present in the array, can be observed. Such fact may suggest that for infinitely long chains localization could take place for arbitrarily small randomness strength. I prefer however to be cautious about this last

point and leave the problem open to future investigations.

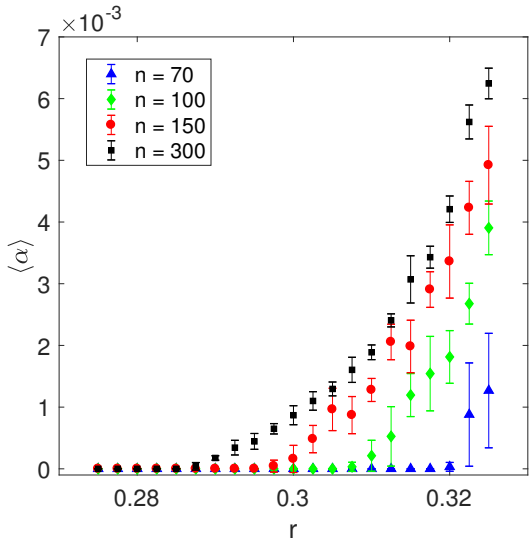

Figure 8.10: The phase transition from diffusive to localized regime is illustrated by plotting the average localization exponent $\langle\alpha\rangle$ and relative standard deviation versus the randomness strength r, for laser chains having different number of elements n (see legend). The amount of randomness necessary to achieve localization decreases by increasing the array size. Each point has been calculated averaging over five values of α. Each α has been obtained from 150 different realizations of the disorder with the same strength r. The remaining parameters used are the same as in Fig.8.9.

What is worth mentioning is that the localization process observed here is not a trivial one. It has been verified that for every value of the disorder strength r used in the simulations, the lasers are always operating in the excitable regimes and excitability waves can propagate normally through the array if all the coupling coefficients are set identically equal to $K_0 - r$, the minimum possible value achievable during the random determination of the coupling terms. A proof in this sense is given in Fig.8.8, where for $n = 150$ lasers, if all the lasers are identically coupled with the minimum possible coupling achievable with the parameters used in Fig.8.10, propagation of excitable waves is not inhibited. This check supports the fact that the observed localization phenomenon is due to a non trivial dynamical scattering process, where dissipation for sure plays a relevant role, that can not be explained by an artificial local breaking of the links between neighbor elements of the array.

Gaining access on how the noise strength affects excitable dynamical systems is crucial towards understanding their operation and achieving a better control over their performances: such point is indeed evident in the case of the coherence resonance processes discussed in the first section of the present Chapter, for this reason it is interesting to

briefly comment on how the localization exponent $\langle\alpha\rangle$ depends on the additive noise strength D. Some results in this sense are depicted in Fig.8.11: a decrease in the localization exponent is observed for increasing the noise strength in the central laser of the array.

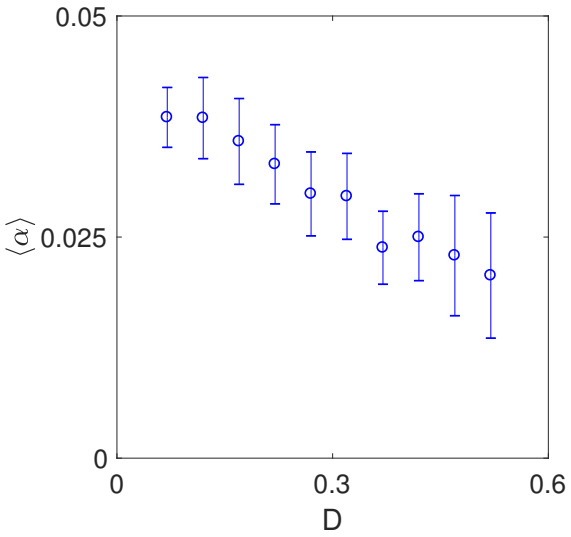

Figure 8.11: The average localization exponent is plotted versus the noise strength D for $n = 150$ coupled lasers. Each point, and relative standard deviation, is the result of an average over 20 different values of $\langle\alpha\rangle$ each one obtained through 150 realizations of the disorder and with the same value of D. Parameters used are $K_0 = 0.5$ and $r = 0.4$.

The two results discussed above constitute a very preliminary and modest step towards the study and understanding of the collective phenomena in coupled excitable lasers: more effort is needed both concerning the development of suitable mathematical models that properly account for the above mentioned phenomenology and concerning their experimental study. It would be also interesting to study the dynamics of coupled excitable lasers in different geometries for instance considering a laser matrix (2D geometry) instead of a chain (1D geometry), and to understand wether technological applications of those systems could be envisaged.

I can anticipate that, a numerical study still in progress reveals the fact that both synchronization and disorder induced localization take place also when the coupling coefficient is imaginary and when the alpha-factor is included in the lasers equations. Predicting synchronization and localization in presence of imaginary couplings is relevant for instance in view of their potential experimental observation in array of coupled micropillar lasers [102, 103] where the coupling among the laser cavities is due to evanescent waves.

9 Spatiotemporally localized solutions on the finite background of the nonlinear Schrödinger equation: the Bogoliubov-de Gennes bullets

9.1 Towards spatio-temporal localization...

Up to now in this thesis we have focussed our attention on light pulses or solutions which are localized in time. Historically in nonlinear dynamics localized solutions in general have been considered a very attractive and fascinating research object. Some equations such as the nonlinear Schrödinger equation, the Korteweg-de Vries equation and the Kadomntsev-Petviashvili equation to cite just a few, are integrable, which means they can be solved exactly through the inverse scattering transform technique [104, 105]. In certain parameter regions such equations admit soliton solutions, e.g. solutions that are localized and also that are robust upon collisions. If we restrict our attention to the nonlinear Schrödinger equation we can mention the two celebrated soliton solutions: the fundamental bright soliton for the so called focussing and the dark soliton for the defocussing case respectively. In nonlinear optics we can have both spatial and temporal solitons due to the interplay between Kerr nonlinearity and diffraction or dispersion accordingly [106]. Bright solitons exist when the diffraction and nonlinearity or when dispersion and nonlinearity compensate each other. In the first case we speak about spatial solitons or non diffracting light beams, while in the second case we speak about of temporal solitons or non dispersing pulses. There has been a substantial effort in the recent years to combine the concept of both spatial and temporal localization, with the ambitious goal to obtain the so-called light bullets: solitonic solutions that remain confined and propagate without spreading neither along the propagation direction (temporal confinement), nor diffracting in the transverse direction with respect to the propagation direction (spatial confinement). The idea has

been first suggested by Silberberg [107] and some experimental attempts to observe such bullets have been done, evidencing however some stability problems [108, 109].

Besides solitons defined in a strict mathematical sense from the integrability of the evolution equations through inverse scattering transform, some localized solutions have been predicted by studying theoretically and experimentally dissipative equations like the complex Ginzburg-Landau equation [110] or perturbed versions of the nonlinear Schrödinger equation as well as in other nonlinear equations [111]. Such localized solutions are customary referred to in the literature as solitons in a broad sense.
All the above mentioned bright solitons in the nonlinear Schrödinger equation or in the complex Ginzburg-Landau equation "live" on a vanishing field background. If the background is finite and different from zero the nonlinear Schrödinger equation admits so called breathers solutions. Breathers are solitons that undergo a periodic dynamics. The most general breathers solution has been derived by Kuznetsov [112]. Later, two particular cases of the Kuznetsov breather have been discussed, the so-called Peregrine soliton [113] and the Akhmediev breather [114]. The existence of such peculiar solutions still stimulates an active research interest both from the theoretical [115] and the experimental point of view [116]. On the other hand another class of solitons exists in presence of periodic potentials. It is well known that in presence of periodic potential the dispersion relation exhibits a band structure, like in the case of crystalline structure in solid state physics. It can be shown that for modes close to the first band edges, localized structures called gap-solitons can be found [117]. Gap solitons have been studied extensively both in nonlinear optics for light propagating in photonics crystals, where the periodic potential is realized through a periodic modulation of the refractive index. For two dimensional modulation of the refractive index spatial gap-solitons can be observed for light propagating orthogonally to the modulation plane[118]. Temporal gap-solitons can be instead observed for instance in fibre Bragg gratings where the one-dimensional modulation of the refractive index takes place along the propagation direction of the light through the fibre [119]. Gap solitons have been observed also in other physical systems such as Bose-Einstein condensates where the periodic potential can be realized by means of an optical lattice [117, 120].

9.2 Controlling the excitations dispersion relation through the potential

We suggest here that there is possibility to build spatiotemporally localized solutions, living on the finite non-vanishing field background, in a two-dimensional nonlinear Schrödinger equation, describing a a field defined in space and evolving in time for instance an atomic Bose-Einstein condensate in presence of a periodic potential:

$$\frac{\partial A}{\partial t} = i\nabla^2 A + ic|A|^2 A + i4m[\cos(q_x x) + \cos(q_y y)]A. \tag{9.1}$$

Where A is the field envelope defined in space and evolving in time t, c is the nonlinearity coefficient, m the potential strength while $q_{x,y}$ determine the periodicity of the potential along the two spatial directions of coordinates x and y. Indeed in the mean field approximation such equation called also the Gross-Pitaevskii equation in the Bose-Einstein condensates community, describes the dynamics of a Bose-Einstein condensate [121]; the periodic potential can be practically created by using an optical lattice [122]. Throughout all the study we have taken the nonlinearity coefficient $c < 0$. Hence the equation is defocussing and no bright solitons could in principle exist.

Let's for the moment consider the vanishing potential case ($m = 0$). We examine now the dispersion relation of the weak excitations on top of the condensate, the so called Bogoliubov-de Gennes modes. In a Bose-Einstein condensate they correspond to sound waves propagating on top of the spatially homogeneous stationary state [121]. In one spatial dimension $\left(\nabla^2 = \frac{\partial^2}{\partial x^2}\right)$ the dispersion relation is a parabola that in the limit of strong background becomes linear close to the origin, while in two spatial dimensions the dispersion relation consists of paraboloids determined by the following relation:

$$\omega = \pm k\sqrt{(k^2 + 2|A_0|^2 c)}; \tag{9.2}$$

where $k = |\vec{k}| = \sqrt{k_{||}^2 + k_{\perp}^2}$ being $k_{||}$ and $k_{\perp}$ the components of the wavevector $\vec{k}$ in the parallel and orthogonal direction with respect to the propagation one. Eq.9.2 can be obtained by substituting the following *ansatz*:

$$A(t, \vec{r}) = A_0 e^{ic|A_0|^2 t}\left[1 + b_+(\vec{r}, t)e^{i\vec{k}\cdot\vec{r}} + b_-(\vec{r}, t)e^{-i\vec{k}\cdot\vec{r}}\right] \tag{9.3}$$

into Eq. 9.1 and linearizing with respect to the small Bogoliuobov modes amplitudes $|b_{\pm}| << A_0$.

The analytical computation of the dispersion relation in presence of a periodic potential is in general problematic. A useful numerical technique that we use in order to compute the dispersion of the excitations accounting for the modifications induced by the potential (when $m \neq 0$) is the following.Starting from an homogeneous background of amplitude A_0 we introduce a small perturbation to every spatial spectral mode and let the corresponding field amplitude evolve in time for a certain temporal interval T recording the field amplitude $A(\vec{r}, t)$ values in the entire space and time domain. A simple spatio-temporal Fourier transform give hence the spectrum $\tilde{A}(\vec{k}, \omega)$. For every fixed value of ω, the set of obtained wave numbers (k_x, k_y) constitutes the so-called isofrequency curves. Isofrequency curves are very important analysis tools for the wave propagation which are are widely used for instance to study the properties of photonic crystals. In general they indicate the curvature that the phase front acquires upon propagation hence allowing an understanding of the focalization, collimation or spreading nature of the waves in those systems. Due to the mathematical similarity of the problem we are considering in this Chapter our study can benefit from such cross-disciplinary interaction. Coming back to our system, in case of nonvanishing potential the dispersion still exhibits paraboloid shape, that cut at certain frequency give circular isofrequency curves with increasing radius for larger and larger ω. When the isofrequency curves are concave a wavepacket of excitations on top of the homogeneous background will spread due to diffraction. However, for sufficently high ω, discontinuities in the isofrequency curves called bandgaps appear (See Fig.9.1). Waves having wavevectors lying in the bandgaps cannot propagate. In correspondence to the apparence of bandgaps we can observe also a flattening of the isofrequency lines. This flattening corresponds to the so called self-collimation regime. A wave-packet whose spectrum lies entirely on the flat isofrequency lines propagates without suffering any diffraction. We can call such wave-packet spatial soliton or solitonic beam. In this sense we have an ingredient to achieve spatial localization. Self-collimation has been indeed studied and observed in photonic crystals [123, 124, 125].

We now want to ask the following question: how can we use the periodic potential to achieve temporal localization? Temporal spreading of a wave-packet, e.g. a

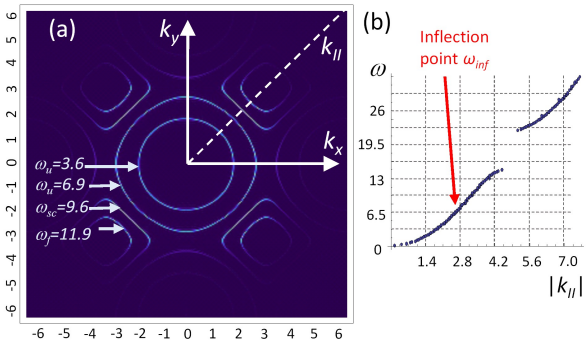

Figure 9.1: In a) the isofrequency lines of the Bogoliubov excitations are presented for different values of ω (indicated on the plot). Increasing ω we have first the diffracting regime ($\omega = \omega_u$), then the aparence of the bandgaps with the flattening of the isofrequency curves for $\omega = \omega_{sc}$ and later on the change of curvature of the isofrequency lines with corresponding focussing regime ($\omega = \omega_f$). The suffix sc stands for self-collimation and wave-packets with a wavevector corresponding to this value experience no diffraction upon propagation. In b) the dispersion relation ω versus $k_{||}$ is shown: the red arrow indicates the longitudinal inflection point, wave-packets with wavevectors centered around this point experience no dispersion. The parameters used are $m = 1$, $q_x = q_y = 6.67$, $c = -0.05$ and $A_0 = 0.5$.

spreading taking place in a reference frame co-moving with the wave-packet, occurs in general because the different spectral component travel at different velocities, e.g. a group velocity dispersion exists. The group velocity dispersion in fibre optics is defined as the second derivative of the propagation constant with respect to the frequency [25]. In the notation that we are considering in this Chapter the temporal and spatial coordinates are interchanged, hence the analogous of the group velocity dispersion is the second derivative of ω with respect to $\vec{k}_{||}$, where $\vec{k}_{||}$ is the wavevector oriented along the propagation direction of a pulse. Now, if one chooses a wave-packet of excitations whose spectrum is centered around a wavevector that lies in correspondence to the inflection point of the curve ω versus $\vec{k}_{||}$ (temporal inflection point), there $\frac{\partial^2 \omega}{\partial \vec{k}_{||}^2} = 0$, and no dispersion is present. Inspired by this consideration we can indeed think that wave-packets of excitations having an infinite extent in the direction transverse to the propagation one remain localized in the co-moving reference frame upon evolution if the central wave-vector is chosen in correspondence to the inflection point of the curve ω versus $\vec{k}_{||}$ (Fig.9.1b)): such solutions are the temporal solitons or solitonic pulses.

9.3 Linear Bogoliubov-de Gennes bullets

We have now both ingredients ready to obtain the so-called Bogoliubov de-Gennes bullets, we just need to combine them in a suitable way. If we choose a Gaussian wave-packet of excitations with amplitude a_0, wavevector $\vec{k_0}$, longitudinal and transverse width, $w_{||}$ and $w_{\perp}$ accordingly to Eq. 9.4:

$$a(\vec{r}) = a_0 exp\left\{i\vec{k}_0 \cdot \vec{r}\right\} exp\left\{\left[-\quad \frac{(x-y)^2}{w_{||}^2} + \frac{(x+y)^2}{w_{\perp}^2}\right)\right]\right\} \tag{9.4}$$

and locate it on top of the homogeneous field background by choosing a wavevector $\vec{k}_0$ that corresponds simultaneously to the longitudinal and transverse inflection points, we will achieve simultaneously a non diffracting and non dispersing regime and our wave-packet can propagate without spreading neither along the direction of propagation nor along the direction transverse to it. If the nonlinearity coefficient is small and/or the intensity of the wave-packet is much smaller than the background (with a background amplitude that is non negligible) we call the spatiotemporally localized wave-packet of excitations: *linear Bogoliubov-de Gennes bullet*. The results of numerical simulations are summarized in Fig. 9.2 and Fig. 9.3 and show that such bullets exist emphasizing their difference with usually dispersive pulses. Note that in the intensity profiles depicted in Fig.9.2, in all the plots, the spatial Fourier components with wave numbers $k_x = q_x$ and $k_y = q_y$, corresponding to the the potential periodicities, have been removed (only in the plotting). This has been done in all the intensity plots presented in this Chapter.

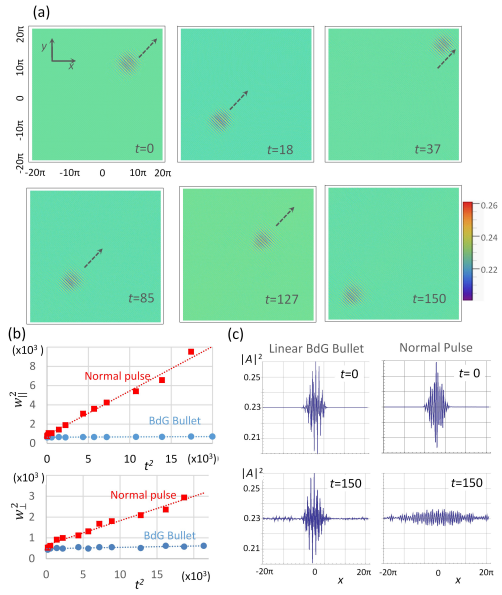

Figure 9.2: In a) the snapshots of the temporal evolution of the linear Bogoliubov-de Gennes excitations are shown (the black arrows denote the propagation direction). The bullet width, both in the longitudinal and transverse direction, remains unchanged upon propagation, while if the wavevector is not choosing to satisfy the bullet condition then excitations wave-packets broaden significantly in time b). In c) a 1-D section of the initial conditions of the simulations and the results after an evolution for $t = 150$ in both cases of spreading pulse and linear bullet. Parameters used are: $m = 1$, $q_x = q_y = 6.67$, $A_0 = 0.5$, $c = -0.05$, $a_0 = 0.05$ and initial widths $w_\perp = w_{||} = 18.5$. The spreading pulse has wavevector $\vec{k}_0 = 1.45(\hat{x} + \hat{y})$, while for the linear bullet $\vec{k}_0 = 2.45(\hat{x} + \hat{y})$.

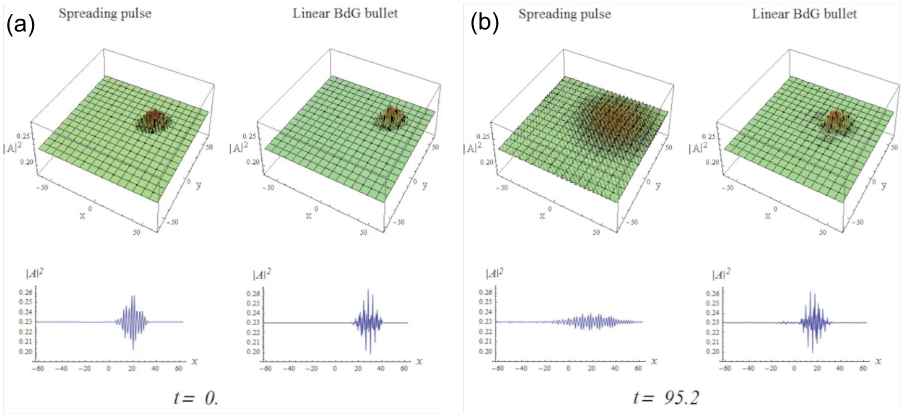

Figure 9.3: In a) the spreading pulse at $t = 0$ and after temporal evolution (2-D plot and 1-D section) is compared with the linear Bogoliubov-de Gennes bullet b). The latter remains unchanged. Parameters considered are $A_0 = 0.5$, $m = 1$, $q_x = q_y = 6.67$, $c = -0.05$, $a_0 = 0.05$, and $w_\perp = w_{||} = 18.5$; $\vec{k}_0 = 1.45(\hat{x} + \hat{y})$ and $\vec{k}_0 = 2.45(\hat{x} + \hat{y})$ for the spreading pulse and the linear bullet respectively.

It is interesting to comment about the fact that while in Fig.9.2 results about bullets of excitations propagating on the finite background have been reported, in principle one

could also remove the background and have a bullet traveling on the vanishing background.

9.4 Nonlinear Bogoliubov-de Gennes bullets

We define the *nonlinear Bogoliubov-de Gennes bullets* as wave-packets of excitations traveling on the finite field background where the bullet amplitude is comparable with the background amplitude being the latter significantly different from zero, and/or the nonlinearity coefficient is large (about order one). It is indeed possible to observe numerically such objects too. The results are summarized in Fig.9.4. We have identified families of bullets where a fixed relation between intensity peak I_p and width is respected ($I_p \propto w_{||}^{-2}$). The interested reader can also find movies showing the evolution of the stable linear and nonlinear bullets available online as a Supplemental Material of the paper where the results presented in this Chapter have been published [126].

As a general comment it is important to say that since the Bogoliubov-de Gennes

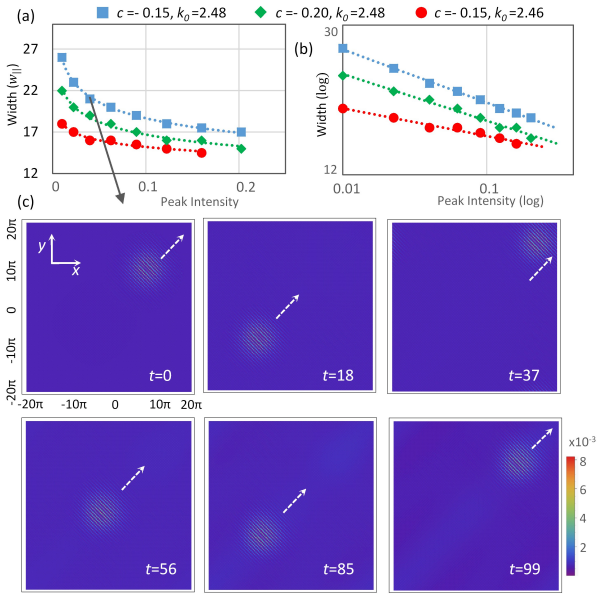

Figure 9.4: In a) the intensity peaks values of the nonlinear bullets are depicted as a function of the bullet width for various values of the nonlinearity coefficient c depicted above. In b) the same results are shown in logarithmic scale. In c) the snapshots of the temporal evolution of one nonlinear bullet are shown, the white arrows denote the propagation direction. Parameters used in the simulations are: $a_0 = 0.2$, $c = -0.15$, $w_\perp = w_{||} = 21$, $m = 1$, $q_x = q_y = 6.67$, $A_0 = 0.5$ and $\vec{k}_0 = 2.48(\hat{x} + \hat{y})$.

bullets exist also in the limit of vanishing nonlinearity, probably they are not solitons

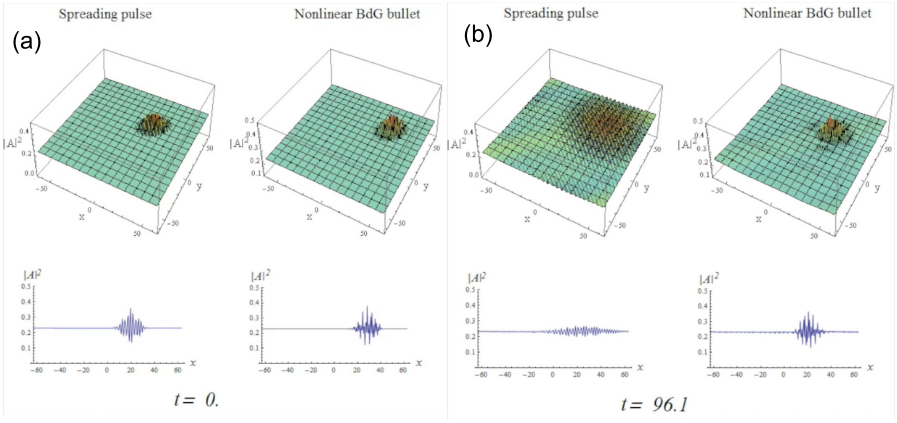

Figure 9.5: In a) a spreading pulse at $t = 0$ and after temporal evolution (2-D plot and 1-D section) is compared with the nonlinear Bogoliubov-de Gennes bullet b). The latter remains unchanged upon propagation. Simulations have been performed with the following set of parameters: $A_0 = 0.5$, $m = 1$, $q_x = q_y = 6.67$, $c = -0.15$, $a_0 = 0.2$, and $w_\perp = w_{||} = 19$; $\vec{k}_0 = 1.45(\hat{x} + \hat{y})$ and $\vec{k}_0 = 2.48(\hat{x} + \hat{y})$ for spreading pulse and nonlinear bullet respectively.

in the strict sense, if one consider solitons to be objects existing thanks to the balance of dispersion or diffraction and nonlinearity (at least in the conservative case). The Bogoliubov-de Gennes bullets may be considered maybe as linear localized solutions that may be also "dressed" with nonlinearity such as X-waves [127, 128, 129, 130]. Also it is important to stress that Bogoliubov-de Gennes bullets have a width that cannot be smaller than a critical value, indeed for very narrow bullets the spectrum will be very large and contain wavenumbers falling into the forbidden bandgap. This fact should be taken into account in possible future experimental studies.

9.5 On the bullets stability

It is very important to stress some points about the preparation of the initial conditions for the bullets. Indeed I comment now in detail about the procedure briefly sketched above. First of all it is necessary to find the system steady state, the spatially periodic Bloch mode with average amplitude A_0 and periodicities q_x and q_y in the x and y directions, respectively. An artificial transient step is needed to "cool down" the system into the stationary Bloch solution. This is obtained by making a transformation to complex time $t \rightarrow t(1 + i\epsilon)$, being ϵ a real parameter much smaller than unity and then integrating Eq.9.1 for a small temporal interval. This transformation mimics dissipation and causes damping of the thermal excitations of the condensate [131], allowing the system to relax to a stationary state. Once the system has reached the ground state, the complex time transformation is removed and the system switches back to the conservative regime. This time is referenced as $t = 0$. Hence the Bogoliubov-de Gennes bullet envelope can be introduced over the steady-state background in the form given by Eq. 9.4. However Eq. 9.4 is just an *ansatz* and not the true bullet solutions, consequently a substantial scattering takes place once the bullet is located on top of the steady-state background. Since periodic boundary conditions have been used in the simulations, the scattered dispersive waves lead to the introduction of strong noise in the system affecting dramatically the stability of the steady state and of the propagating pulse. For this reason, the scattered radiation is sufficiently, although not completely, filtered out of the system before allowing the bullet to propagate. In this sense a certain amount of noise is present in the system and this reveals the fact that bullets are stable with respect to such perturbations. It is possible to test numerically more extensively and quantitatively the stability of the bullets. Two ways have been followed. In the first case, after preparing the initial bullet condition as described before, complex white noise of amplitude n has been added to the field at $t = 0$. In presence of noise the intensity peak of the bullet undergoes oscillations. The variance of the bullet intensity peak, $Var(I_p)$, has been computed after evolution for a long time interval obtained by numerically simulating Eq.9.1. The procedure has been repeated varying the input noise strength n (See Fig.9.6). We can observe that $Var(I_p)$ increases linearly with n^2. The second stability test has been done perturbing the field continuously, at each

integration step during the temporal evolution. The variance of the pulse intensity peak has been calculated at each interval $j\Delta t$ with j an integer ranging from 1 to $T/\Delta t$, with T the total integration time. Results of such numerical stability analysis are presented in Fig.9.7. The variance increases linearly with n^2 in the first perturbation scheme considered and with time in the second one. If the bullets were unstable then the width would increase exponentially.

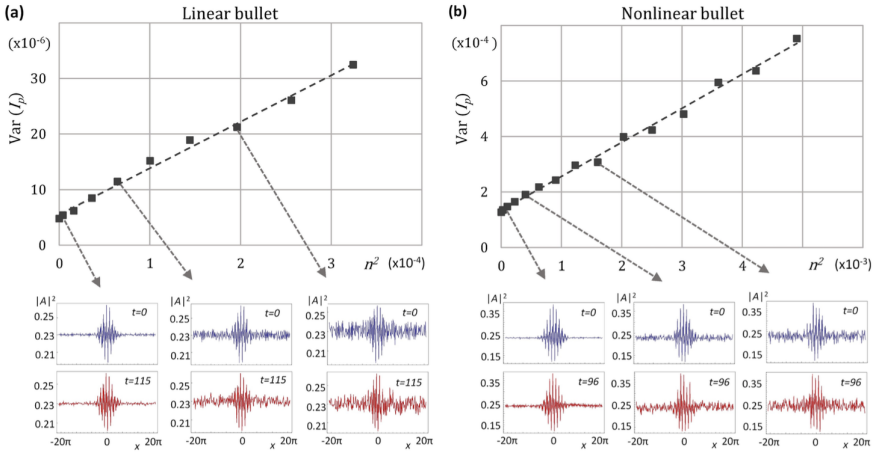

Figure 9.6: The variance of the peak intensity $Var(I_p)$ of the bullet for long intervals of propagation ($t \approx 100$) is plotted as a function of the initial noise intensity n^2 both in the case of linear bullets a), and for nonlinear bullets b). The respective insets show the cross-section of the bullets intensity before propagation (blue) and after propagation (red). The parameters for the bullets are the same as in Fig.9.2 and Fig.9.4 for the linear and nonlinear bullets respectively. Dashed lines correspond to linear fits. Dashed black arrows indicate the bullets at the initial (blue plots) and final (red plots) stage of the evolution for the corresponding value of added noise.

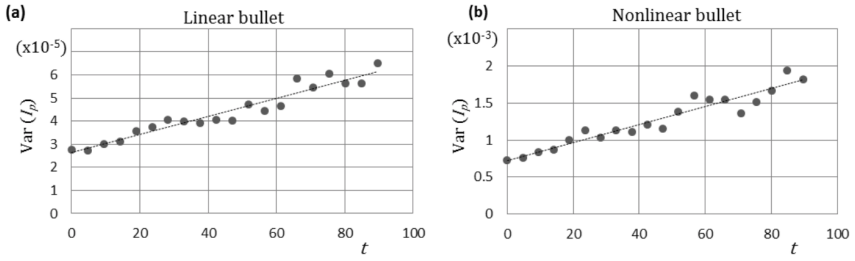

Figure 9.7: The variance of the peak intensity of the bullets, $Var(I_p)$, in the presence of a continuously added noise of constant amplitude, averaged over regular subintervals of the propagation time t. The amplitudes for the noise were $n = 0.0002$ and $n = 0.001$ for the linear and nonlinear bullets respectively. The total propagation time in both cases is $t \approx 95$ and the dots in the plots correspond to the variance calculated on temporal intervals having length $\Delta t = 4.75$. All the parameters for the bullets are the same as in Fig.9.2 (linear) and Fig.9.4 (nonlinear). Dashed lines correspond to linear fits.

It is also very important to stress the fact that the Bogoliubov-de Gennes bullets

differ substantially from the well known gap solitons. Indeed gap solitons exist close to the band edges where the first derivative of the dispersion relation is close to zero $\left(\frac{\partial\omega}{\partial\vec{k}_{||}} \approx 0\right)$. We are instead considering here the case where the second derivative of the dispersion relation is close to zero $\left(\frac{\partial^2\omega}{\partial\vec{k}_{||}^2} \approx 0\right)$. We note that choosing the correct wavevector corresponding to the bullet regime is crucial, indeed if we take a too long one corresponding to the convex curvature of the isofrequency lines we will obtain focussing of the Bogoliubov-de Gennes excitations. Focussing is achieved thanks to the dispersion relation modification induced by the potential notwithstanding the fact that we are considering a defocussing nonlinear Schrödinger equation (see Fig.9.8):

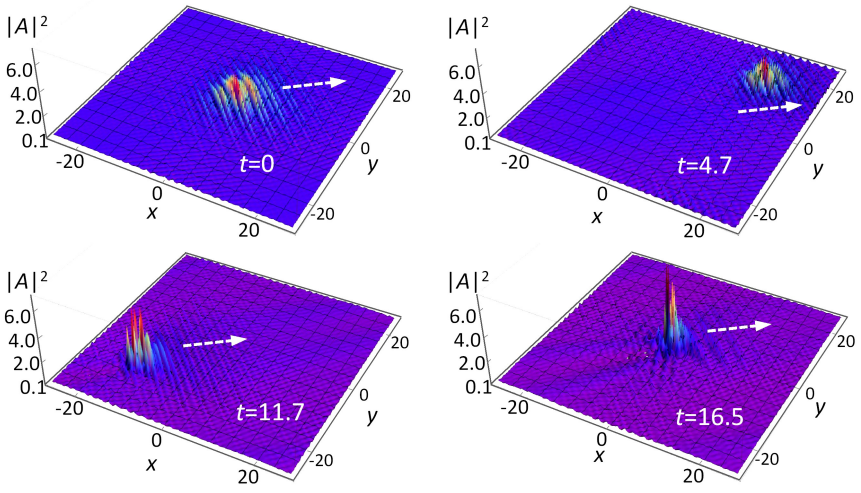

Figure 9.8: Focussing dynamics of a Bogoliubov-de Gennes excitations wave-packet, the white arrows denote the propagation direction. Parameters used are $m = 1$, $q_x = q_y = 6.67$, $c = -0.1$, $A_0 = 0.5$, $a_0 = 1.1$ and $\vec{k}_0 = 2.7(\hat{x} + \hat{y})$; the initial widths are $w_\perp = 10$ and $w_{||} = 14$ respectively.

Future tasks in this research direction are numerous. From the mathematical point of view, analytical solutions of the Bogoliubov-de Gennes bullets must still be found as a well as a rigorous proof of their stability must be given. From the experimental point of view it is interesting to think how to observe the bullets in atomic Bose-Einstein condensates with periodic potential, first of all individuating a realistic range of real world parameters and then studying the practical feasibility of the experiment. Another interesting direction could be to find a suitable photonic system supporting the existence of the Bogoliubov-de Gennes bullets, in this direction the main challenge may be finding a way of implementing the periodic potential in an efficient way. Adapting the proposed localization scheme to dissipative systems where gain and losses play

important roles can be challenging, but it is an option that potentially could be explored too.

10 Appendix: The derivation of the Arecchi-Bonifacio (Maxwell-Bloch) equations

10.1 Interaction of a two-level atom with the electromagnetic field

We present here a derivation of the Arecchi-Bonifacio equations starting from the density matrix of a two-level atomic system interacting with a monochromatic electric field. We will describe how a two-level atom interacts with a non-quantized electromagnetic field through the density matrix formalism (it is of course possible to derive the same equations from a fully quantum approach [132], but such procedure would be redundant for our purposes). This treatment will result in the optical Bloch equations. The same mathematical picture can be obtained studying the dynamics of a spin one-half particle interacting with a magnetic field which oscillates periodically in time; this is the reason for the name Bloch.

In order to take into account the temporal evolution of the electric field amplitude, which varies due to the photon exchanges with the atomic medium, a self consistent analysis is required. For this reason it will be necessary to take into account how the polarization induced by the field in the material medium affects the field itself. This point will be accounted for by coupling the optical Bloch equations with Maxwell equations.

The Hamiltonian which describes an electron with charge $-e$ and mass m interacting with an electromagnetic field is:

$$H = \frac{1}{2m}\left[\mathbf{p} - \frac{e}{c}\mathbf{A}(\mathbf{x},t)\right]^2 + eV(\mathbf{x},t) + U(r). \tag{10.1}$$

Where $\mathbf{x}$ the electron position which can be written as $\mathbf{x} = \mathbf{r}_0 + \mathbf{r}$ being $\mathbf{r}_0$ the nucleus position, and $\mathbf{r}$ the electron position relative to the nucleus; $\mathbf{p}$ is the momentum operator conjugate with $\mathbf{r}$. $\mathbf{A}(\mathbf{x}, t)$ and $V(\mathbf{x}, t)$ are the vector and scalar potential of the external electromagnetic field while $U(r)$ is the spherically symmetric potential which describes the electron-nucleus Coulombian interaction.

The electric field $\mathbf{E}$ and the magnetic field $\mathbf{B}$ are related to the potentials through the well known relationships

$$\mathbf{E} = -\nabla V - \frac{1}{c}\frac{\partial \mathbf{A}}{\partial t} \tag{10.2}$$

$$\mathbf{B} = \nabla \times \mathbf{A}. \tag{10.3}$$

Let's choose the Coulomb gauge where $V = 0$ and $\nabla \cdot \mathbf{A} = 0$ and assume that the radiation field is monochromatic with wavelength λ.

We introduce now the first crucial approximation of our description: we assume that the wavelength λ is much greater than the atomic dimensions, which is equivalent to require $\mathbf{k} \cdot \mathbf{r} \ll 1$ where $\mathbf{k}$ is the radiation wave vector. This is what is called the *dipole approximation*.

It follows that the vector potential can be well approximated in this way:

$$\begin{aligned} \mathbf{A}(\mathbf{r}_0 + \mathbf{r}, t) &= \mathbf{A}(t)\exp[i\mathbf{k}\cdot(\mathbf{r}_0 + \mathbf{r})] + c.c. = \mathbf{A}(t)\exp(i\mathbf{k}\cdot\mathbf{r}_0)(1 + i\mathbf{k}\cdot\mathbf{r} + ...) + c.c. \\ &\approx \mathbf{A}(t)\exp(i\mathbf{k}\cdot\mathbf{r}_0) + c.c. = \mathbf{A}(\mathbf{r}_0, t) \end{aligned} \tag{10.4}$$

losing its operator properties, since its dependence on the position operator $\mathbf{r}$ can be neglected, and becoming a simple complex number. Hence the Schrödinger equation for the electron is:

$$H\psi(\mathbf{r}, t) = \left\{ \frac{1}{2m}\left[\mathbf{p} - \frac{e}{c}\mathbf{A}(\mathbf{r}_0, t)\right]^2 + U(r) \right\} \quad (\mathbf{r}, t) = i\hbar\frac{\partial\psi(\mathbf{r}, t)}{\partial t}. \tag{10.5}$$

In order to split the Hamiltonian into two separate parts, the first one describing the isolated atom and the second one including the coupling with the external field, let us introduce the following gauge transformation defined by the unitary operator

$$T(\mathbf{r}, t) = \exp\left[-i\frac{e}{\hbar c}\mathbf{r}\cdot\mathbf{A}(\mathbf{r}_0, t)\right]. \tag{10.6}$$

Applying T to the Schrödinger equation we have:

$$THT^{\dagger}T\psi = i\hbar T\frac{\partial\psi}{\partial t}, \tag{10.7}$$

but since the Coulomb potential depends just on the position operator $\mathbf{r}$, it commutes with T and $TUT^{\dagger} = U$. The transformation on the remaining part of H is:

$$T\frac{1}{2m}\left[\mathbf{p} - \frac{e}{c}\mathbf{A}(\mathbf{r}_0, t)\right]^2 T^{\dagger} = \frac{1}{2m}\left[T\mathbf{p}T^{\dagger} - \frac{e}{c}\mathbf{A}(\mathbf{r}_0, t)\right]^2. \tag{10.8}$$

We have

$$\begin{aligned} T\mathbf{p}T^{\dagger}\psi &= T(-i\hbar\nabla)\Big\{\exp\left[-i\frac{e}{\hbar c}\mathbf{r}\cdot\mathbf{A}(\mathbf{r}_0,t)\right] \Big\} \\ &= T\Big\{\exp\left[-i\frac{e}{\hbar c}\mathbf{r}\cdot\mathbf{A}(\mathbf{r}_0,t)\right]\left[-i\hbar\nabla\psi + \frac{e}{c}\mathbf{A}(\mathbf{r}_0,t)\right]\Big\} \\ &= \left[\mathbf{p} + \frac{e}{c}\mathbf{A}(\mathbf{r}_0,t)\right] \end{aligned} \tag{10.9}$$

and

$$THT^{\dagger} = \frac{\mathbf{p}^2}{2m} + U(r) = H_0 \tag{10.10}$$

where we have defined H_0 as the Hamiltonian of the isolated atom. Furthermore

$$T\frac{\partial\psi}{\partial t} = \frac{\partial(T\psi)}{\partial t} - \frac{\partial T}{\partial t} \tag{10.11}$$

and since

$$\frac{\partial T}{\partial t} = -i\frac{e}{\hbar c}\mathbf{r}\cdot\frac{\partial\mathbf{A}(\mathbf{r}_0,t)}{\partial t}T = \frac{i}{\hbar}e\mathbf{r}\cdot\mathbf{E}T \tag{10.12}$$

if we define the new wave function $\psi' = T\psi$, the Schrödinger equation becomes

$$H_0\psi' = i\hbar\left[\frac{\partial\psi'}{\partial t} - \frac{i}{\hbar}e\mathbf{r}\cdot\mathbf{E}\psi'\right]. \tag{10.13}$$

Omitting the apex to simplify the notation

$$(H_0 + H_{INT})\psi = i\hbar\frac{\partial\psi}{\partial t} \tag{10.14}$$

where $H_{INT} = -e\mathbf{r} \cdot \mathbf{E}$ is the interaction Hamiltonian.

Let E_1 be the energy of the atom upper level (excited state) and E_2 the energy of the lower level (ground state). We can define the transition frequency:

$$\omega_a = \frac{E_1 - E_2}{\hbar} \tag{10.15}$$

and fixing the zero of the energy between the two levels we have $E_1 = \frac{\hbar\omega_a}{2}$ and $E_2 = -\frac{\hbar\omega_a}{2}$, which are respectively the eigenvalues of the free hamiltonian H_0:

$$H_0|1\rangle = \frac{\hbar\omega_a}{2}|1\rangle, \qquad H_0|2\rangle = -\frac{\hbar\omega_a}{2}|2\rangle. \tag{10.16}$$

The eigenstates can be written in a vector form as follows:

$$|1\rangle = \begin{pmatrix} 1 \\ 0 \end{pmatrix}, \qquad |2\rangle = \begin{pmatrix} 0 \\ 1 \end{pmatrix}. \tag{10.17}$$

A generic atomic state will be then a linear combination of $|1\rangle$ and $|2\rangle$ which constitute a basis for the two dimensional Hilbert space:

$$|\psi\rangle = a|1\rangle + b|2\rangle = \begin{pmatrix} a \\ b \end{pmatrix} \tag{10.18}$$

while a generic observable is described by the hermitean matrix:

$$A = \begin{pmatrix} A_{11} & A_{12} \\ A_{21} & A_{22} \end{pmatrix} \tag{10.19}$$

whose elements are $A_{ij} = \langle i|A|j\rangle$ and satisfy $A_{11}, A_{22} \in \mathbb{R}$ together with $A_{21} = A_{12}^*$ since $A = A^\dagger$.

The two observables of interest are the free hamiltonian

$$H_0 = \begin{pmatrix} \frac{\hbar\omega_a}{2} & 0 \\ 0 & -\frac{\hbar\omega_a}{2} \end{pmatrix} \tag{10.20}$$

and the dipole moment operator

$$e\mathbf{r} = \begin{pmatrix} 0 & \mathbf{d} \\ \mathbf{d}^* & 0 \end{pmatrix}. \tag{10.21}$$

We have assumed that the states $|1\rangle$ and $|2\rangle$, have definite and opposite parity, so that:

$$\mathbf{d}_{11} = \mathbf{d}_{22} = 0, \quad \mathbf{d}_{12} = \mathbf{d}_{21}^* = \langle 1|e\mathbf{r}|2\rangle = \mathbf{d}. \tag{10.22}$$

Defining the Rabi frequency:

$$\Omega_R = \frac{2\mathbf{d}\cdot\mathbf{E}}{\hbar} \tag{10.23}$$

H becomes hence

$$H = H_0 - e\mathbf{r}\cdot\mathbf{E} = \frac{\hbar}{2}\begin{pmatrix} \omega_a & -\Omega_R \\ -\Omega_R & -\omega_a \end{pmatrix}. \tag{10.24}$$

The atomic frequency appears now to be split into two new frequencies and the splitting depends on the field strength. This phenomenon is the so called Rabi splitting.
In order to describe the temporal evolution of the physical observables of the system it is convenient to define the the density operator $\rho(t)$. ρ is positive defined, self-adjoint and has unitary trace. It can be described by a matrix whose elements are given by: $\rho_{ij} = \langle i|\rho|j\rangle$.
Its temporal evolution is ruled by the Liouville-Von Neumann equation of motion:

$$\dot{\rho} = -\frac{i}{\hbar}[H, \rho], \tag{10.25}$$

that for the matrix elements says:

$$\dot{\rho}_{ij} = -\frac{i}{\hbar}\sum_k (H_{ik}\rho_{kj} - \rho_{ik}H_{kj}). \tag{10.26}$$

For the two-level atom the density matrix is a 2×2 matrix with just 3 independent elements (due to hermiticity) ρ_{11}, ρ_{22} and ρ_{12}. ρ_{11} represent the population of the state $|1\rangle$ while ρ_{22} the population of $|2\rangle$. The unitarity of the trace which implies

$\rho_{11} + \rho_{22} = 1$, describes the probability conservation.

Out of diagonal terms describe the so-called coherences and are the feature of the system "quantumness". The mean value of a generic observable can be calculated through the following prescription:

$$\langle A(t) \rangle = Tr\left[\rho(t)A\right]. \tag{10.27}$$

Hence the expectation value of the dipole moment operator reads:

$$\langle e\mathbf{r} \rangle = Tr(\rho e\mathbf{r}) = Tr\left[\begin{pmatrix} \rho_{11} & \rho_{12} \\ \rho_{12}^* & \rho_{22} \end{pmatrix} \begin{pmatrix} 0 & \mathbf{d} \\ \mathbf{d} & 0 \end{pmatrix}\right) = \mathbf{d}Tr\begin{pmatrix} \rho_{12} & \rho_{11} \\ \rho_{22} & \rho_{12}^* \end{pmatrix} = \mathbf{d}(\rho_{12} + \rho_{12}^*). \tag{10.28}$$

This expression shows the connection between out of diagonal terms and the electric dipole moment of the atom. This result allows to obtain an expression for the macroscopic dipole moment induced in a material whose N atoms per unit volume can be modeled as two-level systems:

$$\mathbf{P} = N\langle e\mathbf{r} \rangle = Nd(\rho_{12} + \rho_{12}^*)\hat{\mathbf{u}}. \tag{10.29}$$

d is the modulus of $\mathbf{d}$ and $\hat{\mathbf{u}}$ is a unitary vector.

Exploiting the constraints of hermiticity and unitarity of the trace of ρ we can formulate the equation of motion for the independent density matrix elements following Eq.10.26:

$$\dot{\rho}_{12} = -\frac{i}{\hbar}\left[(H_{11} - H_{22})\rho_{12} + H_{12}(\rho_{22} - \rho_{11})\right] \tag{10.30}$$

$$\dot{\rho}_{11} = -\frac{i}{\hbar}\left[H_{12}\rho_{21} - H_{21}\rho_{12}\right]. \tag{10.31}$$

Substituting the hamiltonian of Eq.10.24 into Eq.10.30 and Eq.10.31, we obtain:

$$\dot{\rho}_{12} = -i\omega_a\rho_{12} + \frac{i}{2}\Omega_R(1 - 2\rho_{11}) \tag{10.32}$$

$$\dot{\rho}_{11} = \frac{i}{2}\Omega_R(\rho_{12}^* - \rho_{12}). \tag{10.33}$$

We can restrict ourselves to the case where the electric field is a plane wave propagating along the direction z and polarized along $\hat{\mathbf{e}}$:

$$\mathbf{E}(z,t) = E(z,t)\hat{\mathbf{e}}, \quad E(z,t) = \frac{E_0}{2}e^{i(kz-\omega t)} + c.c.. \tag{10.34}$$

Since the Rabi frequency is directly dependent on the electric field, substituting Eq.10.34 into Eq.10.23 we get:

$$\mathbf{\Omega}_R(z,t) = \mathbf{\Omega} e^{i(kz-\omega t)} + c.c. \tag{10.35}$$

with

$$\mathbf{\Omega} = \frac{\mathbf{d}\cdot\hat{\mathbf{e}}E_0}{\hbar}. \tag{10.36}$$

Assuming that $\mathbf{P}$ and $\mathbf{E}$ are parallel ($\hat{\mathbf{u}} = \hat{\mathbf{e}}$) we have

$$\mathbf{\Omega} = \Omega = \frac{dE_0}{\hbar}. \tag{10.37}$$

It follows naturally that the temporal dependence of the macroscopic polarization P, should be the same as the electric field one. This implies to write down ρ_{12}, which entails the main dependence of P, in a consistent way introducing a complex amplitude r and a phase:

$$\rho_{12} = re^{i(kz-\omega t)}. \tag{10.38}$$

Eq. (10.34) suggests that P can be rewritten as:

$$\mathbf{P}(z,t) = P(z,t)\hat{\mathbf{e}} \tag{10.39}$$

with

$$P(z,t) = \frac{P_0}{2}e^{i(kz-\omega t)} + c.c., \quad P_0 = 2Ndr. \tag{10.40}$$

It is physically relevant introducing a variable which takes into account the population difference between the two atomic levels:

$$r_3 = \rho_{11} - \rho_{22} = 2\rho_{11} - 1. \tag{10.41}$$

r_3 is positive if the upper level is more populated than the lower one, negative otherwise. The substitution of Eq.10.35, 10.37 and 10.41 into Eq.10.32 and Eq.10.33, gives two

first order coupled differential equations for the variables r and r_3:

$$\dot{r} = i(\omega - \omega_a)r - \frac{i}{2}\left(\Omega + \Omega^* e^{-2i(kz-\omega t)}\right) r_3 \tag{10.42}$$

$$\dot{r_3} = i\left(\Omega r^* - \Omega^* r - \Omega r e^{2i(kz-\omega t)} + \Omega^* r^* e^{-2i(kz-\omega t)}\right). \tag{10.43}$$

A final approximation is necessary to accomplish the deduction of the Bloch equations: the terms oscillating at twice the optical frequency can be neglected without substantial loss of information since their rapid oscillation does not affect the dynamics which occurs on time scales larger than the optical period. This is the *rotating wave approximation*. Furthermore, introducing the detuning between the field and atomic frequencies, $\delta = \omega - \omega_a$, we obtain the optical Bloch equations for a two level atomic system:

$$\dot{r} = -i\delta r - \frac{i}{2}\Omega r_3 \tag{10.44}$$

$$\dot{r_3} = i(\Omega r^* - \Omega^* r). \tag{10.45}$$

10.2 The Arecchi-Bonifacio (Maxwell-Bloch) equations

Up to now we have supposed the the electric field interacting with the atomic system doesn't modify its amplitude in the interaction. We didn't consider that it gains and loses photons due to the stimulated emission and absorption processes. In order to describe these facts it is necessary to take into account self consistently the field dynamics itself introducing the so called Maxwell-Bloch equations.

Let's suppose that our material is non magnetic and that no free charges or currents are present; in this case Maxwell equations are:

$$\nabla \times \mathbf{E} = -\frac{1}{c}\frac{\partial \mathbf{B}}{\partial t} \tag{10.46}$$

$$\nabla \cdot \mathbf{B} = 0 \tag{10.47}$$

$$\nabla \cdot \mathbf{D} = 0 \tag{10.48}$$

$$\nabla \times \mathbf{B} = \frac{1}{c}\frac{\partial \mathbf{D}}{\partial t}. \tag{10.49}$$

The constitutive relation

$$\mathbf{D} = \mathbf{E} + 4\pi\mathbf{P}, \tag{10.50}$$

connects the displacement field **D** with the electric field **E** through the medium polarization **P**.

Applying the rotor to both side of the first Maxwell equation Eq.10.46 and exploiting Eq.10.49 and Eq.10.50, we get:

$$\nabla \times (\nabla \times \mathbf{E}) = \nabla(\nabla \cdot \mathbf{E}) - \nabla^2 \mathbf{E} - \frac{1}{c^2}\frac{\partial^2 \mathbf{E}}{\partial t^2} = -\frac{4\pi}{c^2}\frac{\partial^2 \mathbf{P}}{\partial t^2}. \tag{10.51}$$

For a plane wave the electric field has zero divergence. We assume that it propagates along the direction z with linear polarization along x and **P** is parallel to **E**, so that the vectorial Eq.10.51 becomes a scalar one:

$$\frac{\partial^2 E}{\partial z^2} - \frac{1}{c^2}\frac{\partial^2 E}{\partial t^2} = \frac{4\pi}{c^2}\frac{\partial^2 P}{\partial t^2} \tag{10.52}$$

where $E = E(z,t)$ and $P = P(z,t)$. The wave equation (Eq. 10.52) contains a source term proportional to the medium polarization, i.e. the polarization induced by the field acts as a source producing itself an electric field.

Let us assume that the field is a monochromatic plane wave propagating along the positive direction of the z axis and analogously for the polarization:

$$E(z,t) = \frac{1}{2}E_0(z,t)e^{i(kz-\omega t)} + c.c., \quad P(z,t) = \frac{1}{2}P_0(z,t)e^{i(kz-\omega t)} + c.c.. \tag{10.53}$$

A substantial simplification is obtained by assuming that the envelopes vary only slightly on spatial and temporal scales comparable to the carrier periods. This assumption is the so called *slowly varying envelope approximation* (SVEA).

The SVEA can be expressed mathematically in the following way:

$$\left|\frac{\partial E_0}{\partial z}\right| \ll k|E_0|, \quad \left|\frac{\partial P_0}{\partial z}\right| \ll k|P_0|, \quad \left|\frac{\partial E_0}{\partial t}\right| \ll \omega|E_0|, \quad \left|\frac{\partial P_0}{\partial t}\right| \ll \omega|P_0|. \tag{10.54}$$

The expressions for the fields in Eq.10.53 can be written as the following sum:

$$E(z,t) = E^+(z,t) + E^-(z,t), \quad P(z,t) = P^+(z,t) + P^-(z,t) \tag{10.55}$$

with

$$E^+(z,t) = \frac{1}{2}E_0(z,t)e^{i(kz-\omega t)}, \quad E^-(z,t) = \frac{1}{2}E_0^*(z,t)e^{-i(kz-\omega t)} \tag{10.56}$$

and analogously for $P(z,t)$.

Hence Eq.10.52 can be split in two distinct equations; let us consider the one with the + sign. Left-hand side of Eq.10.52 can be written as

$$\left(\frac{\partial}{\partial z}+\frac{1}{c}\frac{\partial}{\partial t}\right)\left(\frac{\partial}{\partial z}-\frac{1}{c}\frac{\partial}{\partial t}\right)E^{+}. \tag{10.57}$$

The action of the linear operators defined in the brackets is the following:

$$\begin{aligned}\left(\frac{\partial}{\partial z}-\frac{1}{c}\frac{\partial}{\partial t}\right)E^{+} &= \frac{1}{2}e^{i(kz-\omega t)}\left(ikE_0+\frac{\partial E_0}{\partial z}+i\frac{\omega}{c}E_0-\frac{1}{c}\frac{\partial E_0}{\partial t}\right)\approx 2ikE^{+} &(10.58)\\ \left(\frac{\partial}{\partial z}+\frac{1}{c}\frac{\partial}{\partial t}\right)E^{+} &= \frac{1}{2}e^{i(kz-\omega t)}\left(ikE_0+\frac{\partial E_0}{\partial z}-i\frac{\omega}{c}E_0+\frac{1}{c}\frac{\partial E_0}{\partial t}\right)\\ &= \frac{1}{2}e^{i(kz-\omega t)}\left(\frac{\partial}{\partial z}+\frac{1}{c}\frac{\partial}{\partial t}\right)E^{+} &(10.59)\end{aligned}$$

where we have applied the SVEA in Eq.10.58. The left-hand side of Eq.10.52 becomes then

$$\frac{\partial^2}{\partial z^2}-\frac{1}{c^2}\frac{\partial^2}{\partial t^2}\Bigg)E^{+}=2ik\frac{1}{2}e^{i(kz-\omega t)}\left(\frac{\partial}{\partial z}+\frac{1}{c}\frac{\partial}{\partial t}\right)E^{+}. \tag{10.60}$$

Applying the SVEA to the right-hand side we get:

$$\begin{aligned}\frac{\partial^2 P^{+}}{\partial t^2} &= \frac{\partial}{\partial t}\left[\frac{\partial P^{+}}{\partial t}\right]=\frac{\partial}{\partial t}\left[\frac{1}{2}e^{i(kz-\omega t)}\left(-i\omega P_0+\frac{\partial P_0}{\partial t}\right)\right]\approx &(10.61)\\ &\approx -i\omega\frac{\partial}{\partial t}\left[\frac{1}{2}e^{i(kz-\omega t)}P_0\right]=-i\omega\frac{1}{2}e^{i(kz-\omega t)}\left(-i\omega P_0+\frac{\partial P_0}{\partial t}\right)\approx\omega^2\frac{1}{2}e^{i(kz-\omega t)}P_0.\end{aligned}$$

The scalar wave equation with source term, Eq.10.52, obtained equating Eq.10.61 and Eq.10.60 acquires the following form:

$$\frac{\partial E_0}{\partial z}+\frac{1}{c}\frac{\partial E_0}{\partial t}=2\pi ikP_0. \tag{10.62}$$

In an analogous way, considering the equations for E^{-} and P^{-} we can get an equation for E_0^{*} and P_0^{*} which is exactly the conjugate of Eq.10.62.

We emphasize the fact that the SVEA introduces a fundamental simplification of the problem reducing a second order differential equation, Eq. 10.52, to a first order one: Eq.10.62.

It is worth noting that outside the plane wave approximation, in order to describe

the field propagation in the transverse directions, the Laplacian operator in Eq.10.51 should contain also a transverse part: $\nabla_\perp^2 = \partial_x^2 + \partial_y^2$. This results in an additional diffraction term into Eq.10.62 which would become:

$$\frac{1}{2ik_0}\nabla_\perp^2 E_0 + \frac{\partial E_0}{\partial z} + \frac{1}{c}\frac{\partial E_0}{\partial t} = 2\pi i k_0 P_0. \tag{10.63}$$

We have defined k_0 as the longitudinal component of the carrier wave vector, outside the plane wave approximation the wave vector can assume also transverse components. Up to now we have considered just reversible effects neglecting the dynamics related to dissipative phenomena. Let us see how dissipative processes can be included into the Maxwell-Bloch equations.

The atomic excited state can decay through both spontaneous emission and anelastic collisions, i.e. non radiative de-excitations. We can write the de-excitation rate as $\gamma_\downarrow = A + \gamma_a$, where A is the Einstein coefficient for spontaneous emission and γ_a the rate of non radiative de-excitations. The same processes will contribute obviously to increase the population of the ground state. We are implicitly assuming that A and γ_a refer to processes connecting the two levels, in a more complicated scheme where other atomic levels are present we should introduce also dissipative terms which are related to those additional levels.

The populations are also altered by thermal excitations or pumping processes which transfer atoms from the ground to the excited level. Let's call $\gamma_\uparrow$ the rate at which these processes occurs. Hence we can write two rate equations which describe the dissipative dynamics:

$$\dot{\rho}_{11} = -\gamma_\downarrow \rho_{11} + \gamma_\uparrow \rho_{22} \tag{10.64}$$

$$\dot{\rho}_{22} = \gamma_\downarrow \rho_{11} - \gamma_\uparrow \rho_{22}. \tag{10.65}$$

The rate equation for the population difference $r_3 = \rho_{11} - \rho_{22} = 2\rho_{11} - 1$ is:

$$\begin{aligned} \dot{r}_3 &= 2\rho_{11} = -2\gamma_\downarrow \rho_{11} + 2\gamma_\uparrow (1 - \rho_{11}) = -2(\gamma_\downarrow + \gamma_\uparrow)\rho_{11} + 2\gamma_\uparrow = \\ &= -(\gamma_\downarrow + \gamma_\uparrow)(r_3 + 1) + 2\gamma_\uparrow = -(\gamma_\downarrow + \gamma_\uparrow) r_3 + \gamma_\uparrow - \gamma_\downarrow = \\ &= -\gamma_{||}(r_3 - \sigma). \end{aligned} \tag{10.66}$$

Where we have defined:

$$\gamma_{||} = \gamma_{\downarrow} + \gamma_{\uparrow}, \quad \sigma = \frac{\gamma_{\uparrow} - \gamma_{\downarrow}}{\gamma_{\downarrow} + \gamma_{\uparrow}} \tag{10.67}$$

The temporal evolution of variable r_3 is then:

$$r_3(t) = \sigma + [r_3(0) - \sigma]\, e^{-\gamma_{||} t}. \tag{10.68}$$

Hence $\gamma_{||}$ is the decay rate of the population inversion. The parameter σ discriminates between an absorber, for $\sigma < 0$, when population is mostly located on the ground level and consequently the radiation interacting with the atoms is absorbed, and an amplifying medium, $\sigma > 0$, where the excited level is the most populated (population inversion regime) and the interacting electric field is amplified through the stimulated emission process.

The polarization itself is affected by a decay due to the elastic collisions between the atoms that induce shifts of the atomic transition frequency ω_a. This fact causes a broadening of the gain linewidth whose width is defined by Ω_G (in the literature such term is also denoted by the symbol $\gamma_{\perp}$).

Coming back to the Maxwell-Bloch equations we can add to them the dissipative terms:

$$\frac{1}{c}\frac{\partial \Omega}{\partial t} + \frac{\partial \Omega}{\partial z} = ik4\pi N \frac{d^2}{\hbar} r \tag{10.69}$$

$$\frac{\partial r}{\partial t} = -i\delta r - \frac{i}{2}\Omega r_3 - \Omega_G r \tag{10.70}$$

$$\frac{\partial r_3}{\partial t} = i(\Omega r^* - \Omega^* r) - \gamma_{||}(r_3 - \sigma). \tag{10.71}$$

We introduce now a more compact notation where the dynamical variables are dimensional and the parameter number is reduced. We define:

$$f = \frac{\Omega}{\sqrt{\gamma_{||}\Omega_G}}, \quad p = \frac{2i}{\sigma}\sqrt{\frac{\Omega_G}{\gamma_{||}}} r, \quad D = \frac{r_3}{\sigma}, \quad g = \frac{2\pi k N d^2}{\hbar \Omega_G}\sigma. \tag{10.72}$$

Introducing the normalized detuning

$$\Delta = \frac{\delta}{\Omega_G} = \frac{\omega_a - \omega}{\Omega_G} \tag{10.73}$$

we obtain the equations:

$$\begin{aligned}
\frac{1}{c}\frac{\partial f}{\partial t} + \frac{\partial f}{\partial z} &= gp & (10.74)\\
\frac{\partial p}{\partial t} &= \Omega_G \left[fd - (1 + i\Delta)p \right] & (10.75)\\
\frac{\partial D}{\partial t} &= -\gamma_{||} \left[\frac{1}{2}(fp^* + f^* p) + D - 1 \right]. & (10.76)
\end{aligned}$$

This set of equations constitute the starting point for the study of the laser dynamics. The equations have been derived under the following hypothesis: dipole, slowly varying envelope, rotating wave and plane wave approximation. They can be (and indeed have been [17]) generalised in order to account for the most diverse cavity configurations, boundary conditions, and to include external injection as well. In particular cases they can be reduced to simplified rate equations models.

11 List of journal publications

Here are listed the journal papers where the scientific results presented in this thesis have been, or are about to be, published.

- A. M. Perego, N. Tarasov, D. V. Churkin, S. K. Turitsyn, and K. Staliunas. Pattern formation by dissipative parametric instability. *Physical Review Letters*, 116:028701, 2016.

- N. Tarasov, A. M. Perego, D. V. Churkin, K. Staliunas, and S. K. Turitsyn. Mode- locking via dissipative Faraday instability. *Nat. Commun.*, 7:22441, 2016.

- A. M. Perego. High-repetition-rate, multi-pulse all-normal-dispersion fibre laser. *Optics Letters*, 42(18):3574-3577, 2017.

- A. M. Perego, S. Smirnov, K. Staliunas, S. Wabnitz and D. V. Churkin. Faraday instability laser. Submitted for publication (currently in review at the moment of thesis submission).

- A. M. Perego, S. K. Turitsyn and K. Staliunas. Gain through losses in nonlinear optics. Submitted for publication (currently in review at the moment of thesis submission).

- A. M. Perego, F. Gustave, B. Garbin, S. Barland, F. Prati and G. J de Valcárcel. A rigorous framework for mode-locking in lasers. To be submitted for publication.

- A. M. Perego and M. Lamperti. Collective excitability, synchronization, and array- enhanced coherence resonance in a population of lasers with a saturable absorber. *Physical Review A*, 94:033839, 2016.

- M. Lamperti and A. M. Perego. Disorder-induced localization of excitability in an array of coupled lasers. *Physical Review A*, 96:041803, 2017.

- S. Kumar, A. M. Perego, and K. Staliunas. Linear and nonlinear bullets of the Bogoliubov-De Gennes excitations. *Physical Review Letters*, 118:044103, 2017.

Bibliography

[1] M. Faraday. On a peculiar class of acoustical figures; and on certain forms assumed by groups of particles upon vibrating elastic surfaces. *Philos. Trans. R. Soc. Lond.*, 121:299–340, 1831.

[2] T. B. Benjamin and F. Ursell. The stability of the plane free surface of a liquid in vertical periodic motion. *Proc. R.Soc. A*, 225:505, 1954.

[3] V. E. Zakharov and L. A. Ostrovsky. Modulation instability: The beginning. *Phys. D*, 238:540–548, 2009.

[4] V. I. Bespalov and V. I. Talanov. Filamentary structure of light beams in nonlinear liquids. *JETP Lett.*, 3:307, 1966.

[5] T. B. Benjamin and J. E. Feir. The disintegration of wave trains on deep water Part 1. Theory. *J. Fluid Mech.*, 27:417, 1967.

[6] A. M. Turing. The chemical basis of morphogenesis. *Philos. Trans. R. Soc. Lond.*, 237:37, 1952.

[7] L. A. Lugiato and R. Lefever. Spatial dissipative structures in passive optical systems. *Phys. Rev. Lett.*, 58:2209, 1987.

[8] M. Haelterman, S. Trillo, and S. Wabnitz. Additive-modulation-instability ring laser in the normal dispersion regime of a fiber. *Opt. Lett.*, 17:745, 1992.

[9] F. Copie, M. Conforti, A. Kudlinski, A. Mussot, and S. Trillo. Modulational instability in dispersion oscillating fiber ring cavities. *Phys. Rev. Lett.*, 116:143901, 2016.

[10] K. Staliunas and V. S. Sánchez-Morcillo. *Transverse Patterns in Nonlinear Optical Resonators*. Springer, 2003.

[11] K. Staliunas and V. J. Sánchez-Morcillo. Turing patterns in nonlinear optics. *Opt. Commun.*, 177:389–395, 2007.

[12] M. Mahric. *Fiber optics parametric amplifiers and related devices*. Cambridge University Press, 2007.

[13] V. Gordienko, M. F. C. Stephens, A. E. El-Taher, and N. J. Doran. Ultra-flat wideband single-pump Raman-enhanced parametric amplification. *Opt. Exp.*, 25:4810–4818, 2017.

[14] M. Nakazawa, K. Suzuki, and H. A. Haus. The modulational instability laser. I. Experiment. *IEEE J. Quantum Electron.*, 25:2036–2044, 1989.

[15] C. J. S. de Matos, D. A. Chestnut, and J. R. Taylor. Low-threshold self-induced modulational instability ring laser in highly nonlinear fiber yielding a continuous-wave 262-GHz soliton train. *Opt. Lett.*, 27:915–917, 2002.

[16] E. M. Pessina, G. Bonfrate, F. Fontana, and L. A. Lugiato. Experimental observation of the Risken-Nummedal-Graham-Haken multimode laser instability. *Phys. Rev. A*, 56:4086, 1997.

[17] L. Lugiato, F. Prati, and M. Brambilla. *Nonlinear Optical Systems.* Cambridge University Press, 2015.

[18] L. D. Landau and E. M. Lifshitz. *Mechanics, Vol. 1.* Butterworth-Heinemann, 3rd Edition, 1976.

[19] F. Melo, P. Umbanhowar, and H. Swinney. Transition to parametric wave patterns in a vertically oscillated granular layer. *Phys. Rev. Lett.*, 72:172–175, 1994.

[20] J. F. Drake, P. K. Kaw, Y. C. Lee, G. Schmid, C. S. Liu, and M. N. Rosenbluth. Parametric instabilities of electromagnetic waves in plasmas. *Phys. Fluids*, 17:778, 1974.

[21] V. Petrov, Q. Ouyang, and H. L. Swinney. Resonant pattern formation in a chemical system. *Nature*, 388:655–657, 1997.

[22] K. Staliunas, S. Longhi, and G. J. De Valcárcel. Faraday patterns in Bose-Einstein condensates. *Phys. Rev. Lett.*, 89:210406, 2002.

[23] P. Engels, C. Atherton, and M. A. Hoefer. Observation of faraday waves in a Bose-Einstein condensate. *Phys. Rev. Lett.*, 98:095301, 2007.

[24] P. Coullet, T. Frisch, and G. Sonnino. Dispersion-induced patterns. *Phys. Rev. E*, 49:2087, 1994.

[25] G. P. Agrawal. *Nonlinear Fiber Optics.* Academic Press, San Diego, 2006.

[26] L. Pitaevski and S. Stringari. *Bose-Einstein Condensation and Superfluidity.* Oxford University Press, 2016.

[27] S. Rota Nodari, M. Conforti, G. Dujardin, A. Kudlinski, A. Mussot, S. Trillo, and S. De Biévre. Modulation instability in dispersion-kicked optical fibers. *Phys. Rev. A*, 92:013810, 2015.

[28] A. Mussot, M. Conforti, S. Trillo, F. Copie, and A. Kudlinski. Modulation instability in dispersion oscillating fibers. *Adv. Opt. Photonics*, 10:1–42, 2018.

[29] M. Matera, A. Mecozzi, M. Romagnoli, and M. Settembre. Sideband instability induced by periodic power variation in long-distance fiber links. *Opt. Lett.*, 18:1499, 1993.

[30] N. Smith and N. J. Doran. Modulational instabilities in fibers with periodic dispersion management. *Opt. Lett.*, 21:570–572, 1996.

[31] J. C. Bronski and J. N. Kutz. Modulational stability of plane waves in nonreturn-to-zero communications systems with dispersion management. *Opt. Lett.*, 21:937, 1996.

[32] F. Kh. Abdullaev, S. A. Darmanyan, A. Kobyakov, and F. Lederer. Modulational instability in optical fibers with variable dispersion. *Phys. Lett. A*, 220:213–218, 1996.

[33] K. Staliunas, C. Hang, and V. V. Konotop. Parametric patterns in optical fiber ring nonlinear resonators. *Phys. Rev. A*, 88:023846, 2013.

[34] M. Conforti, A. Mussot, A. Kudlinski, and S. Trillo. Modulational instability in dispersion oscillating fiber ring cavities. *Opt. Lett.*, 39:4200, 2014.

[35] M. Droques, A. Kudlinski, G. Bowmans, G. Martinelli, and A. Mussot. Experimental demonstration of modulation instability in an optical fiber with a periodic dispersion landscape. *Opt. Lett.*, 37:4832, 2012.

[36] A. M. Perego, N. Tarasov, D. V. Churkin, S. K. Turitsyn, and K. Staliunas. Pattern formation by dissipative parametric instability. *Phys. Rev. Lett.*, 116:028701, 2016.

[37] I. S. Aranson and L. Kramer. The world of the complex Ginzburg-Landau equation. *Rev. Mod. Phys.*, 74:99, 2002.

[38] I. Carusotto and C. Ciuti. Quantum fluids of light. *Rev. Mod. Phys.*, 85:299, 2013.

[39] N. Tarasov, A. M. Perego, D. V. Churkin, K. Staliunas, and S. K. Turitsyn. Mode-locking via dissipative faraday instability. *Nat. Commun.*, 7:22441, 2016.

[40] E. G. Turitsyna, S. V. Smirnov, S. Sugavanam, N. Tarasov, X. Shu, S. A. Babin, E. V. Podivilov, D. V. Churkin, G. Falkovich, and S. K. Turitsyn. The laminar-turbulent transition in a fibre laser. *Nature Photonics*, 7:783–786, 2013.

[41] S. Coen and M. Haelterman. Modulational instability induced by cavity boundary conditions in a normally dispersive optical fiber. *Phys. Rev. Lett.*, 79:4139, 1997.

[42] A. M. Perego. High-repetition-rate, multi-pulse all-normal-dispersion fiber laser. *Opt. Lett.*, 42(18):3574–3577, 2017.

[43] P. V. Mamyshev. All-optical data regeneration based on self-phase modulation effect. In *Optical Communication, 1998. 24th European Conference on*, volume 1, pages 475–476 vol.1, 1998.

[44] S. Pitois, C. Finot, L. Provost, and D. J. Richardson. Generation of localized pulses from incoherent wave in optical fiber lines made of concatenated Mamyshev regenerators. *J. Opt. Soc. Am. B*, 25:1537–1547, 2008.

[45] K. Sun, M. Rochette, and L. R. Chen. Output characterization of a self-pulsating and aperiodic optical fiber source based on cascaded regeneration. *Opt. Express*, 17:10419, 2009.

[46] T. North and C. Brès. Regenerative similariton laser. *APL Photonics*, 1:021302, 2016.

[47] K. Regelskis, J. Želudevičius, K. Viskontas, and G. Račiukaitis. Ytterbium-doped fiber ultrashort pulse generator based on self-phase modulation and alternating spectral filtering. *Opt. Lett.*, 40:5255, 2015.

[48] Z. Liu, Z. M. Ziegler, G.L. Wright, and F. W. Wise. Megawatt peak power from a Mamyshev oscillator. *Optica*, 4:649, 2017.

[49] M. Karlsson. Modulational instability in lossy optical fibers. *J. Opt. Soc. Am. B*, 12(11):2071–2077, 1995.

[50] E. Roldán, G.J. de Valcárcel, and F. Mitschke. Role of field losses on the Risken–Nummedal–Graham–Haken laser instability: application to erbium-doped fibre lasers. *Applied Physics B*, 76(7):741–748, Jul 2003.

[51] R. Krechetnikov and J. E. Marsden. Dissipation-induced instabilities in finite dimensions. *Rev. Mod. Phys.*, 79:519–553, Apr 2007.

[52] T. Tanemura, Y. Ozeki, and K. Kikuchi. Modulational instability and parametric amplification induced by loss dispersion in optical fibers. *Phys. Rev. Lett.*, 93:163902, 2004.

[53] R. W. Boyd. *Nonlinear Optics*. Academic Press, 3rd Edition, 2007.

[54] G. H. M. van Tartwijk and G. P. Agrawal. Maxwell-Bloch dynamics and modulation instabilities in fiber lasers and amplifiers. *JOSA B*, 14:2618–2627, 1997.

[55] V. Lucarini, J. J. Saarinen, K. E. Peiponen, and E. M. Vartiainen. *Kramers-Kronig Relations in Optical Materials Research*. Springer, 2005.

[56] F. Castelli, M. Brambilla, A. Gatti, F. Prati, and L. A. Lugiato. The LLE, pattern formation and a novel coherent source. *The European Physical Journal D*, 71(4):84, 2017.

[57] S. Liu, Z .and Coulibaly, M. Taki, and N. Akhmediev. Kerr frequency combs and triangular spectra. *Opt. Lett.*, 42:2126, 2017.

[58] H. A. Haus. A theory of forced mode locking. *IEEE Journal of Quantum Electronics*, 11:323, 1975.

[59] H. Haus. Mode-locking of lasers. *IEEE Journal of Selected Topics in Quantum Electronics*, 6:1173, 2002.

[60] D. Kuizenga and A. E. Siegman. FM and AM mode locking of the homogeneous laser - part I: Theory. *IEEE Journal of Quantum Electronics*, 6(11):694–708, 1970.

[61] A. E. Siegman. *Lasers*. Oxford University Press, 1990.

[62] F. X. Kärtner, D. M. Zumbühl, and N. Matuschek. Turbulence in mode-locked lasers. *Physical Review Letters*, 82:4428, 1999.

[63] A. G. Vladimirov and D. Turaev. Model for passive mode locking in semiconductor lasers. *Phys. Rev. A*, 72:033808, 2005.

[64] A. G. Vladimirov, D. Rachinskii, and M. Wolfrum. *Modeling of Passively Mode-Locked Semiconductor Lasers in "Nonlinear Laser Dynamics: From Quantum Dots to Cryptography", edited by Kathy Lüdge*. Wiley, 2012.

[65] F. Arecchi and R. Bonifacio. Theory of optical maser amplifiers. *IEEE Journal of Quantum Electronics*, 1(4):169–178, 1965.

[66] B. McNeil. Due credit for Maxwell-Bloch equations. *Nat. Phot.*, 9:207, 2015.

[67] K. Staliunas. Laser Ginzburg-Landau equation and laser hydrodynamics. *Phys. Rev. A*, 48:1573–1581, Aug 1993.

[68] G. L. Oppo, A. M. Yao, F. Prati, and G. J. de Valcárcel. Long-term spatiotemporal dynamics of solid-state lasers and vertical-cavity surface-emitting lasers. *Phys. Rev. A*, 79:033824, 2009.

[69] E. Roldán, G. J. de Valcárcel, F. Prati, F. Mitschke, and T. Voigt. *Multilongitudinal mode emission in ring cavity class B lasers, in O. G. Calderon and J. M. Guerra (eds.)* Trends in Spatiotemporal Dynamics in Lasers, Instabilities, Polarization Dynamics and Spatial Structures. Research Signpost, 2005.

[70] M. Pang, W. He, X. Jiang, and P. St. J. Russel. All-optical bit storage in a fibre laser by optomechanically bound states of solitons. *Nat. Phot.*, 10:454, 2016.

[71] A. K. Wójcik, P. Malara, R. Blanchard, T. S. Mansuripur, F. Capasso, and A. Belyanin. Generation of picosecond pulses and frequency combs in actively mode locked external ring cavity quantum cascade lasers. *Applied Physics Letters*, 103:231102, 2013.

[72] D. G. Revin, M. Hemingway, Y. Wang, J. W. Cockburn, and A. Belyanin. Active mode locking of quantum cascade lasers in an external ring cavity. *Nat. Commun.*, 7:11440, 2016.

[73] Y. Wang and A. Belyanin. Active mode-locking of mid-infrared quantum cascade lasers with short gain recovery time. *Opt. Express*, 23(4):4173–4185, Feb 2015.

[74] A. Gordon, C. Y. Wang, L. Diehl, F. X. Kärtner, A. Belyanin, D. Bour, S. Corzine, G. Höfler, H. C. Liu, H. Schneider, T. Maier, M. Troccoli, J. Faist, and F. Capasso. Multimode regimes in quantum cascade lasers: from coherent instabilities to spatial hole burning. *Phys. Rev. A*, 77:053804, May 2008.

[75] J. D. Murray. *Mathematical Biology: I. An Introduction*, volume 1. Springer-Verlag, 3rd Edition Berlin Heidelberg, 2002.

[76] E. M Izhikevich. Neural excitability, spiking and bursting. *International Journal of Bifurcation and Chaos*, 10(06):1171–1266, 2000.

[77] J. L. A. Dubbeldam, B. Krauskopf, and D. Lenstra. Excitability and coherence resonance in lasers with saturable absorber. *Physical Review E*, 60(6):6580, 1999.

[78] S. Barbay, R. Kuszelewicz, and A. M. Yacomotti. Excitability in a semiconductor laser with saturable absorber. *Optics Letters*, 36(23):4476–4478, 2011.

[79] M. Turconi, M. Giudici, and S. Barland. Drift-induced excitable localized states. *Physical Review Letters*, 111(23):233901, 2013.

[80] M. Turconi, F. Prati, S. Barland, and G. Tissoni. Excitable solitons in a semiconductor laser with a saturable absorber. *Physical Review A*, 92(5):053855, 2015.

[81] B. J. Shastri, A. N. Tait, M. Nahmias, B. Wu, and P. Prucnal. Coincidence detection with graphene excitable laser. In *CLEO: Science and Innovations*, pages STu3I–5. Optical Society of America, 2014.

[82] B. J. Shastri, M. A. Nahmias, A. N. Tait, B. Wu, and P. R. Prucnal. SIMPEL: Circuit model for photonic spike processing laser neurons. *Opt. Expr.*, 23(6):8029–8044, 2015.

[83] B. J. Shastri, M. A. Nahmias, A. N. Tait, A. W. Rodriguez, B. Wu, and P. R. Prucnal. Spike processing with a graphene excitable laser. *Scientific Reports*, 6(4):19126, 2016.

[84] A. M. Perego and M. Lamperti. Collective excitability, synchronization, and array-enhanced coherence resonance in a population of lasers with a saturable absorber. *Physical Review A*, 94:033839, 2016.

[85] M. Lamperti and A. M. Perego. Disorder-induced localization of excitability in an array of coupled lasers. *Phys. Rev. A*, 96:041803, 2017.

[86] J. L. A. Dubbeldam and B. Krauskopf. Self-pulsations of lasers with saturable absorber: dynamics and bifurcations. *Optics Communications*, 159(4):325–338, 1999.

[87] B. Hu and C. Zhou. Phase synchronization in coupled nonidentical excitable systems and array-enhanced coherence resonance. *Physical Review E*, 61(2):R1001, 2000.

[88] M. G. Rosenblum, A. S. Pikovsky, and J. Kurths. Phase synchronization in driven and coupled chaotic oscillators. *Circuits and Systems I: Fundamental Theory and Applications, IEEE Transactions on*, 44(10):874–881, 1997.

[89] J. F. Lindner, B. K. Meadows, W. L . Ditto, M. E. Inchiosa, and A. R. Bulsara. Array enhanced stochastic resonance and spatiotemporal synchronization. *Physical Review Letters*, 75(1):3, 1995.

[90] P. W. Anderson. Absence of diffusion in certain random lattices. *Physical Review*, 109:1492, 1958.

[91] B. Kramer and A. MacKinnon. Localization: theory and experiment. *Rep. Prog. Phys.*, 56:1469–1564, 1993.

[92] H. Hu, A. Strybulevych, J. H. Page, S. E. Skipetrov, and B. A. van Tiggelen. Localization of ultrasound in a three-dimensional elastic network. *Nature Physics*, 4:945, 2008.

[93] R. Dalichaouch, J. P. Armostrong, S. Schultz, P. M. Platzman, and S. L. McCal. Microwave localization by two-dimensional random scattering. *Nature*, 354:53, 1991.

[94] J. Billy, V. Josse, Z. Zhanchun, A. Bernard, B. Hambrecht, P. Lugan, D. Clément, L. Sanchez-Palencia, Bouyer P., and A. Aspect. Direct observation of Anderson localization of matter waves in a controlled disorder. *Nature*, 453:891, 2008.

[95] M. P. Van Alabada and A. Lagendijk. Observation of weak localization of light in a random medium. *Physical Review Letters*, 55(24):2692, 1985.

[96] D. S. Wiersma, P. Bartolini, A. Lagendijk, and R. Righini. Localization of light in a disordered medium. *Nature*, 390:671, 1997.

[97] T. Schwartz, G. Bartal, S. Fishman, and M. Segev. Transport and Anderson localization in disordered two-dimensional photonic lattices. *Nature*, 446:52, 2007.

[98] M. Segev, A. Silberberg, and D. N. Christodoulides. Anderson localization of light. *Nature Photonics*, 7:197, 2013.

[99] L. Martin, G. Di Giuseppe, A. Perez-Leija, R. Keil, F. Dreisow, M. Heinrich, S. Nolte, A. Szameit, A. F. Abourrady, D. N. Christodoulides, and E. A. Saleh. Anderson localization in optical waveguide arrays with off-diagonal coupling disorder. *Optics Express*, 19:13636, 2011.

[100] Y. Lahini, A. Avidan, F. Pozzi, M. Sorel, M. Morandotti, D. N. Christodoulides, and Y. Silberberg. Anderson localization and nonlinearity in one-dimensional disordered photonic lattices. *Physical Review Letters*, 100:013906, 2008.

[101] J. B. Pendry. Off-diagonal disorder and 1D localisation. *J. Phys. C: Solid State Phys.*, 15:5773–5778, 1982.

[102] F. Selmi, R. Braive, G. Beaudoin, I. Sagnes, R. Kuszelewicz, T. Erneux, and S. Barbay. Spike latency and response properties of an excitable micropillar laser. *Phys. Rev. E*, 94:042219, 2016.

[103] F. Selmi, R. Braive, G. Beaudoin, I. Sagnes, R. Kuszelewicz, and S. Barbay. Relative refractory period in an excitable semiconductor laser. *Phys. Rev. Lett.*, 112:183902, 2014.

[104] S. Novikov, S. V. Manakov, L. P. Pitaevskii, and V. E. Zakharov. *Theory of solitons: The inverse scattering method*. Plenum, 1984.

[105] M. Ablowitz and H. Segur. *Solitons and the inverse scattering transform*. SIAM Studies in Applied Mathematics, 1981.

[106] Y. S. Kivshar and G. P. Agrawal. *Optical Solitons*. Academic Press, 2003.

[107] Y. Silberberg. Collapse of optical pulses. *Opt. Lett.*, 15:1282, 1990.

[108] X. Liu, L. Qian, and F. W. Wise. Generation of optical spatiotemporal solitons. *Phys. Rev. Lett.*, 82:4631, 1999.

[109] S. Minardi et al. Three-dimensional light bullets in arrays of waveguides. *Phys. Rev. Lett.*, 105:263901, 2010.

[110] N. Akhmediev and A. Ankiewicz. *Dissipative Solitons*. Springer, 2005.

[111] S. Trillo and W. Torruellas. *Spatial Solitons*. Springer, 2001.

[112] E. A. Kuznetsov. Solitons in a parametrically unstable plasma. *Sov. Phys. Dokl.*, 22:507, 1977.

[113] D. H. Peregrine. Water waves, nonlinear Schrödinger equations and their solutions. *J. Aust. Math. Soc. Series B, Appl. Math.*, 25:16, 1983.

[114] N. N. Akhmediev, V. M. Eleonskii, and N. E. Kulagin. Exact first-order solutions of the nonlinear Schrödinger equation. *Theor. Math. Phys.*, 72:809, 1987.

[115] V. E. Zakharov and A. A. Gelash. Nonlinear stage of modulation instability. *Phys. Rev. Lett.*, 111:054101, 2013.

[116] B. Kibler, J. Fatome, C. Finot, G. Millot, F. Dias, G. Genty, N. Akhmediev, and J. M. Dudley. The Peregrine soliton in nonlinear fibre optics. *Nat. Phys.*, 6:790, 2010.

[117] E. A. Ostrovskaya and Y. S. Kivshar. Matter-wave gap solitons in atomic bandgap structures. *Phys. Rev. Lett.*, 90:160407, 2003.

[118] J. W. Fleischer, M. Segev, N. K. Efremidis, and D. N. Christodoulides. Observation of two-dimensional discrete solitons in optically induced nonlinear photonic lattices. *Nature*, 422:147, 2003.

[119] B. J. Eggleton, R. E. Slusher, C. M. de Sterke, P. A. Krug, and J. E. Sipe. Bragg grating solitons. *Phys. Rev. Lett.*, 76:1627–1630, 1996.

[120] B. Eiermann, T. Anker, M. Albiez, M. Taglieber, P. Treutlein, K. P. Marzlin, and M. K. Oberthaler. Bright Bose-Einstein gap solitons of atoms with repulsive interaction. *Phys. Rev. Lett.*, 92:230401, 2004.

[121] L. P. Pitaevskii and S. Stringari. *Bose-Einstein Condensation*. Clarendon, 2003.

[122] O. Morsch and M. Oberthaler. Dynamics of Bose-Einstein condensates in optical lattices. *Rev. Mod. Phys.*, 78:179, 2006.

[123] R. E. Slusher and B. J. Eggleton. *Nonlinear Photonic Crystals*. Springer, 2003.

[124] H. Kosaka, T. Kawashima, A. Tomita, M. Notomi, T. Tamamura, T. Sato, and S. Kawakami. Self-collimating phenomena in photonic crystals. *Appl. Phys. Lett.*, 74:1212, 1999.

[125] D. N. Chigrin, S. Enoch, C. M. Sotomayor Torres, and G. Tayeb. Self-guiding in two-dimensional photonic crystals. *Opt. Express*, 11:1203, 2003.

[126] S. Kumar, A. M. Perego, and K. Staliunas. Linear and nonlinear bullets of the Bogoliubov-de Gennes excitations. *Phys. Rev. Lett.*, 118:044103, 2017.

[127] C. Conti, S. Trillo, P. Di Trapani, G. Valiulis, A. Piskarkas, O. Jedrkiewicz, and J. Trull. Nonlinear electromagnetic x waves. *Phys. Rev. Lett.*, 90:170406, 2003.

[128] P. Di Trapani, G. Valiulis, A. Piskarkas, O. Jedrkiewicz, J. Trull, C. Conti, and S. Trillo. Spontaneously generated x-shaped light bullets. *Phys. Rev. Lett.*, 91:093904, 2003.

[129] M. A. Porras, C. Conti, S. Trillo, and Di Trapani. Paraxial envelope x waves. *Opt. Lett.*, 28:1090–1092, 2003.

[130] C. Conti and Trillo. Nonspreading wave packets in three dimensions formed by an ultracold bose gas in an optical lattice. *Phys. Rev. Lett.*, 92:120404, 2003.

[131] M. L. Chiofalo, S. Succi, and M. P. Tosi. Ground state of trapped interacting Bose-Einstein condensates by an explicit imaginary-time algorithm. *Phys. Rev. E*, 62:7438, 2000.

[132] R. Bonifacio and L. A. Lugiato. Cooperative radiation processes in two-level systems: Superfluorescence. *Phys. Rev. A*, 11:1507–1521, 1975.